FAILURE PROCESSES IN UNIDIRECTIONAL COMPOSITE MATERIALS

by

Mannur Jaganathan Sundaresan

Dissertation submitted to the Faculty of the
Virginia Polytechnic Institute and State University
in partial fulfillment of the requirements for the degree of

DOCTOR OF PHILOSOPHY

in

Engineering Mechanics

APPROVED:

E.G. Henneke, II, Chairman

J.C. Duke, Jr.,

J.N. Reddy

K.L. Reifsnider

C.W. Smith

October, 1988

Blacksburg, Virginia

FAILURE PROCESSES IN

UNIDIRECTIONAL COMPOSITE MATERIALS

by

Mannur Jaganathan Sundaresan

E. G. Henneke, II, Chairman

Engineering Mechanics

(ABSTRACT)

Failure processes in unidirectional composite materials subjected to quasi-static tensile load along the fiber direction are investigated. The emphasis in this investigation is to identify the physical processes taking place during the evolution of failure in these materials. An extensive literature review is conducted and the information relevant to the present topic is summarized. The nature of damage growth in five different commercially available composite systems are studied. In-situ scanning electron microscopy is employed for identifying the failure events taking place at the microscopic level. Acoustic emission monitoring is used for estimating the rate of damage growth on a global scale and determining the size of individual failure events.

The results of this study has shown the important roles of the matrix material and the interphase in determining the tensile strength of unidirectional composite materials. Several failure modes occuring at the microscopic scale are revealed for the first time. Further, the results indicate that dynamic fracture participates to a significant extent in determining the failure process in these materials. Based on the results of this study the influence of various parameters in determining the composite strength is described.

Acknowledgements

The author would like to thank the following people for their contribution to this work

- Dr. E. G. Henneke, II, for his guidance and support during the course of this investigation.

- Drs. K. L. Reifsnider, J. N. Reddy, J. C. Duke, Jr., and Prof. C. W. Smith for serving in the authors advisory committee.

- Chuck Chandler, Bob Davis, B. Shaver and Archy Montgomery for their assistance in the fabrication of test specimens and fixtures.

- Mike deBusk for his assistance in the laboratory.

- Karen Swanson for her assistance in the SEM work.

- his brother, M. J. Gurunathan who made it possible for the author to pursue education beyond high school.

- his wife Vasanthy without whose many sacrifices and love this work would not have been possible.

Table of Contents

List of Tables

List of Illustrations

1.0: INTRODUCTION

The longitudinal strength of unidirectional composite materials is an important parameter, which often determines the ultimate strength of composite structures. The strength of such an unidirectional material is determined by the mechanical properties of the constituents, namely, the fiber, the matrix and the interface, and their interactions. At the present time there is a large variety of fibers, matrices and interfaces available and it is potentially possible to synthesize composite sytems to optimally suit different applications. To realize this potential, a good understanding of the failure processes operative in different composite systems is essential.

The macroscopic failure of a unidirectional composite lamina, under quasi-static tensile load is the result of a sequence of microscopic failure events. Since the fibers themselves have a statistical distribution of strength instead of a single value of strength, the damage in unidirectional resin matrix composites starts as a distribution of random single fiber fractures, at relatively low load levels. These isolated fiber fractures create further damage in the surrounding material in the form of matrix or interfacial failure or additional fiber fractures. Thus, groups of adjacent fiber fractures are formed and as the load increases, the size of those groups grow. In the meantime, more isolated fiber fractures continue to occur throughout the composite volume. It is generally assumed that one of these "isolated initi-

ators" grows and eventually cause unstable fracture across the entire specimen width. The mechanics of growth of these "isolated initiators" into critical dimensions, determines the strength of the composite material.

There are a number of factors which influences the nature and rate of damage growth in unidirectional composite materials. These include fiber strength statistics, matrix and interfacial properties, and internal residual stresses. Hence, the failure process in these materials is quite complex. By necessity, the researchers in this area are forced to study isolated aspects of the failure process.

A very extensive literature exists on this topic. A large number of theoretical investigations concentrat on the influence of fiber strength statistics in determining the ultimate strength of the composite materials. Others analyze the micromechanics of failure using analytical and numerical techniques. Experimental techniques ranging from optical microscopy to acoustic emission monitoring have also been used to study the failure process. These theoretical and experimental investigations have provided valuable insight into the composite failure processes. However, many gaps remain in our understanding of the failure of unidirectional composite materials.

For example a number of important parameters required as inputs for theoretical models are not available. These include the actual values of stress concentration around broken fibers and the ineffective length for real composite systems. The nature and sequence of failure events in different composite systems have not been clearly established. Further, no analytical framework appears to exist for the quantitative prediction of the influence of various parameters such as matrix toughness and the interfacial strength on the strength of the composite material.

1.1. Objective:

The objective of the present study is to understand the fundamental physical processes involved in the failure of unidirectional composite materials under quasistatic tensile load along the fiber direction. As a part of this program, a comprehensive literature review was undertaken. Major efforts were made in assembling the published literature in this area and presenting it in a coherent manner.

In the experimental program the failure processes in actual composite systems currently in use in aerospace applications were monitored. In-situ scanning electron microscopy (SEM) and acoustic emission monitoring technique (AET) were used for studying the failure behavior. SEM provides information about the failure events at the microscopic scale and AET provides information about the rate of damage growth on a global scale. Hence the two experimental techniques complement each other.

In chapter 2, a detailed literature review on the failure processes in unidirectional composite materials, is given. Chapter 3 describes the technique and results of SEM studies of the failure process. The acoustic emission monitoring of the failure processes is described in chapter 4. In chapter 5, the results of chapters 3 and 4 are examined along with a perspective of the literature review and a description of the evolution of failure processes in unidirectional composites is provided.

2.0: Failure Mechanics of Unidirectional Composite Materials: A Review

2.1.0. Introduction

The importance of the understanding of the failure processes of unidirectional composite materials and quantifying them needs hardly be emphasized. In most laminates, the ultimate strength is determined by the strength of the lamina whose fibers are aligned with the load direction, both under static as well as under fatigue loading conditions.

At present, the most common approach for determining composite strength is an empirical one, in which the composite of a given set of constituents is tested in the form of coupons, the A and B confidence levels are estimated and extrapolated to obtain the safe strength in actual structures for design purposes. Though this is a viable approach, it is quite expensive and needs new data to be generated for each combination of fiber, matrix and interface and enviornmental conditions. More importantly, the understanding of the physical process is essential if one is to find an optimal combination of fiber matrix and interface for a given application.

Conventionally it has been assumed that the function of the fiber is to carry the load, while the matrix keeps the fibers in their proper position and protects them from the environment.

Hence, the early investigators obtained the strength of the composite from the rule of mixtures in the form [96,182]

$$\sigma_{comp} = V_{fib}\,\sigma_{fib} + (1 - V_{fib})\,\sigma_{matrix} \qquad (2.1)$$

where σ_{comp} is the ultimate strength of composite, σ_{fib} is the average strength of fiber , σ_{matrix} is the stress in the matrix at the ultimate strength of the composite and V is the fiber volume fraction.

Soon it became apparent that the composite strength is not determined by the average strength of the fibers, but rather by the statistical distribution of the strength of the fibers and the way in which the load from a broken fiber is transferred to the rest of the material. It has been only recently that it was appreciated that the matrix and interface have important roles in determining how the load from a broken fiber is redistributed.

The review is organized as follows: First, the properties of the constituent materials - fibers, matrix and interface are reviewed. Then the type of internal stress distribution in a unidirectional lamina with and without broken fibers is examined. Experimentally observed fracture surface morphology and other experimental results which may provide information on the nature and chronology of the failure process are examined. The available statistical and other strength theories and their results are summarized along with some comparisons between experimental and theoretical results. Finally an alternate model of failure process is suggested.

2.2.0. Properties of fiber.

The main property of interest in fibers is the strength distribution. Besides the strength, other properties which can affect the composite failure behaviour are the fiber diameter,

modulus, thermal expansion coefficient, and chemical structure of the fiber surface which interacts with the matrix to form an interfacial layer. Lovell [107], Hiramatsu [87], Hughes [89] and Riewald [155] provide a compilation of the properties of available fibers for structural applications. Significant recent additions to the available fibers are the ulltrahigh strength carbon fiber having one million psi strength, the ultrahigh modulus carbon fiber having 120 million psi modulus, and a variety of ceramic fibers for high temperature applications.

2.2.1 Strength: The strength distribution of fibers is determined by internal flaws introduced during manufacture as well as due to handling, consolidation into the composite and to environmental and other factors in service. For example, defects in virgin carbon fibers could be due to misaligned or discontinuous fibrils or entraped foreign particles, each category of which can give rise to a different level of strength reduction.

Jones [95] studied the strength limiting flaws present in pitch based fibers and their influence on the Weibull strength parameters. Moreton [128] reviews several studies related to the dependence of PAN based carbon fibers' strength on the manufacturing process and discusses the mechanisms of fracture of individual fibers.

The Weibull "extreme value statistics theory" is the most widely used method for characterizing the strength distribution of fibers. In this theory, it is assumed that the fibers have flaws of varying severity randomly distributed along the length of the fibers. But for a given segment of a fiber, the strength is governed by the most severe of these defects present in that segment. The probability of failure of a fiber segment of unit length as a function of stress can be expressed as [67]

$$F(\sigma) = 1 - \exp\left[-\left(\frac{\sigma}{\sigma_0}\right)^m \right] \tag{2.2}$$

where the two parameters, Weibull modulus 'm' and characterstic strength σ_0, completely characterize the strength distribution of the fiber, hence the name "two parameter Weibull distribution". The parameter σ_0 is simply a nondimensionalising parameter and is numerically equal to the stress at which the probability of failure is equal to {1 - (1/e)} i.e., 0.632. The modulus 'm' is an inverse measure of variability of fiber strength, the greater the value m, the smaller is the strength variability. From this distribution for unit length, the strength of a fiber segment of length 'l' can be calculated as

$$F_l(\sigma) = 1 - \exp\left[-l\left(\frac{\sigma}{\sigma_0}\right)^m\right] \tag{2.3}$$

The average strength of the fiber can be expressed as [67]

$$\sigma_{av} = \sigma_0(l)^{-\frac{1}{m}}\,\Gamma\left(1 + \frac{1}{m}\right) \tag{2.4}$$

where Γ is the gamma function. The above equation indicates a linear relation between the logarithm of average strength of fibres and logarithm of length and a plot of log σsubav versus log l is a straight line with slope equal to -1/m. Thus it is possible to estimate the average strength at any length from the above plot, constructed from experimental data of average strength measured at two or more lengths. It is convenient to measure the filament strengths at lengths of 1" or greater. But the statistical strength theories require strength distributions at much smaller lengths called the "ineffective length" whose magnitude is of the order of 0.004" and it is almost impractical to measure fiber strengths at this length. Because of this difficulty, the common practice is that strength data from several larger gage lengths like 1", 2", 5", and 10" are used to extropolate and to obtain the strength at the scale of the ineffective length.

The actual variation of the strength with length as well as the conformity of the true strength distribution with the Weibull model has been investigated by several investigators including Metcalfe and Schmitz [123] for glass fibers and Barry [24], Hitchon and Phillips [88] and Bader

and Priest [14] for carbon fibers and Phoenix [137] for boron fibers. Different methods of estimating Weibull parameters from a given strength data set and the errors involved in these estimations are examined by Talreja [174].

These investigators have found that even at a given gage length, the two parameter Weibull model does not accurately represent the actual strength distribution, and of greater concern was their finding that the extrapolation of strength data measured at longer gage lengths to the very short lengths of the order of the "ineffective length" is inapplicable and gives unconservative estimates. For example Metcalfe and Schmitz found [123] that the strength increased rapidly with a reduction in gage length down to a length of about 0.5" inches and thereafter there is much smaller increase in strength as the gage length reduces. Harlow and Phoenix [80] have modelled this type of strength distribution by a double Weibull function

$$F(\sigma) = 1 - \exp\left[-(\frac{\sigma}{\sigma_0})^m - (\frac{\sigma}{\tilde{\sigma}_0})^{\tilde{m}} \right] \tag{2.5}$$

where $\tilde{\sigma}$ and $\tilde{m}$ correspond to those flaws controlling the strength at very short fiber lengths. Based on the experimental results of Metcalfe and Schmitz on glass fibers, Harlow and Phoenix assume $\tilde{m} = 10m$. As Harlow and Phoenix observe, the strength at long gage lengths is almost exclusively determined by the parameters σ_0 and m, whereas at very short lengths, the parameters $\tilde{\sigma}$ and $\tilde{m}$, dominate. The influence of σ_0 and m corresponding to short gage lengths probably will not be seen except at the extreme lower tail region of the strength distribution. When plotted on Weibull probability paper, the double Weibull distribution forms two intersecting straight lines on the log scale and the point of intersection is given by [80],

$$\delta^* = \frac{\sigma_0}{\tilde{\sigma}_0} \frac{m\tilde{m}}{(\tilde{m} - m)} \tag{2.6}$$

The ratio $\sigma_0/\tilde{\sigma}_0$ for fibers whose length is equal to the ineffective length is termed the strength truncation ratio and appears to be equal to 0.65 for glass fibers. Harlow and Phoenix [80] observe that the second Weibull term in equation (2.5), in effect places a ceiling on the maximum possible strength near $\tilde{\sigma}_0$. It should be noted that all these estimates are based on Metcalfe and Schmitz data published in 1964 and fiber manufacturing has considerably evolved from that time. Hence current fiber properties are likely to be different. Further, for other fibers like carbon, boron, and kevlar, even this kind of rough estimate is not available.

Kasai and Saito [98] have compiled a considerable amount of information about the strength distributions of usual reinforcing fibers, available in the literature up to 1979. They found that for a 90% correlation between the model and actual data, a three parameter Weibull function is essential. A three parameter Weibull distribution for fibers of unit length takes the form

$$F(\sigma) = 1 - \exp\left[-\left(\frac{\sigma - \sigma'}{\sigma_0}\right)^m\right] \tag{2.7}$$

The main difference between the two parameter and three parameter Weibull distribution is that for the two parameter distribution, the minimum fiber strength possible is zero whereas for the three parameter, it would be equal to σ' . From a comparison of experimental results with the two and three parameter Weibull models, the fiber strength distribution in the lower tail region appears to be more accurately modelled by three parameter distribution. This can be observed in the results of Bader and Priests [14]. The two parameter Weibull function has a tendency to under-estimate the strength at the lower tail region and over-estimate the strength at the upper tail region. For the common fibers used in composites, the shape parameter m, which is an indication of fiber strength variability, ranges from 2 to 7, in general.

As we shall see in the later sections, the statistical strength theories point to the fact that the strength of a composite is largely determined by the strength distribution of the fibers in the lower tail region. Hence, it is more effective to improve the minimum strength of the fibers rather than the average strength of fibers, if improvement in composite strength is desired.

2.2.2. Modulus: Barry [24], while testing the early carbon fibers (1972) of the type Modmor Is, IIs and IIIs, found that the modulus of fibers also varied considerably, upto 30%. Also, for type I the ultimate strain increased with an increase in the modulus, while for IIs, remained independent of modulus, and for IIIs, decreased with an increase of the modulus.

The ratio of the average fiber strength to modulus, i.e. average strain, at failure is another parameter of interest, since it would determine both the strain energy released during fiber break and the extent to which the matrix may be strained in the composite. The strain to failure is minimum for boron and high modulus carbon fibers and maximum for kevlar and S- glass fibers.

2.2.3. Toughness: All the common reinforcing fibers excepting kevlar fibers are brittle in the sense no stress relieving mechanisms within the fibers, such as plasticity, are present and they are very susceptible to impact damage. However, individual kevlar fibers break by fibrous failure and are considerably tougher.

2.2.4. Thermal expansion coefficient: The relative values of the thermal expansion coefficient of fiber compared to that the matrix determine the extent of residual thermal stresses present in the composite, when it is cooled down from the cure temperature to room temperature [131,132]. Some of the fibers have anisotropic thermal expansion. Typical values are listed in table I.

2.3.0. Properties of Matrix Material and Interface

Even though the matrix itself carries a very small share of the load in the composite, its behaviour near a failed fiber, largely determines how the load from the broken fiber is redistributed and the efficiency of this redistribution in turn determines the composite strength. The relevant properties of the matrix are shear modulus, strain at failure, Poisson's ratio,

Table I: Thermal expansion characteristics, from Nairn [131].

Material	Property	Value
Graphite fibers	α_L	- 0.36 ppm/°C
-do-	α_T	18 ppm/°C
-do-	ΔV	0.54% (177° Cto25° C *
Kevlar 49	α_L	-2 ppm/° C
-do-	α_T	59 ppm/° C
-do-	ΔV	1.8% (177 C to 25° C)*
3501 - 6 Epoxy	α	40 ppm/° C
-do-	ΔV	1.8% (177° C to 25° C)*
Polysulphone	ΔV	3.2% (185° to 25° C)*
Polyethylene terephthalate	ΔV	13.6% (200° C to 25° C)*
Polyethylene	ΔV	22% *

*Volume contraction due to cooldown from composite fabrication temperature to room temperature.

fracture toughness, shear deformation and yield mechanisms, strain rate sensitivity, thermal expansion and moisture absorption characteristics.

2.3.1. Stress - strain behaviour: Zimmerman, Adams and Walrath [195] recently carried out detailed characterization of a commonly used resin, Hercules, 3502 and three other candidate resins. The properties measured included ultimate strength and strain, fracture toughness, thermal expansion coefficient, moisture absorption and fracture surface characteristics. According to their results the ultimate tensile strength for these resins, in bulk form, ranges from 4 to 8 ksi. It is interesting to note that the shear strengths are generally larger than tensile strengths and range from 7 to 12 ksi. The ultimate tensile strain of Hercules 3502 was about 1% and shear strain was about 3.5%. The other three new resin formulations had larger ultimate shear strains and one of them had an ultimate shear strain of 14%. There was also considerable variation in the above properties with temperature and humidity. The general trend was that the elastic modulus decreases and ultimate strain increases with increase in temperature and moisture content.

2.3.2. Yield and Fracture: The yield and fracture strength of epoxy resins could be modified considerably by the dispersion of rubber particles - the fracture toughness could be increased to greater than twice the unmodified toughness values [55,181,192]. But this increase is gained at a sacrifice to the modulus which is not desirable from the point of view of composite transverse stiffness. Thermoplastic resins have ultimate strains of the order of 10 to 150% under uniaxial loading.

The above stress strain behaviours were measured under a uniaxial state of stress for bulk epoxy specimens. However, it is not clear how these properties relate to the constrained in-situ behaviour of the resin within the composite, where a triaxial state of strain prevails. Some of the micromechanisms of resin deformation and failure in bulk polymers are discussed in reference [192]. Recently, the microscopic deformation of the resin within com-

posite materials has been studied by scanning electron microscopy. Bradley and Cohen [32], while studying the interlaminar fracture process, noted that while some resins are capable of extensive microvoid development and plastic deformation, others behave in a completely brittle manner. For example, Hexcel 185 resin underwent extensive microcraking whereas Hercules 3502 had a single brittle crack growth. Sato et.al. [157], while studying short fiber thermoplastic (polyamide) composites, found that the matrix bordering fiber ends underwent extensive localised plastic deformation and distributed microcrack growth.

2.3.3. Strain rate effects: It is possible that the strain rate dependence of the matrix deformation behaviour becomes important, since the fiber fracture essentially loads the surrounding matrix under impact conditions, for a very short duration of time. Any increase in modulus and yield stress level of the matrix under such conditions, can cause a corresponding increase in the transient stress concentration in the neighbouring fibers (section 2.4.2) and also possibly alter failure behaviour of the matrix.

It appears quite probable that the strain rate does affect the yield strength and the modulus of the matrix materials. The yield strength of 1100-0 aluminium increases by 25% at a strain rate of 850/sec and triples at 10^4 /sec. according to Clifton [44] and Malvern [115]. There is also a corresponding increase in the modulus. Vinh and Khalil [187] report that for polyimide resin there is a three fold increase in yield strength and ten fold increase in modulus when strain rate is increased to 110/sec. Armenakas [10] report that the modulus doubled when strain rate was increased from 0.00044/sec to 0.44/sec for one type of epoxy.

2.3.4. Thermal expansion coefficients:: table I, the thermal expansion coefficients of some of the common resins are listed. It is clear that the differential thermal contraction between fiber and matrix can cause residual thermal stresses in the composite. Of particular concern is the high thermal expansion coefficient of thermoplastic matrices in which the cure shrinkage can be as large as 22% by volume.

2.3.5. Interface: Fiber matrix bond strength, and hence the stress redistribution from a broken fiber into the surrounding material is largely determined by the interface properties. Fiber manufacturers generally give specific surface treatments to the fibers, which determine the interfacial strength.

Drzal [57,58] conducted a detailed study of the influence of the interface on the composite strength. As manufactured, the carbon fiber surface has a defective surface layer of very low shear strength, which causes failure along the fiber surface, if fabricated into composite and loaded. Specific oxidation treatments remove this defect laden surface, and further add some chemically reactive components to the surface. Both of these increase the interfacial shear strength considerably.

Drzal tested carbon/epoxy composites, as well as monofibers embedded in semicured epoxy matrix, under three different fiber surface conditions: (i) untreated, (ii) surface treated with oxidation, and (iii) surface treated fibers coated with a thin layer of epoxy which upon curing along with the bulk composite produces a high modulus and higher strength interface. His tests revealed the significant effect of the interfacial conditions on composite strength.

In mono-fiber composite tests, the untreated fibers seemed to completely debond and slide after a fiber break. The shear stress from the fiber transferred to the resin mainly by friction. The surface treated fiber debonded after fiber break to a length of the order of one diameter, and caused considerable stress concentration in the matrix. As the strain was increased, the debond length increased to several diameters long. The surface coated fiber had no debond, but had the maximum stress concentration among the three types of surface preparations and further, caused a transverse crack propagation through the matrix.

These effects clearly manifested themselves in the respective composites also. Composites made from untreated fibers displayed fracture surface with large degree of fiber pullout while the composites with surface treatment had much shorter fiber pullout. In contrast the com-

posite with fiber coating had almost planar fracture surface, indicating fracture propagation just as in isotropic brittle materials.

Drzal et. al., [56] devised a means of estimating the approximate interfacial shear strength in composite materials. They used a specimen in which a single fiber was embedded in matrix material and was subjected to a gradually increasing axial strain while being monitored under an optical microscope. As the strain increased the fiber fragmented into smaller and smaller segments untill the individual segments reached the "critical length". Beyond this strain level there was no further fiber fragmentation. The length of these segments was measured. The axial stress in the middle of each segment is assumed to be the fiber strength at that length. From these data the average shear strength at the fiber matrix interface is obtained by simple force equilibrium.

Bascom et. al., [15] determined the mono-fiber fragmentation length in a number of systems having different combinations of fibers and matrix materials. One of their findings was that the ineffective length of AS4 fiber in thermoplastic matrix was much longer than that in thermoset matrices. Di Landro [54] obtained relatively low values of interfacial shear strength in a carbon fiber thermoplastic composite material. From these results and from his other chemical analyses he concluded that the low value of shear strength was due to the absence of chemical bonding between the fiber and the matrix and the fiber in these composites was constrained by the matrix purely by frictional forces.

Sawada et. al., [159] measured the interfacial shear strength in carbon fiber polyimide composites, for various fiber surface treatments. Their results suggest that the interfacial shear strength in these composites is primarily determined by the chemical bonding and is very little influenced by the mechanical anchoring due to the fiber surface roughness. Piggot and Andison [142] conducted single fiber pullout tests from different matrix materials and measured the force required to extract the fibers, as a function of embedded length.

Adams [3] tested unidirectional composites with several combinations of fiber sizings and matrix materials under transverse tension, to estimate the interfacial strength for each of the combinations. His results indicate the general trend that unsized fiber surface, epon 828 sizing and polysulphone sizing result in similar transverse tensile strength, whereas PVA sizing leads to transverse strength reductions.

Bender [131] demonstrated that the interfacial bond has considerable influence on the strength of silicon carbide fiber ceramic matrix composite materials. By suppressing the formation of strong bond between the fiber and the matrix, the strength and toughness were enhanced by over 100%.

Recently, there have also been efforts to improve composite properties by providing a thick interface. Subramanian [168] investigated the static and impact strengths of composites in which the carbon fibers were coated with flexible interlayers. He obtained a 20% increase in static strength for the composite with coated fibers, compared to the composite with no fiber coating. The relatively weaker interface, capable of debonding, was attributed as the reason for the increase in strength. This, however, was obtained at an expense of interlaminar shear strength. Agarwal [4] studied the effect of finite thickness interface on the load transfer length in short fiber composite using the finite element technique. As one may expect, a stiffer interface reduces the load transfer length.

The interface ability to remain intact or fail near fiber breaks is considerably influenced by the existing normal stress on the fiber matrix interface in the composite. In the presence of large compressive residual stresses, the interfacial failure is arrested within a short distance from the fiber break, because the frictional shear stresses effectively reduce the stress singularity at the interfacial crack tip. Kelly and Zweben [108] consider the conditions under which unstable interfacial debonding can occur. As the results of Adams and coworkers [2,195] indicate, the interfacial stresses on an unbroken fiber surface can range from compressive to tensile stresses in the range of -10 ksi to 10 ksi, depending on the matrix resin,

applied load and hygro-thermal environment. It appears likely that tensile interfacial normal stress promotes fiber matrix debonding near a fiber break, whereas compressive interfacial normal stress suppresses fiber matrix debonding and promotes the extension of fiber crack into the matrix.

2.4.0. Stress concentration around broken fibers

The actual stress distribution around a broken fiber in an unidirectional composite is complex because of the three dimensional character of the problem, the nonlinear response of the matrix and possible debonding of the fiber matrix interface. Several simplifying assumptions are necessary to render the problem tractable. The first and most widely used assumption, due to Hedgepeth [83], is the so called "shear lag" type of deformation of the composite near a fiber break. Under this assumption the fiber carries all the axial load and the matrix carries only shear load. Further, the fibers are constrained to deform in the axial direction only. Thus lateral displacements and bending of fibers are precluded. These assumptions effectively decouple the equilibrium equation in the axial direction from those in the other two transverse directions. Thus, instead of solving three coupled partial differential equations, one needs to solve only a single second order differential equation. Further, most analyses consider that the matrix is elastic and that no failure either in matrix or the interface occurs.

2.4.1 Two dimensional fiber array, elastic matrix: Hedgepeth [83] and Hedgepeth and Vandyke [84] obtained stress concentration factors, corresponding to the first unbroken fiber, next to a single and multiple fiber breaks, in two dimensional and three dimensional fiber arrays. The stress concentration factor K_r in this first intact fiber in a two dimensional array takes the form [83]

$$K_r = [4:6:8::::(2r + 2)] / [3:5:7::::(2r + 1)] \tag{2.8}$$

for r = 1,2,3,.... . The fiber stress concentration varies from 1.33 for a single fiber break to a value of 0.3 for ten continuous breaks. The shear lag theory predicts that the maximum shear stress τ_{max} occurs at the broken fiber end and is given as (Hikami and Chou as quoted in Goree [70])

$$\tau_{max} = \sigma_{\infty} \left[\frac{G_{matrix}\, A_{fiber}}{E_{fiber} h\, t} \quad \frac{\pi(2m-1)!}{2^{2m}\{(m-1)!\}^2} \right]^{1/2} \tag{2.9}$$

where h is the interfiber spacing, t is the monolayer thickness and m is the number of continuous fiber breaks. This formula would give, for a single fiber break, τ_{max} = 13.5 ksi for a fiber stress of 200 ksi in graphite/epoxy. This is beyond the strength capability of most resin matrices. The corresponding value for ten continuous fiber breaks is 67 ksi. Hence we may expect considerable amount of plastic flow and shear fracture of the matrix, particularly near multiple fiber breaks.

The stress concentration factor (SCF) in two dimensional arrays was the topic of numerous investigators. Fukuda and Kawata [61] using an approximate discretization technique, determined the stress concentration factor and ineffective length for a model in which the matrix was also capable of supporting axial load. For low fiber volume fraction, the SCF was lower and fiber ineffective length δ was much larger, compared to the shear lag analysis.

Fukuda and coworkers [62-65] in a series of papers using shear lag theory, determined the fiber stress concentration factors for a variety of different broken and unbroken fiber sequences. Their analysis included (i) the SCF in the first and second unbroken fibers for continuous fiber breaks of various sizes (ii) the SCF in hybrid composites consisting of alternately high modulus (low elongation) and low modulus (high elongation) fibers.

One of their findings was that in a hybrid composite, the high modulus fiber suffers lesser SCF due to neighbouring low modulus fiber breaks as compared to the SCF in an all high

modulus composite. This factor at least partially explains the so called hybrid or synergistic effect in hybrid composites.

Argon [7] and Agarwal [5] determined the strain field at the fiber end for somewhat different situations from the present one under consideration. Argon considered a single fiber embedded in a matrix and determined the shear strain concentration at the end of the fiber by an approximate analysis and obtained the peak shear stress to be nearly nine times the average normal strain in the matrix. Agarwal performed a finite element analysis of aligned discontinuous fiber composite with epoxy matrix. He found that considerable plastic flow occurs in the matrix, even at 0.5% strain of the composite.

Whitney and Drazal [190] provided an approximate closed form solution for the axisymmetric stress distribution around the fiber break in the case of a single fiber encassed inside a matrix material, as in the case of Drazal's fiber fragmentation test, for measuring the interfacial shear strength [section 2.3.5].

Ko [101] used the finite element technique to determine the stresses in core-sheath type of monofiber composite materials. Two types of composites were considered - a composite in which the central fiber was broken and another in which the annular matrix was cracked. A parametric study of the dependence of various stresses on the moduli ratio and the differences in Poisson's ratio was done. For the broken fiber case considered in this paper, the axial stress concentration factor in the matrix and the radial interfacial stress concentration factor near the fiber break exhibited a moderate dependence on the modulus ratio but a strong dependence on the Poisson's ratio mismatch. For E(fiber)/E(matrix) = 50 and Poisson's ratio(fiber) = Poisson's ratio(matrix) = 0.25, the axial SCF in the matrix was 9 and for the same combination except Poisson's ratio(matrix) = 0.5, the SCF in the matrix was 52. Corresponding figures for the radial SCF in the interface are 2 and 58 respectively.

Avery and Herakovich [12] provided an elasticity solution for the thermal stresses present in core-sheath type monofiber composite with both transversely isotropic as well as transversely anisotropic fibers. Two types of idealized transverse anisotropy, namely, circumferentially aligned basal planes and radially aligned basal planes, are discussed. The stresses, as well as possible failure modes for each type of anisotropy, assuming purely from thermal stresses are discussed.

2.4.2. Two dimensional array, elasto-plastic matrix: Hedgepeth and Vandyke [84] analyzed the stress distribution in composite, with an elastic, perfectly plastic matrix. They obtained the stress concentration factor for a single fiber break as a function of the ratio P/P(limit) where P(limit) is defined as the load at which plasticity initially sets in and P is the current load. Under these conditions the stress concentration factor in the first intact fiber reduces from the value of 1.33 for the elastic case to 1.18 for an elasto-plastic case with P/P(limit) of 6. Further increase in P/P(limit) beyond this value reduces the stress concentration factor only by a small amount. The spread of the plastic region in the matrix around the fiber break, is almost linear up to P/P(limit) = 6, and at this load level the length of the plastic zone is three times the fiber diameter.

Reedy [150], while analyzing the crack extension in a notched boron - aluminium linear array illustrated the effect of matrix plasticity on the stress concentration factor in the first intact fiber. He used a shear lag based finite element technique for analysis and considered the matrix shear behaviour to follow modified the Ramberg - Osgood relationship of the form

$$\begin{aligned} \frac{\gamma}{\gamma_y} &= \frac{\tau}{\tau_y} \qquad \text{when } \frac{\tau}{\tau_y} \leq 1 \\ &= \left(\frac{\tau}{\tau_y}\right)^N \quad \text{when } \frac{\tau}{\tau_y} > 1 \end{aligned} \tag{2.10}$$

where τ_y is the shear yield stress and the exponent N characterizes the material plastic strain hardening behaviour. It may be noted that for a value of N=1, the matrix is perfectly elastic,

and for N=9 the matrix is almost elastic- perfectly plastic. The variation of stress concentration with the yield stress τ_y and exponent N are provided by Reedy. He assumed the stress level in boron fibers to be 3586 MPa and varied the matrix yield strength in the range of 17 to 138 MPa. It can be seen from his results that the stress concentration factor could be reduced upto 1.1 if suitably ductile matrices are used.

Because of matrix yielding, the value of the fiber stress concentration factor is likely to reduce at higher load levels. Further, near multiple fiber breaks, the resin is likely to be subjected to even greater levels of stress, and, hence, the stress concentration predicted for multiple fiber breaks by the elasto-plastic analysis is likely to be even smaller than the elastic predictons. Analytical results for such cases do not seem to be readily available . Reedy [151] also considered the effect of fiber debonding and frictional load transfer on the stress concentration factor and the length of the overstressed region in the first intact fiber. He found that the stress concentration factor decreases and the length of the overstress region increases as the frictional interfacial shear stress reduces in magnitude. For a Kevlar/epoxy mono-layer with a fiber strength of 134 GPa and interfacial shear strength of 30 GPa, he determined the extent of debonding, considering different levels of frictional interface shear stresses. For a value of frictional stress equal to half the interfacial strength he found that the stress concentration factor was 1.08 and the overstress length was 60 times the fiber diameter.

2.4.3. The ineffective length - Two dimensional case: A parameter needed in the statistical strength prediction of composite material is the overload length of the first unbroken fiber near the damage or equivalently twice the length δ within which the broken fiber attains average strain levels in the composite. Rosen [156] estimated this length for a single fiber break, using shear lag theory, for a linear fiber array and found this to depend on the moduli ratio of the fiber and matrix, and the fiber volume fraction. For example, according to his estimates, for carbon/epoxy with a fiber volume fraction of 0.6, the value of δ is eight times the fiber dia, if the matrix is elastic. Thus, the ineffective length is sixteen times the fiber diameter.

Armanekas [9] experimentally determined the ineffective length in glass/epoxy, with a fiber volume fraction of 10% to range from 40 to 75 times the fiber diameter whereas Rosen's model for this volume fraction predicted it to be 40 times the fiber diameter. For continuous fiber breaks, it is obvious that the overstressed length increases.

2.4.4. Dynamic stress concentration factor - 2D case: The stress concentration factor considered in all the above analyses was due to the static overload caused by the broken fibers. However the time duration required for a dynamic crack to traverse a single fiber is so small (of the order of few nanoseconds i.e., 10^{-9} sec) that the surrounding matrix and fibers are essentially loaded under impact conditions. Hedgepeth [83] found that the transient stress, immediately following fiber fracture, was greater than the static predictions and he obtained a dynamic response factor, which is the ratio of dynamic SCF to the static SCF for various number of fiber breaks. The dynamic response factor ranged from 1.15 for single break to 1.27 for a large number of fiber breaks [83]. Thus the dynamic stress concentration factor for single fiber break becomes 1.53.

Ji [94] examined the distribution of this dynamic SCF along the length of the nearest neighbour and found that the overload length under dynamic conditions is considerably larger than the static prediction - for example for graphite/epoxy, even at a distance of 50 diameters from the fiber break, a SCF of 1.1 exists.

2.4.5. Accuracy of the shear lag analysis: Recently Reedy [152] evaluated the accuracy of the SCF predicted by shear lag analysis by comparing it with those determined by three dimensional finite element analysis. He considered boron/aluminium and kevlar/epoxy composites and modelled the matrices to be elastoplastic. His results indicate that, for elastic matrix, a considerable gradient of the stresses exists across the width of the first unbroken fiber. The edge nearest to the broken fiber is loaded to a greater extent than the farther regions, i.e., the first unbroken fiber is under a considerable amount of bending. However matrix yield and

flow reduces these bending stresses. For boron/ aluminium with elastic matrix, there is about a 25% difference in the stresses between extreme points across the fiber width, and for Kevlar epoxy this difference is of the order of 40%. However, Reedy compared the average fiber stress predicted by FEM with shear lag results and concluded that the shear lag predictions are quite accurate. The shear lag model assumes that the fiber can only extend in the axial direction and no transverse bending is allowed. This appears to be the reason why the shear lag theory fails to reveal the bending stresses in the first unbroken fiber.

In addition, in actual composites the interfiber spacing is not uniform and there is considerable fiber contiguity. When the interfiber distance varies, we may expect the SCF also to vary - the lesser the fiber seperation, the greater the SCF is likely to be.

The analysis of Gecit and Erdogan [68] concerning laminated structure is of direct relevance in understanding the above two effects. From their analysis it is possible to estimate (i) the stress intensity factor in the matrix near the fiber break and (ii) the SCF in the neighbouring fiber, as a function of interfiber spacing. For alternate broken and unbroken fibers their analysis would yield the following results: for interfiber separation of 0.1 dia and 0.05 dia the stress concentration factors at the surface of the unbroken fiber, respectively, would be 2.3 and 2.8. As the interfiber separation reduces further towards zero, the SCF tends to infinity, i.e., the stress concentration turns into "Stress Intensity". Though the resin plasticity and interfacial failure are expected to alleviate the above stress intensification,when the interfiber spacing is very small, it is still likely to be quite significant.

2.4.6. Stress Concentration factor : Three dimensional case: Fewer results regarding stress concentration in composites with fibers arranged in three dimensional array are available compared to the two dimensional case. Hedgepeth and Vandyke [84] extended the shear lag theory of two dimensions to the three dimensional case and determined the stress concentration factors corresponding to breaks in fiber groups of up to 36 in hexagonal array. Their results [84] on stress concentration factors is reproduced in table 2. It may be noted that even

for such a large number of fiber breaks and elastic matrix behaviour, the stress concentration factor does not exceed 2.0. If elastoplastic matrix behaviour or interfacial failure is present, the stress concentration values are likely to be even smaller.

2.4.7. Ineffective length : Three dimensional case: The calculation of the ineffective length for a three dimensional array is not as straight forward as in the case of the two dimensional array. The shear rigidity of the matrix in the 2D case is well defined and is equal to Gh where G is shear modulus of resin and h is the interfiber distance. This parameter is undefined in the three dimensional case. Batdorf [16,19,22,23] devised an electrical analogue, through which both the effective shear regidity of the matrix as well as the ineffective length could be experimentally obtained. He found that, the differential equations of the shear lag theory and those of the electrical potential distribution in an array of cylindrical conductors in an electrolyte, are identical. By choosing suitable conductors and electrolyte and applying a potential across the ends of the conductor, the shear lag theory could be exactly simulated. The electrical potential at different points along the fibers correspond to the axial stresses in the fibers, and this potential could be easily measured by an electrical probe. Thus, he was able to evaluate the complete stress distribution around broken fibers and estimate the effective shear rigidity Gh for a variety of configurations.

2.4.8. Three dimensional state of stress at a fiber break: The shear lag analysis does not give complete information on the three dimensional state of stress near a fiber break. Though no directly related results seem to be available, the results of Haener and Ashbaugh [82] are of interest. They consider an hexagonal array composite which is loaded uniformly at the ends, but only on the matrix surfaces leaving the fiber ends stress free. They found that for glass epoxy, the interfacial normal stress was tensile and is of the order of 0.3 times the applied stress.

Table II: Stress concentration factors in an hexagonal array of fibers corresponding to an hexagonal group of fiber breaks, from Garg [67].

M_1	M_2	LCF_a	LCF_b
1	1	1.104	1.104
3	7	2.252	1.410
5	19	1.374	1.630
7	37	1.476	1.874

Notes: M_1 is the number of broken fibers on the major diagonal of hexagonal group of broken fibers. M_2 is the total number of broken fibers in that group. LCF_a is the load concentration factor at the first unbroken fiber on the major diagonal. LCF_b is the maximum load concentration facor due to the group of fiber breaks.

Spencer and Smith [166] consider a mono-fiber composite model - coaxial cylinders of fiber and matrix with a fiber break - and determined the interfacial normal and shear stresses. They also found considerable interfacial tensile stress near the fiber break.

2.4.9. The influence of internal triaxial stresses in the composite: The analyses reviewed so far considered the load redistribution around broken fibers to be independent of the prevailing state of stress before the fiber break. This may be accurate as long as material behaviour is linear and no internal damage other than fiber break occurs. However, considerable matrix yielding and interfacial debonding is known to occur during fiber fracture, and the extent and mode of those damages are likely to be affected by the internal state of stress before the fiber break. Of primary concern in this regard are the interfacial normal stress and the axial stress in the matrix. The former has influence on the extent of debond at the interface while the latter might affect the possible plastic deformation and cracking of the matrix.

Adams and coworkers [2,195] have carried out a considerable amount of study on the three dimensional state of stress in unidirectional composites with square array of fibers, without any damage, i.e., no fiber breaks. They consider both hygrothermal stresses as well as stresses induced due to axial loading. They used a generalized plane strain elastoplastic finite element analysis, in which the matrix deforms with a nonlinear stress strain relationship, but is not permitted any cracking.

Their analysis considers [195], carbon/epoxy composites containing AS4 fibers and four different types of resins - 3502 and three other new toughened epoxy formulations. The principal differences between these resins are their rigidities, the extent of nonlinearity present under room temperature conditions and their sensitivity to moisture and elevated temperature. Following are some of their results of direct relevance to the present topic: (i) There is a considerable amount of thermal residual stress in the matrix, due to the cooldown from cure temperature to room temperature and these residual stresses are affected by the extent of resin plastic flow - residual stresses being lesser for resins with greater plastic strain ca-

pability. The finite element prediction of the maximum tensile principal stress for 3502 resin due to this cooldown alone is about 9 ksi. This is greater than the ultimate strength of the resin, which is only 5.5 ksi, (ii) The interfacial normal stress is compressive and equal to 5.23 ksi (iii) These stresses in the matrix were relieved to various extents by moisture absorption as well as elevated temperature. For example, the interfacial normal stress becomes tensile and equal to 2 ksi at 3.8% moisture content and room temperature, and this interfacial tensile stress increases to 4 ksi at 100°C and 3.8% moisture content (iv) Under a longitudional tension of 320 ksi, at room temperature dry conditions, the maximum tensile principal stress in the matrix reaches 18.6 ksi and interfacial normal stress reaches -6.3 ksi. (v) For other resin formulations with greater plasticity, the stresses are different and generally are lesser.

It is important to consider the implications of these matrix stresses, present in an undamaged composite, upon the damage process following a fiber break. The resin is already severely stressed and under this condition the resin's capability of both transferring shear loads as well as its ability of arresting propagating cracks are likely to be affected. On the other hand, the considerable amount of interfacial compressive stress in a dry, room temperature condition is likely to provide large frictional stresses, if the interface should debond. The high level of frictional stresses are likely to limit the debond length. These frictional stresses may, however, vanish under elevated temperature and moist conditions, probably promoting interfacial debonding at fiber breaks. It may also be noted that the core region of the matrix in between the fibers is under triaxial tension, and under these conditions the resin plastic flow may not be as much as indicated by the uniaxial test results. Hence it is possible that the matrix damage is likely to be even greater than what is indicated by the finite element predictions. Lastly, it may be noted that, for other composite materials with glass or kevlar fibers, the resin is likely to be strained to much higher levels because strain to failure of glass- epoxy for example is of the order of 2% compared to about 1% for carbon epoxy.

2.4.10. Influence of thermal expansion mismatch: An early investigation concerning fiber reinforced ceramics by Aveston [13] illustrates the dominant influence of the thermal expansion mismatch between the matrix and fiber on the strength and failure mode of composites. The composite under study was silicon fiber reinforced cordierite. By suitable heat treatment process, the crystalline structure and hence the thermal expansion coefficient of the cordierite matrix could be varied over a wide range - from a value greater than the thermal expansion coefficient of the SIC fiber to values considerably less than that of the fiber. Aveston's tests indicated that the strength of this composite increased to almost threefold when the matrix thermal expansion coefficient was reduced from the maximum value to the minimum value. Correspondingly the failure morphology changed from brittle planar crack to fibrous failure. Aveston attributed these changes to the alteration of the residual interfial normal stresses and its effect on the fiber matrix debonding.

Later, Lim, Piggot and Bailey [110] illustrated a similar effect of this thermal expansion mismatch in carbon/epoxy composite. They found that a reduction in this mismatch, brought about by certain additives to the epoxy matrix, resulted in considerable improvement in the toughness of the composite.

2.4.11. Stress intensity factors due to interfacial cracks: The cracks from the fiber breaks, until very close to the final failure, are either blunted in the matrix due to plastic deformation or arrested by the interface failure. The effectiveness of this crack arrest process depends on the mechanical properties of the constituent phases [77]. There were numerous investigations [77,37] on a related problem - cracks near bimaterial interfaces - starting with those of Zak and Williams [194]. In most of these investigations, however, elastic material behaviour and plane stress or plane strain conditions were assumed. Hancock [77] summarizes some of these results and describes the influence of the mechanical properties of the constituents on the crack growth behaviour in composites. Important points from his summary, relating to the stress field around the broken fiber that corresponds to a crack in the

stiffer material are: (i) as the ratio of the modulus of the fiber to that of the matrix becomes larger, the strength of the singularity at the crack tip approaches unity, and (ii) the interfacial stresses are an order of magnitude larger than the largest principal stress in the less stiff phase, i.e., the matrix.

2.4.12. The influence of off axis plies on the unidirectional layers: The zero degree plies in a multidirectional laminate are subjected to constraint stresses in the transverse direction, due to the differences in Poissons ratio between zero degree laminae and off axis laminae. Stinchcomb [167] determined the magnitude of the transverse stress in zero degree plies due to this constraint. For example, the transverse stress in a unidirectional ply is 1.4 ksi and -1.7 ksi if it is constrained by a single 90 ply and a 45 ply respectively. These overall transverse stresses in turn produce nonuniform stresses within the matrix. Kriz [102] observes that at 76 K, the zero degree ply strength is lower on the average by about 23% and has greater scatter when unconstrained compared to the strength of the same zero degree ply constrained by 90 and 45 degree plies.

2.4.13. Dynamic crack propagation and crack arrest: So far, all the analyses considered tacitly assumed that the crack propagates across a single fiber width and is arrested in the matrix without dynamically propagating into the neighbouring fibers. Also, it is assumed that the matrix toughness is adequate for the purpose of arresting the propagating cracks from the fibers. However, as we shall see, this is not always the case and the capability of the matrix and interface to arrest a dynamic crack, from a fracturing fiber, cannot be taken for granted.

Daniel [50] was probably the first to study experimentally this aspect. He considered the ability of a propagating crack in a fiber to cut across the matrix and into the adjacent fiber. His model consisted of square glass bars, representing fibers, and similar bars of Homalite, representing matrix, arranged in a linear array. The dynamic crack was initiated at the central fiber at a notch by impact loading. The dynamic crack propagation and stress field were

observed through photoelastic fringes photographed by a high speed, Cranz- Schardin camera. The results indicate that the crack from the notched fiber succeeded in propagating through the matrix into the neighbouring fiber, but in doing so branched into two. Apparently, it arrested at the next interface. However, the photoelastic fringe pattern indicated traces extending into the third and fourth fibers. But post-test visual examination showed no traces of crack corresponding to the photoelastic fringes in the third and fourth fibers.

When the same specimen was subjected to impact for the second time, the cracks propagated into the second and third fibers exactly along a path indicated by the earlier photoelastic traces. This observation points to the possibility that stress waves emanating from a fiber break can cause microscopic damage in the neighbouring fibers, which nevertheless do not fracture. However, the scale, i.e., size, of fibers in Daniel's experiments were quite different from those in actual composites. In contrast, the fiber fractures in Rosen's [156], Zwebens [196], and Armenaka's [9] experiments appear to arrest in the matrix. But the interfiber matrix layer in these cases was quite large.

Dally and Kobayashi [49] studied the dynamic crack propagation in duplex specimens, consisiting of two different segments, bonded together with a very tough adhesive layer. The first segment was a low toughness material - Homalite - in which the dynamic crack was initiated and the second segment was a relatively tougher epoxy, used for arresting the dynamic crack. They found that the ability of the adhesive layer to arrest a propagating crack was determined by two factors: (i) the load under which the dynamic crack was initiated and (ii) the thickness of the adhesive layer. A lower load level or thicker adhesive layer promoted crack arrest in the adhesive layer.

In a series of papers, Theocaris and coworkers [176-180] considered the dynamic crack propagation in composite materials. They used an experimental model of composite material in which the fiber and matrix were simulated by two plasticised epoxy resins of differing moduli. The "fiber" and "matrix layer" in their model were typically 2 cm and 4 cm wide, re-

spectively. A dynamic crack was initiated at a notch in one of the phases by axial impact loading. The crack speed and stress intensity factor during crack propagation were monitored by the method of caustics and photographically recorded using a Cranz - Schardin camera. They observed that the interface between the two phases acted as a barrier for the dynamic crack, in that the fast running crack momentarily stopped at the interface. After a brief interval of time the crack reinitiated, while the singularity gradually disappeared in the crack initiating phase and after this brief period reappeared in the second phase. They attributed this crack arrest mechanism to the disturbance of the dynamic stress wave field by the material discontinuity at the interface. In certain cases the dynamic crack arrested at the interface and apparently travelled along the interface on either side of the arrested crack, to form a 'T', until it met weak points in the second phase and branched into the second phase.

They also found [177] that a preexisting crack, orthogonal to a dynamically propagating crack, does not constitute an efficient barrier. Instead, the preexisting crack merely diverts the propagating crack from its original plane and leads it to reinitiate as two individual cracks at the end of the preexisting crack. From the above branching phenomenon, it appears that the mere debonding of the interface in reinforced composite may not be able to remove the singularity of a propagating crack. There must be some mechanisms such as friction by which the singularity at the debond is alleviated, for the crack to be effectively arrested.

Recently, Theocaris [179] considered the dynamic crack propagation through models of composite materials having a central region of one material bounded on either side by a material of different modulus and toughness. The influence of the mechanical properties of the two materials on the crack velocity and bifurcation were studied. In their matrix - fiber - matrix model in which the crack initiated from the matrix and for the dynamic loading conditions in their test, the crack velocity and tendency to branching depended primarily on the ratio of moduli of "fiber" to that of "matrix". The higher this ratio the greater was the velocity and tendency to branch. In the "fiber-matrix-fiber" model, there was a lesser tendency for the

crack to branch in the matrix. However, when the strain rate was increased from 4/sec to 24/sec there was a greater tendency for the cracks to branch in the matrix phase.

2.5.0. Failure Process in composite and fracture surface morphology

As described in the introduction, the failure process in a unidirectional composite material under longitudinal tension is a sequence of events, starting as randomly occuring isolated fiber fractures, followed by the formation of groups of broken fibers and eventual failure of the entire structure. Because of the microscopic dimensions of the fibers and the opaque nature of the composite, it is very difficult to directly observe these failure processes. Hence experimental studies had to limit themselves to monofiber composite, a single fiber embedded in transparent resin, or fiber bundles embedded in transparent resin. Other studies used the inferences from fracture surface morphology or techniques such as deplying. The rate at which the fiber fractures occur with increasing load has been also estimated by indirect means such as acoustic emission monitoring.

2.5.1. Failure modes in different composite systems: Typically, different composite systems exhibit different fracture surface morphologies. High modulus carbon/epoxy has an almost flat fracture surface. High strength carbon/epoxy factuure surface has relatively long fiber pullout, but macroscopically looks flat. Glass/epoxy and kevlar/epoxy composites fail by the failure mode commonly referred to as "brooming" or "paint brush" mode, which exhibits extensive splitting of the matrix along the entire length of the specimen, and fibers separate out to give the appearance of a paint brush. Even within a given composite system, the failure mode can be altered by the experimental conditions. For example, Suvorova [173] describes the change in failure mode caused by changes in strain rate in carbon/epoxy. A somewhat fibrous failure mode operating at low strain rates changes into more brittle and almost planar fracture at high strain rates.

2.5.2. Failure in monofiber and fiber bundle composites: Mullin [130] studied failure in monofiber composite, i.e., a single carbon fiber embedded in a transparent matrix, and determined the influence of matrix fracture toughness and interfacial shear strength. Increasing interfacial shear strength or reducing matrix fracture toughness changed the failure mode from the highly energy absorbing failure process of fiber debonding to the low energy failure mode of transverse fracture of the resin. This trend correlated well with the fracture behaviour of bulk composites. Low toughness resin and high interfacial strength promoted brittle transverse fracture of composite, while a low interfacial strength lead to increased strength as well as the paint brush type of failure mode.

Mullin [129] noted that in boron-epoxy monofilament composite, three different kinds of matrix and interface failures can occur. The mode of failure and the extent of these damages depended on the strain rate and the load level at which fiber fracture occured. Under quasistatic loading, when fiber stress was low, there was neither fracture propagation into the matrix nor interfacial failure. However when the fibers failed at high load levels, there was either a single disk shaped matrix crack perpendicular to the fiber, or two cone shaped matrix cracks starting at the fiber break, initially at 45 degree to the fiber axis. But these cone shaped cracks gradually grew to be almost perpendicular to the fiber. When the matrix was very ductile, no matrix cracks formed and the fiber merely detatched and slid inside the matrix cavity to a small distance. One can make out from Mullin's photographs that apparently the Poisson's expansion at the fiber end, and consequent friction, seemed to arrest this interfacial debonding and sliding.

At low strain rate (0.008/sec) the disk shaped matrix cracks were arrested within a distance of a few diameters and the surrounding matrix was able to sustain the presence of many such cracks under increasing load. However when the strain rate was increased to 0.8/sec - a hundred fold increase- the cracks from the fiber failures grew in an unstable manner and the matrix could no longer effectively arrest these cracks.

A multifiber linear array of composite with interfiber distance of 0.024" was also tested at these two strain rates. At the lower strain rates, the model was able to sustain a large number of fiber failures. However at the high strain rate, the specimen was not able to sustain the fiber fractures and failed at the third fiber fracture. This indicates the importance of the applied strain rate on the fracture strength.

Clarke and Bader [41] used optical microscopy to monior the failure behaviour of a monofiber composite containing a 100 micrometer diameter silicon carbide fiber embedded in transparent PMMA matrix. They observed both a single radial matrix crack at the site of fiber fracture and multiple shear cracks in the matrix for a considerable distance along the length of the fiber from the point of fracture. Marshall, Cox and Evans [119] examined unidirectional composites with ceramic matrix, using optical microscopy. In this composite system, the matrix exhibited extensive cracking normal to the fiber direction well before the composite ultimate failure.

Lorenzo and Hahn [106] studied the failure modes in glass and graphite composites subjected to static as well as fatigue load. They used optical microscopy to monitor the damage growth in real time. Their models consisted of fiber bundles of either graphite T300 or glass fibers embedded in one of the two types of resins - Epon 815 and Epon 828 epoxy. These two resins in bulk form had ultimate strains of 9% and 14% respectively, and different levels of fracture toughnesses. Their graphite and glass fiber bundles contained approximately 3000 and 200 fibers respectively. These models were monitored using an optical microscope, with magnifications of up to 200, under normal as well as polarized light. Carbon/epoxy single bundle specimen failed at a strain of 1.3%, whereas glass epoxy specimen failed at strains ranging from 4% to 6%. Multibundle composites failed at lower strains - carbon epoxy at 1.2% and glass epoxy at 3.6% strain. Notable among their results is the formation of distributed matrix microcracking normal to the fiber axis. These microcracks were confined to the space between adjacent fibers and never grew to either break the fibers or to bridge them. These cracks were larger and more frequent in glass epoxy, while they were preferentially

located near the fiber matrix interface in graphite epoxy. The significant differences between graphite and glass composite were: In graphite/epoxy very little or no interfacial failure at fiber breaks were seen, whereas glass epoxy had substantial interfacial failure. In glass epoxy, fiber failure occured in a more distributed manner and accumulation of breaks, across many independent sections, occured in a gradual manner as the load was increased. However in graphite epoxy, even though scattered fiber fractures occured, accumulation occured across a single section and even here the accumulation of fiber fractures were much faster, ie. the final failure followed soon after the fiber break accumulation started. There was considerable fiber pullout in glass epoxy, but none in graphite epoxy.

2.5.3. Observation of failure process through SEM: Sato [158] used a miniature three point bending specimen to observe the failure process, in real time under a scanning electron microscope. He noted that, even though random fiber fractures occured at low load levels until about 70% of ultimate load, these isolated fractures did not initiate any matrix damage or fracture of neighbouring fibers. At about 90% of final load, matrix shear cracks seemed to link adjacent, but axially staggered, fiber fractures. Prior to formation of these matrix shear cracks, void bands in the matrix were found with the voids' major dimension of the order of 0.2 microns and inclined at 45 degree to fiber axis, and some of these grew to a size of about 5 microns. Near the ultimate load, a group of fibers broke in stairstep pattern and delaminated and the specimen fracture immediately followed.

Sato [157] also examined a glass - thermoplastic matrix composite, in a similar manner. Even though this was a short fiber composite, the type of matrix deformation near fiber ends is of interest. The matrix deformed and plastically flowed to a much greater extent, compared to epoxy resin, and there was extensive shear microcracking in the matrix.

2.5.4. Fiber damage measurement through deplying: Deplying has been extensively used to examine the fiber fractures in the interior of laminates in carbon/epoxy composites.

Reifsnider and Jamison [91,154] documented the damage to fibers in the interior of multidirectional laminates by this technique. They observed that multiple fiber fractures of up to the order 4 were observed before the final fracture in laminates loaded under fatique. Recently, Jamison [92] measured the extent of fiber fractures in statically loaded $[0]_8$ laminate by deplying at different load levels. Fiber fractures started to appear at load levels of about 60% of the ultimate and appeared to grow exponentially. Near the ultimate failure the average fiber fracture density was approximately 3 per square mm.

2.5.5. Monitoring Fracture in Boron/Aluminium by X-ray imaging: The failure sequences in boron/aluminium composites have been studied by x-ray imaging by several investigators. To begin with, we may note that the diameter of boron fibers are much larger compared to other fibers. The cross sectional area of a single boron fiber is greater than that of a hundred carbon fibers. Herring [86] carried out a detailed investigation of the failure sequences in boron/aluminium. He found that in this material there was very little accumulation of random fiber failures, and in general the first fiber failure, usually occuring at specimen edges, initiated an unstable crack, cutting across the entire width of the specimen. He obtained a remarkable x-ray image of a crack which was arrested after breaking about twenty fibers. This arresting of a dynamic crack rarely occurs in boron-aluminium. The important features of interest in this photograph were: (i) the first fiber which initiated the fracture had only a single crack across its width, whereas the remaining fibers were severly shattered, i.e., had up to 5 or 6 crack branches across the width of each fibers. (ii) the matrix marterial remained intact even after the fracture had sequentially propagated across the fibers. It was only later that the matrix fractured in a ductile manner, (iii) in the initiating fiber, the crack surfaces moved apart after fracture and opened axially by a considerable distance - about a fourth of the fiber diameter. But the separation of fracture surfaces in the remaining fibers were negligible - indicating the possibility that it was not the static overloading which was sustaining the crack propagation, but some kind of stress wave loading. Hence, Herring suggested that the ultimate failure of boron/aluminum is initiated and sustained by stress waves.

Herring investigated these failure processes in boron-aluminium composite in which the bond between fiber and matrix was made intentionally stronger than in the usual fabrication process. The fabrication process was also deliberately varied, so that five different batches of composite specimens were obtained, each having a different fiber strength distribution. Adverse conditions which existed during the fabrication process caused fiber strength to degrade substantially in some of the batches. The minimum fiber strength, average fiber strength and average composite strength corresponding to these batches are shown in table III.

Herring's most important finding was that, if the minimum fiber strength was above 170 ksi, then the composite failure was caused by the first fiber failure. If the minimum fiber strength was below this value, then there was a gradual accumulation of random fiber fractures untill 170 ksi. At 170 ksi stress, however this stable damage accumulation changed into an unstable stress wave induced fracture. He concluded that the threhsold for self-sustaining stress wave induced dynamic crack propagation in these materials was 170 ksi. But the nature of the stress wave responsible for these fractures remained unexplained.

Prewo [144] examined single boron fiber fractures by radiography and found that fibers failed by a single crack when the failure occured at low loads, whereas the fibers failing at higher loads had multiple cracks, and all these cracks appeared to start from a single point on the surface of the fiber. Leddet and Bunsell [104] present optical micrographs which show the fracture propagating from one fiber to the next, apparently dynamically with considerable fragmentation. There was very little axial separation of the crack surfaces and the aluminium matrix did not show indications of plastic deformation.

2.5.6. Fracture surface morphology and SEM studies: Analysis of fracture surface and morphological features is an important aid in understanding the microscopic failure processes involved in the fracture of unidirectional composite materials. There have been numerous publications on the fractography of unidirectional failure surfaces. Grove and Smith [73]

Table III
Boron Fiber and Boron/Aluminum Strength Properties,from Herring [86]

Batch Number	I	II	III	IV	V
Minimum fiber Strength (ksi)	50	60	90	180	230
Ave. Fiber Strength (ksi)	230	260	270	300	350
Ave. Composite Strength (ksi)	170	170	170	180	230

provide a compendium of failure analysis for composite materials, detailing the various techniques available for the fractography of these materials.

In an early investigation, Beaumont and Harris [28] found that the fracture morphology and crack growth stability was dependent on the fiber surface treatment. They tested high modulus carbon epoxy composites (Morganite type I/epon 828) with fiber surfaces under three different conditions: (i) fiber surface untreated (ii) fiber surface untreated and composite exposed to moisture (iii) fiber surface treated by oxidation. In three point bend test they found that the composite with surface treated fibers failed with almost flat surface with rapid crack growth and the other two types failed with extensive fiber pullout and the crack extension was much more gradual. The load at fracture for the composite with untreated fibers was twice that of composites with fiber surface treatment.

Miller and Wingert [125] studied fracture surfaces in three different systems of high modulus carbon/epoxy composites at different temperature and humidity levels - dry condition at −54° C, 21°C and 132°C as well as wet conditions at 21°C and 132 °C . Their system B composite probably illustrates more clearly the interrelationship between the strength, environmental conditions and fracture morphology. The tensile strength for this system at different conditions are reproduced in table IV. Specimens tested at −54° C and 21° C dry conditions exhibited very few individual fiber pullouts and even these few were less than two fiber diameters long. A prominent feature was that the surface appeared as a collection of plateaus, at slightly different levels, each plateau consisiting of a group of fibers, each group consisting of up to thirty fibers. The matrix appeared well bonded to the fibers with no apparent interfacial failure. At 132° C dry condition, the plateaus became less frequent and considerably more fiber pullout is seen. The resin appears to be still adhered to the pulled out fibers. But a significant amount of crumbled resin particles are seen on the lateral sides of the fibers. SEM micrographs corresponding to 21° C/wet conditions indicate increased fiber pullout and somewhat lesser adherence of matrix to the fiber surfaces. But no matrix crumbling, as in 132° C/dry conditions, is seen. At 132° C/wet conditions there was the

greatest amount of fiber pullout with almost no plateaus and fiber surfaces were completely devoid of adhering resin, indicating that the fiber matrix separation occurred preferentially at the interface. There were also no crumbled resin particles. We may infer from this information that three competing failure mechanisms are operative in this composite material and the dominating one of these is determined, probably, by the hygrothermal conditions and consequent internal stress distribution. These three mechanisms are: (i) self similar crack growth across a group of fibers (ii) random fiber break and pullout resulting in resin shear fracture and (iii) random fiber break and pullout resulting in interfacial failure.

It appears that there is an increase in strength when self similar crack growth is suppressed and failure by staggered fiber fractures and pullout is promoted. However, for this composite when there is very extensive pullout as in the case of 132° C/wet condition, strength appears to be lowered.

Purslow [147,148] conducted a detailed fractographic study on graphite epoxy composites. He made use of the radial lines occurring on the individual fiber fracture surfaces to trace the chronological sequence of fiber breaks. In high modulus graphite-epoxy composite, he found that fibers failed in groups. He was able to identify the source of fracture in individual groups and trace the growth of branches from this source into the entire group. From this type of reasoning, he was able to infer that the tiered plateaus on the failure surface are the result of fractures starting from randomly located single fiber faults and spreading across small groups of fibers. He also states that on fracture surfaces it is possible to identify those breaks of individual fibers and small groups of fibers which occured earlier, independent of the final crack propagation. Purslow concluded that, even though there are random fiber breaks before the ultimate failure, the final fracture is not a mere linking up of these preexisting fiber breaks, and these random fiber breaks seem to have very little effect on the final tensile fracture process. Purslow [148] also showed that the fracture appeared to propagate preferentially from fiber to fiber, if fiber contiguity existed, rather than getting into the matrix and reaching other fibers. Thus, the fiber distribution affects fracture mode. In areas where fibers are

densely packed and contiguous, the fracture is likely to occur in a brittle mode and in those areas where there is sufficient width of matrix in between fibers, the fracture probably may be less brittle.

In [0/90] laminates, Purslow [147] found evidence for the fracture of the zero degree fibers to have been caused by stress waves - the waves originated by the failure of a small group of zero degree fibers, and were collimated by the cracks in the 90 degree layers. These stress waves appeared to spread the fracture across the entire width of the specimen . In another publication, Purslow [149] describes the shear failure of epoxy resin inside the composite . When the matrix is subjected to shear, a band of microtensile cracks appear at 45 degrees to the fiber axis and grow under strain until they coalese and form the so-called "cusps". Probably, this observation is applicable to conditions existing under fiber pullout also. The crumbled matrix mentioned regarding Miller and Wingert's results were probably formed in this manner.

Clements [42,43] recently performed a detailed investigation of the interrelation between the strength, fracture surface morphology and environmental conditions. Specimens were of 8 ply unidirectioinal laminates made from T300/5208 graphite epoxy and were tested under different combinations of moisture and temperature conditions. A summary of strengths is listed in table V, from table III of reference 35.

Clements noted that the actual behaviour of the composites tends to be obscured by such extraneous factors as the machining induced edge damages and tab failures. Fibers get damaged at specimen edges while the tensile coupons are being cut, and these damages could be removed by polishing off a thin layer of material from the specimen edges. This kind of polishing was found to improve the strength by upto 25 %. In some of the specimens, due to certain adverse chemical changes in the matrix caused by the contamination of fiber surfaces, the same carbon/expoxy composite became completely brittle and failed with an almost perfectly planar surface, at lower stress levels. The strength data shown above were obtained

after excluding such defective specimens and are likely to reflect true material properties. These results indicate that either moisture saturation or elevated temperature acting alone had a tendency to increase the strength over that at room temperature dry condition. However for this composite, the combined effect of moisture and temperature is probably a reduction in strength.

The fracture morphology ranged from an almost perfectly plane surface to a hill-valley structure with considerable fiber pullout. Clements classifies the mode of failure causing planar fractures as "low energy mode" and that causing hill valley features on the failure surface as "high energy mode". However the failure surfaces rarely belonged exclusively to one mode, but are generally dominated one mode or the other and in certain cases there was an equal proportion of the two modes. Clements found that both moisture absorption and elevated temperature promoted the high energy failure mode and dry room temperature conditions promoted the low energy failure mode. Almost all specimens with chemically degraded resin failed by the low energy mode.

Even among the normal specimens under the same environmental conditions, the surface morphology varied from specimen to specimen. For example, at 25 degree wet condition, 50% of the specimens failed in high energy mode, 38% of the specimens failed in low energy mode and the remaining 12% failed in mixed mode, but with a dominance of high energy mode. All the specimens failing in low energy mode had lower strength.

Ginty [69] studied the fracture surface morphology of graphite/ epoxy composites of both high modulus and high strength types. From Ginty's SEM micrographs it appears that the fracture of different plies in the composite appeared to independently progress in different planes and is often separated axially by distances up to ten to fifteen fiber diameters. This was observed in other fractographic studies also [172]. It appears that the resin rich areas between the plies isolate the fracture propagation within individual plies.

Further, there is clear differences between failure surfaces of high modulus and high strength composites. The high modulus MOD I/epoxy failure surfaces looks relatively flat, devoid of fiber pullout. Radial markings, extending over an order of a hundred fiber diameters, could be seen. Even the few fiber pullouts present do not exceed a length of one fiber diameter. The surface appeared to be a collection of plateaus at slightly different elevations and sometimes these plateaus have parabolic shape.

In contrast, the lower modulus T300/934 composite failure surface had hill-valley structure with fiber pullout of up to five fiber diameters long. There were no large plateaus and radial markings running across such plateaus as in high modulus composite.

Using the information gathered from the above fractographic studies, some important conclusions could be made: (i) straight self-similar crack growth, similar to that occuring in brittle isotropic materials, does occur in unidirectional composites within small groups of fibers and, under favourable conditions, even across entire specimens. Fiber breaks caused by stress concentrations, however, are expected to be staggered, since the fiber flaws are statistically located within the overload length near the initiating fiber breaks. Hence stress concentration is not the likely explanation for the brittle self-similar cracks. (ii) The flat fractures appear to be promoted by certain internal states of stress within the composite. We have seen that matrix stresses and interfacial normal stresses are considerably altered because of elevated temperature and moisture conditions, and directly correlating with them are the changes in failure morphology. Thus the fracture mode appears to be significantly influenced by the internal stresses existing before the damage initiation.

2.5.7. Interation of stress waves and fracture: We have seen in section 5.5 that Herring's experimental findings strongly suggest the involvement of stress waves in the fracture process of boron/aluminum composite. It is interesting to note that Vary [186] suggested somewhat similar involvement of stress waves in the fracture process in various isotropic metallic materials. For these materials, Vary found that a direct correlation between stress wave atten-

Table IV
Composite Strength at Different Hygrothermal Conditions
from Miller and Wingert [125]

Test condition	-54 C/dry	21 C/dry	21 C/wet	132 C/dry	132 C/wet
Strength (MPa)	1442 + 97	1613 + 95	1629 + 106	1658 + 85	1366 + 99

Table V
Composite strength at different hygrothermal conditions, from Clements [43]

Test condition	25° C/dry	25° C/wet	96° C/dry	96° C/wet
Tensile strength (MPa)	1601 ± 69	1765 ± 105	1730 ± 86	1593 ± 276

uation and fracture toughness exists. However, the nature of this interaction remained unexplained. In this connection, it was recently suggested [171] that a component of the stress wave released during the dynamic fracture event travels along the plane of fracture and creates transient tensile stress in the surrounding material. The plausibility of this hypothesis was also demonstrated in a cursory manner. We may also check and ascertain the plausibility of such an explanation from the results of several theoretical [1] and experimental [48] investigations. Even though these investigations do not directly address the above topic, their results contain the necessary information.

The theoretical analysis of the stress wave emitted during the dynamic crack is extremely involved, even in the case of elastic, isotropic materials and only approximate solutions, confined to the initial wavefront of the stress wave emission, seem to be available [1].

2.6.0. Strength distribution of composite materials

Although the tensile strength of unidirectional composites under longitudinal load has been measured by numerous investigators, statistical distribution of composite strength for different fiber systems and environmental conditions do not appear to be readily available. Some of the data available are reproduced in table VI.

2.6.1. Variation of strength distribution with volume: For isotropic brittle materials and ceramics, Weibull statistical strength theory has been widely used to relate the strength of structures to their volume [34]. For specimens uniformally stressed in tension, for such material, the two parameter Weibull theory would relate the volume V_{ten} of the material to the probability of survival S_{ten} at any given stress σ as

$$S_{ten} = \exp\left[-V_{ten}\left\{\frac{\sigma_{ten}}{\sigma_0}\right\}^m\right] \tag{2.11}$$

For specimens under three point bending, because of the nonuniformity in the stress distribution and assuming the specimen fails in tensile mode, the probability of failure in flexure can be shown to be

$$S_{flex} = \exp\left[- V_{flex}\left(\frac{\sigma_{flex}}{\sigma_0}\right)^m \left\{\frac{1}{2(m+1)^2}\right\}\right] \tag{2.12}$$

From these, the ratio of median failure stress in three point bending to that in tension can be shown to be

$$\frac{\sigma_{flex}}{\sigma_{ten}} = \left[2(m+1)^2 \frac{V_{ten}}{V_{flex}}\right] \tag{2.13}$$

Bullock [34] studied whether this theory developed for isotropic materials, which relates strength to the total volume, is valid for unidirectional composite materials. His tests included three different kinds of specimens: impregnated composite tows, tensile coupons containing a volume equivalent to 67 such tows and three point bend specimens. The study included two different kinds of materials - T300/5208 and Modmor II/5208. The Weibull modulus for tensile, flexure and tow specimens was, respectively, 23.3, 24.6 and 29.1 for T300/5208. These should strictly have been equal for the Weibull theory to hold. However the median strength prediction for tensile coupon, calculated from either flexure or tow specimens was in good agreement.

The concept of the weakest link scaling down of bundle strength to that of fiber W(x), employed by Harlow and Phoenix [68] 79 (see section 2.7.5), in deriving the distribution function W(x), in effect is equivalent to the above concept. Experimental results could be used to check such assumptions.

Whitney and Knight [191] performed a more detailed study of the strength versus volume relationship and whether direct application of the Weibull theory is valid for composite materials.

Their test results are included in table V. Contrary to Bullock's [34] conclusions, their data indicate that the direct application of Weibull theory to relate the strength to volume does not hold for composite materials. For example, the Weibull modulus in flexure is almost twice that in tension, but if the direct application of the Weibull theory is to be valid, the Weibull modulus should remain the same in tension as in flexure.

2.6.2. Dependence of composite strength on the resin ultimate strain: Twardy and Bergmann [183] using NOL ring specimens investigated the effect of the matrix material's ultimate strain capability on composite strength. They used a combination of nine different resin formulations, whose strain capability ranged from 1.5% to 2.5%, and three different kinds of fibers whose failure strains were respectively 0.41%, 1.25% and 1.84%. Specimens were loaded at three different strain rates: 0.057%/sec., 1.04%/sec. and 1600%/sec.

At 0.057%/sec strain rate, there was a significant increase in strength due to the increased strain capability of resin - 19 to 73% increase in strength. The high modulus fiber composite showed the largest improvement in strength. At the other two strain rates, the strength remained almost independent of resin strain capability.

McMahon and Taggart [122] conducted a similar study on the influence of the strain capability of the matrix on the composite strength. They tested impregnated strands and tensile coupons with epoxy resin matrices 5208, 5425 and 828 having ultimate strains of 1.5%, 2.5% and 3.5%, respectively. For the 5208 resin composite, the strength appeared to be limited by resin ultimate strain. After a composite strain level of 1.5%, there was no proportional increase in composite strength with increase in fiber strength. They also compared the strengths of impregnated strands with those of tensile coupons and found that with 5208 the ratio of the coupon strength to the strand strength was 0.83, whereas for 5425, it was 0.93, and for 828 it was 0.90.

2.6.3. Effect of prestressing on strength: Though Hedgepeth [83] indicated the presence of dynamic stress concentration factor quite early, it was not until 1975 that this fact was made use of. Mills [126] showed that the composite average strength could be increased and the strength variability be decreased by prestressing the fibers to break them at all points of low strength. They prestressed the fibers by bending, but the actual prestress level is unknown. They found that the average strength for HTS graphite epoxy increased from 168 ksi to 178 ksi and the coefficient of variation reduced from 10.1% to 5.5%. Similar, but lesser increase in properties was seen for other graphite and boron composites. From the design point of view, the benefits are even more significant. Because of reduced variability, the B level for HTS composite had increased from 138 ksi to 161 ksi, due to prestressing.

Table VI: Weibull Strength Parameters of Composite Materials (contd.)

Material	Specimen type	Specimen length	Specimen width	Environmental condition	Weibull scale parameter	Weibull shape parameter m	Source & year publication.
Hercules AS/3501-5a	Tensile 16 ply	6"	0.5"	R.T.	218 ksi	13.3	Whitney & Knight 1980
-do-	3 point flexure 16 ply	6"	0.5"	R.T.	234 ksi	22.9	-do-
Celion 1000 high strength fiber/828	Impregnated tow with 1000 fibers	300 mm	--	R.T.	2.6 GPa	16	Bader & Priest 1982
-do-	-do-	150 mm	--	-do-	2.77 GPa	15	-do-
-do-	-do-	50 mm	--	-do-	2.87 GPa	18	-do-
-do-	-do-	20 mm	--	-do-	2.90 GPa	19	-do-
Celion 1000 single fibers	--	50 mm	--	-do-	2.41 Gpa	6.1	-do-
-do-	--	10 mm	--	-do-	3.25 GPa	5.7	-do-
-do-	--	1 mm	--	-do-	4.53 GPa	5.7	-do-
Carbon/ epoxy	Tensile coupon	8"	1"	R.T.	127 Ksi	20.5	Sun & Yamada 1978
T300/5208	Tensile coupons	N.A.	N.A.	R.T.	227.3 ksi	10.2	Tenn 1981
same data as above,but modelled by 3 parameter weibull distribution:					150.3 ksi	6.76	
				Location parameter is 76.6ksi			

Table VI: Weibull Strength Parameters of Composite Materials.

Material	Specimen type	Specimen length	Specimen width	Environmental condition	Weibull scale parameter	Weibull shape parameter m	Source & year publication.
Narmco 5505 Boron/epoxy	3 point flexure	4"	0.5"	- 65 F	247.5 ksi	27.9	Kaminski 1973
-do-	-do-	-do-	-do-	R.T.	241.1 ksi	26.1	-do-
-do-	-do-	-do-	-do-	350 F	203.8 ksi	19.5	-do-
-do-	-do-	-do-	-do-	420 F	176.4 ksi	8.6	-do-
-do-	Tensile coupon	6"	0.5"	R.T.	192.2 ksi	24.3	-do-
T300/5208	Composite tow with 2000 fibers	--	--	R.T.	360 ksi	29.1	Bullock 1974
-do-	Tensile coupons	N.A.	N.A.	R.T.	207 ksi	23.3	-do-
-do-	3 point flexure	N.A.	N.A.	R.T.	280 ksi	24.6	-do-
T300/5208	Tensile coupon 8ply	6"	0.5"	R.T.	259	17.7	Whitney & Knight 1980
-do-	Tensile coupon 16 ply	-do-	-do-	-do-	241	18.5	-do-
-do-	3point bend 8 ply	-do-	-do-	-do-	344	41.4	-do-
-do-	3 point bend 16 ply	-do-	-do-	-do-	259	36.7	-do-

Chi and Chou [38] experimentally investigated the influence of prestressing the fibers in greater detail. Their composite specimens were impregnated tows made of T300 fiber and epoxy resin. The tows contained approximately one thousand fibers. Fiber Weibull modulus m was 6.2 and mean was approximately 480 ksi. Eight levels of prestress ranging from 74 ksi to 320 ksi were applied to loose fiber bundles and these prestressed bundles were made into composite tow specimens. The resulting composite strength distribution was characterized. The results indicated that the maximum increase in mean strength was obtained for the prestress level of 155 ksi - the mean strength increased by 5%. More important was the increase in strength at the higher survivability levels. For example, the strength corresponding to 90% survival was increased by 10% and for 99.9% survival, was increased by 20%. This is due to the elimination of a portion of the lower tail of the strength distribution.

2.6.4. Dynamic fracture: Kobayashi and Suemasu [109] determined the crack velocities and the heat evolved during the crack propagation for CFRP and GFRP woven composites. They found that in CFRP, the dynamic crack reached high velocities - about 20% of longitudinal wave velocity. But in GFRP, the velocities were quite small-less than 1% of the longitudinal wave velocity. They calculated the amount of heat evolved at the crack tip, from the post fracture temperature profiles on the specimens. The variation of temperature with respect to crack velocity showed differing trends for the two composites. For CFRP, the quantity of heat generated increased exponentially with velocity. However, for glass fiber composite, the heat evolved asymptotically reached a constant value after a certain velocity level.

2.7.0. Composite strength theories

Three different approaches have been used for the prediction of longitudinal strength of unidirectional composite materials. All of them assume that, under quasistatic loading, the failure in these composite materials originates as random single fiber breaks, and the damage

around these single fiber breaks stably grows and at a certain point during loading, becomes unstable and causes the overall failure. The composite failure process is very complicated, and each of the different approaches tends to stress different aspects of the failure. The three approaches are (i) Energy balance criterion, (ii) Numerical and hybrid micro-fracture mechanics and (iii) Statistical strength prediction techniques. In the following sections the first two techniques are briefly reviewed while the third method is considered in greater detail.

2.7.1. Energy balance criterion: This criterion indirectly addresses the strength of the composite, in that it considers fracture toughness of composites. It presupposes that the fracture toughness parameter K_{IC} of a unidirectional composite could be equated with the total dissipation of energy during the failure of composite a [29,46,141]. The various energy dissipation mechanisms operative during failure are: (i) Formation of new fracture surfaces in fiber, matrix and the interface, (ii) Plastic work involved in the deformation of the matrix and (iii) Frictional work done during the extraction of the fibers from the matrix sockets after they have debonded. Of these, the energy consumed due to fiber-matrix interfacial failure and fiber pullout account for the largest share. Hence it is argued [29,141] that the greater the extent and the number of fiber pullout during fracture, the greater would be the toughness and strength. This approach relies on the applicability of fracture mechanics criteria, that at fracture instability the stress intensity factor K_I (or equivalently the strain energy release rate G_I) is equal to the critical stress intensity factor K_{IC} (or G_{IC}, the critical strain energy release rate) for the material, i.e.,

$$K_I(a,b,\sigma) = K_{IC} \text{ or equivalently} \tag{2.14}$$

$$G_I(a,b,\sigma) = G_{IC} \tag{2.15}$$

where K_I and G_I are assumed to be functions of the crack size a, specimen size b and applied stress σ . As discussed by Kanninen [97], in isotropic materials, even in the presence of some extent of inelastic processes at the crack tip, the crack growth can be adequately mod-

elled by linear elastic fracture mechanics, as long as the inelastic process is contained within the K_I dominated region. For this condition to be true, the crack length should be greater than the parameter K_{IC}/σ_y where K_{IC} is the fracture toughness of the material and σ_y is the yield strength . Thus, if the above equation from fracture mechanics is to be applicable to composites, two conditions must be satisfied: (i) a crack tip, with at least some singular character, in an approximate sense, should be present , and (ii) the crack size should be larger than the size of the inelastic region. These two conditions appear to be violated in the energy balance criterion because (i) the damage under consideration is diffuse, because of the matrix yielding and debonding around broken fibers, and a strong singular stress field does not seem to be present, (ii) The inelastic region is of the same order as the assumed crack dimensions. Further, the fiber pullout process itself occurs after a major part of the failure is completed and hence, the contribution of frictional energy consumption towards fracture toughness appears not very convincing.

Dharan [52] reviews some of the earlier applications of LEFM to composite materials and provides expressions for the energy absorptions corresponding to various failure modes such as matrix and fiber fractures, interfacial failure and fiber pullout. His major conclusion is, since the composite materials are inhomogeneous and since cracks rarely propagate in a self-similar manner, LEFM is not applicable for situations such as those encountered in the failure of unidirectional composites.

2.7.2. Finite element and hybrid micro-fracture models: In this approach, the micromechanical failure events occuring during the stable failure process, initiated by single fiber breaks, are modelled by finite element techniques. Even though this technique is in its inception, it appears to have considerable potential, since many complications occuring in the microscale can be taken into account, which otherwise could not be analyzed very effectively.

Kanninen and coworkers [71,97] adopted an hybrid method in which a small inner region encompassing fiber fractures is modelled as heterogeneous material with appropriate fiber,

matrix and interfacial properties. Outside of this region the material is modelled as homogeneous anisotropic material. For the assumed linear elastic brittle constitutive relations, the fracture process was simulated under gradually increasing load. They showed that a number of failure events - fiber breakage, matrix cracking normal to the fibers and fiber bridging, interfacial failure and matrix spiltting parallel to the fibers - can all occur during the stable damage growth. Ouyang and Lu [134] took a similar approach but analyzed the inner region, including the effects of matrix plasticity and finite deformation.

Mahishi and Adams [111,112] consider a mono-fiber composite - a single broken fiber embedded in an annular sheath of matrix material. A finite element analysis, capable of modelling matrix yield and flow, was used to characterize the process of stable crack growth into both the matrix material and interface. They used an energy density criterion to identify fracture initiation and direction of growth. Their analysis indicated that in boron/aluminium [111], the crack from a fiber break predominantly grew into the matrix in a radial direction, and the crack showed lesser tendency to grow along the interface. For graphite/epoxy [112] the crack from the broken fiber propagated into the matrix much faster. The significant influence of the interface on the crack propagation and on the strength of this monofilament model was also illustrated. When the interface was considerably weaker than the matrix (i.e., had only 40% the strength of the matrix), the crack grew preferentially along the interface, thus isolating the matrix from the crack in the fiber. It was only during the final stages of loading that the crack grew into the matrix. This change in mode of failure increased the strength of this model of composite material.

Buchholz et. al., [33] modelled the interfacial debonding and the fiber pull out process in a similar monofiber composite using finite element analysis and crack closure integral method. The energy release rate as a function of debond length is determined. Atkinson et. al., [11] studied a similar fiber pullout process both experimentally and analytically. Their experiments provided information on the regions of debonding and the strain energy release

rates during the debond propagation. Their finite element calculation of the energy release rates compare favourably with their experimental results.

Mahishi [113] used a three dimensional finite element method to simulate the damage growth in a unidirectional lamina containing a square array of fibers under a variety of loading conditions. Defects considered in these models were fiber break, matrix cracks and interfacial debonds. For simulating crack growth, strain energy release rates corresponding to all possible directions of crack growth from the initial defect were determined and these values were compared with the assumed values of critical strain energy release rates in those respective directions. Thus the direction and rate of the incremental damage growth as a function of load increments were determined.

2.7.3. Statistical strength prediction of unidirectional composites: These theories mainly address the statistical strength distribution of the consitituent fibers and their influence on composite strength. The statistical theories assume that the failure process occurs as follows: As the load is gradually increased from zero level there are random isolated fiber fractures called "initiators". Then, the share of load belonging to a broken fiber is locally transfered to the neighbouring fibers through the shear stresses induced in the matrix, but as discussed in section 2.4.3, these stress perturbations in the neighboring fibers are confined within a small axial distance from the plane of the fiber break, and this distance δ is the ineffective length. This causes stress concentration both in the matrix as well as the neighboring fibers and there is an increased tendency for these neighbouring fibers to break. However the actual extent of spread of damage is statistically determined. As the load is gradually increased, a number of fibers surrounding the "initiators" sequentially fail, while the SCF due to this spread of damage keeps increasing. This stable subcritical damage growth, at one stage, turns unstable due to the combined effect of increased load and increased stress concentration and causes catastrophic failure. The statistical strength models aim at determining the lowest load level at which one of these subcritical damages can start propagating unstably. Even though this model is conceptually simple, mathematical analysis of such a stochastic process

is very involved. Hence, gross idealizations were found necessary to keep the problem mathematically tractable. Two distinct statistical models are currently available: (i) the chain of bundle theory and (ii) the theory of growth of multiplets. Several reviews of the statistical strength theories are available [6,67,79,138].

2.7.4. Chain of bundles theory: In this model, the unidirectional composite is imagined to be comprised of narrow segments of fiber bundles joined together, analogous to the way in which individual links are joined together to form a chain. The length of each bundle is equal to twice the ineffective length. All failure events within one bundle are assumed to not influence the strength of other bundles, i.e., there is no spread of damage across the axial ends of the individual bundles. The overall failure of the composite is assumed to occur due to the complete failure of one of these short bundles, analogous to the failure of a chain which is caused by the failure of of one of its links. Hence, the major task in the statistical strength prediction is the determination of the strength distribution of this short bundle. Once the bundle strength is determined, the determination of composite strength is simple. This model originally began with the so called equal load sharing rule in which the presence of the matrix is ignored and the load from the broken fiber is equally distributed among the remaining fibers of the bundle. In the majority of statistical strength theories, the fiber strength is assumed to follow the two parameter distribution.

$$F_l(\sigma) = 1 - \exp\left[-l\left(\frac{\sigma}{\sigma_0}\right)^m\right] \tag{2.16}$$

where $F_l(\sigma)$ is the strength distribution of fibers of length l, σ_0 is the characteristic strength , m, the Weibull modulus and σ the stress.

Daniels [51,67] evaluated the loose bundle strength distribution $G_n(\sigma)$ for a bundle of n fibers and found that for large n, the bundle strength approaches a Guassian distribution and the variability of bundle strength becomes quite small. Daniels expressions for the large bundle strength and standard deviation are [67]:

$$< \sigma_B > = \left[\frac{\delta_m}{\sigma_0^m} \right]^{-\frac{1}{m}} \exp\left(-\frac{1}{m}\right) \tag{2.17}$$

and

$$\Sigma_B = \frac{\delta_m}{\sigma_0^m} \left[\{1 - \exp\left(-\frac{1}{m}\right)\} \exp\left(-\frac{1}{m}\right) \right]^{1/2} N^{1/2} \tag{2.17}$$

respectively.

Gucer and Gurland [67,74], using the analysis of Daniels, constructed the model of chain of bundles with equal load sharing. Thus the bundle strength $G_n(\sigma)$ was equal to Daniel's mean strength $<\sigma_B>$ and the strength of the composite consisting of m such bundles can be shown to be

$$H_{m,n}(\sigma) = 1 - [1 - G_n(\sigma)]^m \tag{2.19}$$

However, the bundle length was undefined in Gucer and Gurland's analysis. Rosen [156] equated the bundle length with twice the ineffective length, after obtaining an expression for the ineffective length. Using the shear lag analysis of Hedgepeth [83], Rosen expressed the ineffective length as

$$\frac{\delta}{d_{fib}} = \frac{1}{2} \left[(V_f^{-1/2} - 1) \frac{E_f}{2G_m} \right]^{1/2} \cosh^{-1} \left[\frac{1 + (1 - \phi)^2}{2(1 - \phi)} \right] \tag{2.20}$$

in which the fiber efficiency factor ϕ is generally assumed to be equal to 0.9. The ineffective length, δ, increases if either the fiber volume fraction, V_f, or the ratio of matrix shear modulus, G_m, to the fiber longitudinal modulus, E_f, decreases.

Shih and Elbert [163] modelled composite systems with interfacial debonding and frictional sliding of the matrix subsequent to the fibers breaks. Based on the interfacial strength and

the magnitude of the sliding friction in the debonded region, they determined the ineffective length and then used Rosen's chain of bundles model to determine the composite strength. Their analysis indicates moderate influence of the interfacial strength on the composite strength. However for a system where chemical bonding is completely absent, the magnitude of the interfacial friction has a significant influence on composite strength.

Later strength models included the effect of stress concentration in the neighbourhood of broken fibers. The stress concentration in the neighboring fibers is maximum at the plane of the fiber break and gradualy reduces to almost unity, at the end of the ineffective length. Zweben and Rosen [197] neglected this variation of stress concentration and conservatively assumed that the stress concentration remains constant over the length δ and is numerically equal to the maximum stress concentration predicted by Hedgepeth [83]. They found that the complete characterization of the failure growth and exact determination of the point of instability were not possible, and instead, calculated the probability of occurence of two and three adjacent fiber failures under increasing load. Comparing these expressions with experimentally observed composite failure stress levels, they concluded that the composite would have high probability of failure when the first double fracture occurred.

Scop and Argon [162], and Argon [6] using a similar approach, determined the probability of occurrence of n adjacent fibers n = 2,3,4, etc. and from these results concluded that the catastrophic fracture is initiated by the occurrence of three adjacent fiber failures.

2.7.5. Strength distribution of composites containing a small number of fibers.: Since earlier attempts to calculate the propabability of failure of composites with a large number of fibers were not very successful, Harlow and Phoenix [80] approached the problem by directly calculating the probability of failure of a composite with a small number of fibers. From the results so obtained they were able to extract information about the behaviour of composites with a large number of fibers. Since this analysis provides considerable insight about the behaviour of statistical strength models, and is virtually exact for the assumptions used, it is

described here in detail. They modelled the failure behaviour in a "linear circular array" in which fibers are placed along the circumference of a circle, so that there are no free edges to the bundle. The existences of free edges, as the one present at the ends of a straight linear array, would complicate the analysis. For such a linear circular array, they assume a local load sharing rule, in which the load shed by a single or a group of adjacent fiber breaks is assumed to be transferred to only the two unbroken fibers bordering this damage i.e., one fiber on either side of the damage. According to this local load sharing rule, the stress concentration factor K_r for r adjacent fiber breaks would be given by

$$K_r = 1 + \frac{r}{2} \tag{2.21}$$

They start with an example of a four fiber composite, which has sixteen different states of failed and surviving fibers [78]. However, considering circular symmetry there are only six unique states and the rest are repetitions. The associated load concentration factors are calcuted from the above load sharing rule. When we consider different combinations of failed and surviving fibers, there are a total of sixteen different states ranging from no fiber failure to the state in which all the four fibers are broken. Each of the fibers are given a number and hence the fibers in this group are identified as fiber 1, 2, 3 and 4. One of the possible failure sequence is that begins with the failure of fiber number 1, followed first by the failure of fiber number 2 and later by that of fiber number 4. Finally the last fiber surviving, the fiber number 3, fails. The probability of occurance of this sequence of failure is given by

$$G_4(\sigma) = F(\sigma)\ [\,F(\tfrac{3}{2}\sigma) - F(\sigma)\,]\ [\,F(2\sigma) - F(\tfrac{3}{2}\sigma)\,]\ [\,F(2\sigma)] \tag{2.22}$$

Some of the other failure sequences include simultaneous failure of two, three as well as all the four fibers. There are in all 51 feasible sequences of failure in this four fiber composite. The probability of failure of the composite is then given by the sum of the probabilities of all these sequences and is given by

$$
\begin{aligned}
G_4(\sigma) \;=\; & 16\ F(4\sigma)\ F(2\sigma)\ F(\tfrac{3}{2}\sigma)\ F(\sigma) - 4\,F(4\sigma)\ F(2\sigma)\ F(\sigma)^2 \\
& - 4\,F(4\sigma)\ F(\tfrac{3}{2}\sigma)^2\ F(\sigma) + \ 4F(4\sigma)\ F(\sigma)^3 - 8F(2\sigma)^2\ F(\tfrac{3}{2}\sigma)\ F(\sigma) \\
& + 2F(2\sigma)^2\ F(\sigma)^2 - 8F(4\sigma)\ F(\tfrac{3}{2}\sigma)\ F(\sigma)^2 + 4F(\tfrac{3}{2}\sigma)^2\ F(\sigma)^2 - F(\sigma)^4
\end{aligned}
\qquad (2.23)
$$

As the number of fibers in the bundle increases, the number of possible failure sequences grows exponentially - a nine fiber bundle would have 87000 sequences, and exact expressions for the failure probability function $G_n(\sigma)$ become too cumbersome. Even with a computer algorithm to follow the above procedure and generate $G_n(\sigma)$ it was difficult to exceed nine fibers. The results so obtained for a 9 fiber composite bundle was provided by Harlow and Phoenix. These results were displayed on Weibull probability paper. The probability distribution of bundle failure $G_n(\sigma)$ was shown down to very low levels, since the lower tail of the $G_n(\sigma)$ is important in determining the overall composite failure. This would be clear, if we consider, for example, the probability of failure of a 100 mm long graphite/epoxy specimen. If we assume $\delta = 0.1$ mm , this specimen, according to the chain of bundles idealization, would contain a chain of 500 mini bundles, each measuring 0.2mm. For this case the probability of failure of the bundle of even 0.001, i.e., one in thousand, would lead to 50% probability of failure of the specimen. Thus, for larger specimens even lower areas of $G_n(\sigma)$ distribution would govern the probability distribution of composite failure.

The probability distribution of a single fiber segment $F(\sigma)$ and that of a chain of nine such segments $F_9(\sigma)$ were both linear . Many important features of the composite strength behaviour can be seen in their figure. The probability distribution function of the bundle strength $G_9(\sigma)$ corresponding to both equal load sharing rule, and local load sharing rule were shown. For the value of fiber Weibull modulus m = 10, the median strength of the composite is 0.78 compared to the median strength of fiber of 0.96. For this bundle, the probability of strength above approximately $\sigma/\sigma_\delta = 0.95$ is zero. In addition, it may be noted that only 50% of the fibers have strength below this load level, according to the fiber strength distribution.

However as we go below $\sigma/\sigma_\delta = 0.63$, the probability of occurrence of bundle failure becomes increasingly small compared to the fiber failure.

The most important result of their study was that they were able to extract information regarding the failure of composites of realistic dimensions from their study of these small composite bundles. An important new distribution function introduced in their analysis was $W_n(\sigma)$, the so called weakest link recalling of the bundle strength back to single fiber size:

$$W_n(\sigma) = 1 - \{1 - G_n(\sigma)\}^{\frac{1}{n}} \tag{2.24}$$

Note that this is a fictitious distribution, defined merely for convenience and has no physical counterpart. From the exact probability distribution for composite bundles starting from $n = 1$ to $n = 9$, corresponding $W_n(\sigma)$ were evaluated and graphically presented by Harlow and Phoenix. These distributions converge to a limiting distribution as n increases. It is clear from their results that convergence, even up to a probability level of 10^{-9} , has been reached within a value of $n = 5$, and for $n = 9$ the convergence is apparently complete. They note that, although this is adequate proof of convergence of the function $W_n(\sigma)$ for engineering purposes, it does not constitute a rigorous proof in the mathematical sense. The real significance of this convergence becomes apparent if we note that the strength distribution $G_n(\sigma)$ of a fiber bundle of size n can be simply evaluated from the relation

$$G_n(\sigma) = 1 - \{1 - W_n(\sigma)\}^n \tag{2.25}$$

Hence if $W_n(\sigma)$ converges and remains unchanged for all values of n above 9, it is no longer necessary to determine directly the strength distribution of large bundles, which anyway is not feasible at the present time. This can be indirectly obtained form the converged limit of $G_n(\sigma)$. The determination of the probability distribution of the strength of composite i.e., the chain of minibundles, then follows from weakest link probability theory as

$$H_{m,n}(\sigma) = 1 - \{1 - W_n(\sigma)\}^{mn} \tag{2.26}$$

The above equation indicates that the strength of the composite containing n parallel fibers of length m $\times$ δ depends on the product m $\times$ n which is the volume of the composite described in terms of the number of individual fiber segments contained in it. There is no preferential dependence on either m or n. This is similar to the Weibull statistics of brittle isotropic materials discussed in section 2.7.1.

The strength of a fiber composite with volume mn = 10^6 can be obtained from the figure mentioned earlier, by merely translating the graph corresponding to $G_n(\sigma)$ upwards by 10^6 and this would result in similar graphs and are provided by Harlow and Phoenix. These graphs are almost linear, indicating that for practical purposes, composite strength can be assumed to follow a Weibull distribution. Thus, the Weibull distribution of the resulting composite could be denoted as

$$H_{mn}(\sigma) \simeq 1 - \{1 - W^{(k)}(\sigma)\}^{mn} \tag{2.27}$$

where the shape and scale parameters m_c and σ_{0c} can be determined. Harlow and Phoenix found that corresponding to the fiber shape parameter variation of 5 to 50, and volume mxn = 10^6, the composite shape parameter varies from 25 to 50, i.e., the variability of composite strength is much lesser compared to that of constituent fibers. The corresponding scale parameter σ_{0c} ranged from 0.51 σ_0 to 1.01 σ_0. For a typical value of fiber Weibull modulus m = 10, this composite has a shape parameter m = 35 and a scale parameter σ_{0c} = 0.63 σ_0.

It may be recalled that Zweben and Rosen [197] and Argon [6] conjectured that the probability of occurrence of two or three adjacent fiber failures is close to the probability of failure of the composite. The above exact strength distribution of Harlow and Phoenix indicate that this approximation is overly conservative, in most cases.

Before closing this section we may note that the local load sharing rule used by Harlow and Phoenix places too severe a stress concentration on the surviving fibers near fiber breaks and is not realistic. This artificially high stress concentration factor could have accelerated the

convergence of $W_n(\sigma)$. The nature of convergence for realistic stres concentration factors is not certain. Further, one of the results of the chain of bundles theory, indicating that the strength of the composite is merely related to the volume and independent of the ratio of length to width, appears to be in contradiction with the results of both Bader and Priest and Whitney and Knight, discussed earlier in section 2.6.1.

2.7.6. Further extensions of chain of bundles model:: The chain of bundles model was extended by Phoenix and coworkers in a series of papers to include various refinements [80,81,139,164]. They considered the following aspects : (i) Providing numerical evidence to support the conjecture that $W_9(\sigma)$ is indeed the converged distribution; that is $W_n(\sigma)$ at $n = 9$ has already converged to the limiting strength distribution for large bundle $W_\infty(\sigma)$, (ii) calculation of the composite strength distributions $H_{mn}(\sigma)$ for more realistic load sharing rules, (iii) calculation of the composite strength distribution $H_{mn}(\sigma)$ corresponding to a double Weibull distribution of fiber strength, (iv) extending the analysis from "linear circular array" to "linear incomplete bundles" where the edge effects may have influence, and (v) extending the analysis to two dimensional hexagonal array. They had to use involved statistical techniques and put in a considerable amount of computational effort for the above extensions. Some of their results are briefly discussed in the following sections.

2.7.7. Convergent sequence of upper bounds: In reference [80] Harlow and Phoenix obtain an upper bound on the probability distribution of the strength of composite materials, based on the occurrence of two or more adjacent fiber failures, using a recursive technique. In this recursive technique, the occurrence of two adjacent fiberbreaks for a larger bundle is obtained from that of the immediately smaller bundle. Composite strength predictions are made for fiber strength distributions corresponding to both a single Weibull function as well as a double Weibull function. Their main conclusions are (i) the probability of occurrence of two adjacent fiber breaks, corresponding to fibers with a double Weibull strength distribution, was almost the same as those corresponding to fibers with a single Weibull distribution, (ii) for typical

values of Weibull modulus m of the order of 5 to 10, this probability of occurrence of two adjacent fiber breaks turns out to be a too conservative upper bound on the actual composite strength distribution.

In a second paper [81], Harlow and Phoenix develop a sequence of convergent upper bounds for the probability distribution of the strength of composite material. The bounds were based on the occurrence of k or more adjacent fiber breaks, where k is sequentially increased as 1, 2, 3, 4 etc., with an understanding that there may exist a critical sequence of size k^*, depending on fiber load L, so that once k^* is reached, there is unstable growth of adjacent fiber breaks and hence the composite fails. They named this criterion as the "k-failure criterion" and showed numerically that the bounding distribution for composite strength takes the form

$$H_{mn}(\sigma) \simeq F_c(\sigma) = 1 - \exp\left[\frac{\sigma}{\sigma_{0c}}^{m_c}\right] \tag{2.28}$$

where the superscript k denotes terms corresponding to k adjacent fiber breaks, and $\pi^{(k)}(\sigma)$ an $O_n^{(k)}(\sigma)$ are certain boundary and error terms, respectively, which tend towards unity and zero, respectively, as n becomes large. Thus for large n

$$H_{mn}^{(k)}(\sigma) = 1 - \{1 - W^{(k)}(\sigma)\}^{mn} \quad \{\pi^{(k)}\sigma + O_n^{(k)}(\sigma)\}^n \tag{2.29}$$

They showed that at any given load σ/σ_δ, these bounds converge rapidly, i.e., the bounds $W^{(k)}(\sigma)$, $W^{(k+1)}(\sigma)$ and $W^{(k+2)}(\sigma)$ are indistinguishable from each other and may be assumed to be numerically equal to the exact distribution $W(\sigma)$. The distributions were obtained for k up to 10 and these indicate that the convergence has been achieved right up to the lower tail values of 10^{-19}. Hence, these distributions may be used to estimate accurately the composite strength distribution for fairly large composite volumes, for the assumptions used.

In typical cases, it appears that the convergence is complete at $k=6$, so that k^* can be taken as 6. Comparing these new results of convergent upper bounds with the earlier estimates of

$W_9(\sigma)$ from small bundles of n=9, Harlow and Phoenix concluded that their earlier conjecture was well supported by the new numerical evidence.

They obtained the strength distribution for composites of size mn = 10^6 and these distributions follow quite closely the Weibull function for both single and double Weibull distribution for the constituent fibers. The shape parameter m for a composite remains in the range 20 to 30, for fiber shape parameters ranging from 5 to 25 and for both kinds of fiber strength distributions. However there is a difference in the mean strength - composites made of fibers having a double Weibull distribution are about 10% weaker in mean strength, compared to those made from fibers having a single Weibull strength distribution.

2.7.8. Modified local load sharing rules: Pitt and Phoenix [139] investigated the effect of modifying the earlier local load sharing rule, such that the load from a group of adjacent fiber breaks is distributed among four of the nearest neighbours, corresponding to two fibers on either side of the break. It is assumed that two thirds of the shifted load is divided equally among the inner adjacent neighbours, while one third is shared by the sub-adjacent neighbours. They used three different techniques to estimate the upper bounds, namely the recursive analysis techniques of Harlow and Phoenix [81] and two other asymptotic techniques, developed by Smith [138] . From these analyses they concluded that the strength distribution of a composite, under this modified load sharing rule, retains the Weibull shape, but there is about 10% a increase in strength compared to the earlier local load sharing rule for a composite volume of mn = 10^6. This increase becomes even larger as the volume increases further. The composite shape parameter m_c turns out to be equal to k x m and is about 25 for the local load sharing rule and 30 for the new tapered load sharing rule. They also asserted that the fracture mode is one in which the adjacent fibers fail sequentially one by one, under increasing load, till the critical crack size k = k * is formed.

2.7.9. Three dimensional case: Smith [164] extended the chain of bundles model to three dimensional situations with fibers arranged in an hexagonal array. They used the asymptotic techniques developed earlier and k-criteria with k up to 7. A local load sharing rule, in which the load shed by a group of broken fibers is redistributed among the immediate outer neighbours, forming a ring around the damage, was used. Unlike the linear or circular array of fibers, the three dimensional array has a great many ways in which multiple fiber breaks can form, and the stress concentratiuon factor, as well as the probability distribution function, need to be evaluated for each of these cases. Using asymptotic techniques and certain approximations they estimated $W_n(\sigma)$ and the composite strength $H_{mn}(\sigma)$ for $mn = 10^6$. Their results indicate that the three dimensional composite is considerably stronger compared to the linear or circular arrays, and strength variability is also considerably reduced. For $m = 10$ and composite volume $mxn = 10^6$ they found that the median strength is 0.53 σ_δ and 0.42 σ_δ and the shape parameter m is 60 and 30, respectively, for 3D and linear fiber arrangements respectively.

2.7.10. Comparison of chain of bundles theory with experiments.: It was only very recently, thaa attempts were made to quantitatively compare the chain of bundles strength estimates with experimental data. Such an evaluation of theoretical results by comparing with experimental data is still hampered because of the nonavailability of actual values of many of the parameters used in the theoretical models. For example, details of fiber strength distribution, ineffective length, fiber debond length, and actual stress concentration factors can only be roughly estimated and actual experimentally measured values are not generally available. Under these conditions investigators tend to treat these parameters as disposable parameters, which are varied to fit the results of theoretical models with the determined composite strength distribution.

The only comparative study available is that due to Watson and Smith [189], who compared the theoretical results with the experimental data of Bader and Priest [14]. Before going to

this comparison, we may note that Bader and Priest found that their composite - impregnated tows containing 1000 fibers - did not meet the strength/length relationship implicit in the Weibull model. The Weibull shape parameter had a tendency to decrease as the composite length was increased. This means the actual variability in composite strength increases as the length is increased, which is contrary to the predictions of the chain of bundles model. The Weibull shape parameter ranged between 15 and 19 for different composite lengths.

Smith [165] and Watson and Smith [189] used the maximum likelihood function to evaluate the conformity of experimental data of fiber strengths and composite strengths with a two parameter Weibull model. Their analysis indicated that there is no strict conformity with the Weibull model, the differences being only modest for single fibers but quite considerable for the impregnated tow composites. These differences indicate a need for reexamining the fundamental assumptions involved in the chain of bundles model [165].

Watson and Smith go on to estimate the strength distribution of a composite bundle i.e., a bundle, of length equal to twice the ineffective length, assuming that the Weibull model is valid for these composites. Further they guess the value of ineffective length δ as 2.5 times the fiber diameter (their assumed bundle length is 5 times the fiber diameter) and the k^* value according to k-failure criteria as equal to 3. $k^* = 3$ implies that unstable failure growth begins on the occurrence of three adjacent fiber breaks. With these parameters, they find good agreement between theoretical predictions and experimental results for the fiber bundle. However, it should be noted that there are a number of weaknesses in this comparison: (i) the estimate of composite bundle strength distribution itself is questionable, since the composite was found not to conform to a Weibull model, (ii) the k-criteria used appears too conservative - earlier Harlow and Phoenix [80] estimated $k^* = 6$ for a linear array, and for a three dimensional array k^* must be at least equal to this if not greater, (iii) the stress concentration factor used for three adjacent fiber fractures was equal to 1.5, compared to Hedgepeth and Vandyke's value of 1.3 even for an elastic matrix, (iv) the value of ineffective length used appears too low.

In conclusion we may note that the predictive cabability of the chain of bundles model at this point looks uncertain and some of the proponents of this model themselves [165] have raised questions about the accuracy of the chain of bundles model. This situation is partly due to the nonavailability of reliable experimental data regarding the input parameters for the strength model.

2.7.11. Theory of growth of multiplets: Batdorf [16] took a major deviation from the chain of bundles model and formulated a theory based on the occurrence of multiple fiber fractures called multiplets. He did not divide the volume of the composite into minibundles, but instead considered the probability of the growth of randomly occurring single fiber breaks, and these initiators growing to critical dimensions. Conceptually, this theory is similar to the chain of bundles theory. Analytically, however, Batdorf's theory is far simpler and probably more practical, in that, it can model certain micromechanical processes which cannot be easily handled by the chain of bundles theory. An example of these is the variation of stress transfer length with an increase in the number of adjacent fiber breaks.

To start with, Batdorf approximates the single Weibull distribution

$$F_1(\sigma) = 1 - \exp\left[-l\{\frac{\sigma}{\sigma_0}\}^m\right] \tag{2.30}$$

after expanding in Fourier series, and retaining the first term only, for small values of σ, as

$$F_1(\sigma) = l\left[\frac{\sigma}{\sigma_0}\right]^m \tag{2.31}$$

If there are totally N fibers of length L each, then the number of singlets or single fiber breaks would be

$$Q_1 = N F(\sigma) = N L\left[\frac{\sigma}{\sigma_0}\right]^m \tag{2.32}$$

Denoting $1/\sigma_0^m$ as k we can pass on to the symbols used by Batdorf. If C is the stress concentration in the neighbouring fibers and assuming that the stress varies linearly from $c_1\sigma$ to σ over the ineffective length δ_1 in the neighbouring fibers, it is possible to determine the probability of failure of the neighbouring fibers. This calculation is simplified if we determine an "effective overload length", λ_1, over which the stress in the neighbouring fibers can be assumed to remain constant and equal to $c_1\sigma$. The probability of failure of a neighbouring fiber under this overload would be

$$P_i \simeq k\lambda_i(c_i\sigma)^m \tag{2.33}$$

where

$$\lambda_1 = \frac{\delta_1 c_1^{m+1} - 1}{c_1^m(c_1 - 1)(m+1)} \tag{2.34}$$

If the fiber has n neighbours in which overstress occurs, then the probability of a singlet becoming a doublet would be

$$P_{1\to 2} = n_1 k\lambda_1(c_1\sigma)^m \tag{2.35}$$

Now considering the whole volume of composite, the number of doublets formed would be

$$Q_2 = Q_1 n_1 k\lambda_1(c_1\sigma)^m \tag{2.36}$$

which can be generalised to any multiplet of order 'i' as

$$Q_{i+1} = Q_i n_i k\lambda_i(c_i\sigma)^m \quad \text{or} \tag{2.37}$$

$$Q_i = N L k^i \sigma^{mi} \prod_{j=1}^{i-1} c_j^m n_j \lambda_j \tag{2.38}$$

where n_i, c_i, λ_i are, respectively, the number of nearest neighbours, the stress concentration factor in the n adjacent fiber and the effective overstress length for a multiplet of order i. A plot of log Q_i versus log σ is a straight line with positive slope indicating that the number of multiplet increases with σ. Batdorf provides a graphical presentation of the failure process according to this theory. According to the assumptions, multiplets can only be formed sequentially in an increasing order as singlet, doublet, triplet etc, and there is no possibility that Q_{i+1} is greater than Q_i. Hence only those portion of lines which obey the above inequality are plotted. These lines form an envelope which is the failure locus of the composite. This can be explained as follows: For any of the multiplet Q_i as σ increases, the number of multiplets increases linearly in the above plot until the corresponding straight line intersects the envelope. Up to this point Q_{i+1} is greater than Q_i according to equation 7.25. Similarly, at the same point $Q_{i+2}$is greater than Q_{i+1} and so on. This, physically, means that the multiplet has become unstable and the final failure immediately follows. Thus any multiplet lying on this envelope forms an unstable configuration and would immediately lead to composite failure.

The load at which the first of such unstable multiplets form is given by the intersection of the envelope with the $Q = 1$ line. Noting that, as the volume of composite increases, Q_i would correspondingly increase and the envelop moves upwards. The result would be a lowering of the stresses at which instability can be caused. In addition, the envelope can be shown to be an approximation of the failure probability diagram similar to the plot of $W(\sigma)$ versus σ obtained by of Harlow and Phoenix [80]. Batdorf showed that in spite of the several approximations made, the estimates of probability of failure of composite from this multiplets theory is in remarkable agreement with the exact results of Harlow and Phoenix [69].

Batdorf and Ghaffarian [18] compared the results of this theory with the experimental data of composite strength obtained by Bullock [34]. Weibull parameters for the fibers were not available from Bullock's data and hence Batdorf and Ghaffarian used several different trial

values to check the theory against experiments. For all plausible values of the fiber's Weibull strength parameters, there was considerable difference between theory and experiment. For example if m=3 was used, λ turned out to be 1.25 mm i.e., more than 125 times fiber]iameter, probably an order of magnitude different from the experimentally observed values [116].

In a further investigation [20], Batdorf and Ghaffarian included the effect of irregular fiber spacing and determined effective stress concentration factors. The effective stress concentration factors which they chose was 1.17 times the stress concentration factors given by Hedgepeth and Vandyke. They compared the theoretical predictons with a new set of experimental data, in which only the mean and the coefficient of variation of the fiber strength and the composite strength were available. From these data they made an estimate of the Weibull parameters for both the fiber strength distribution and composite strength distribution. Using these parameters, and assuming that the fibers were arranged in a square array, they calculated value of λ. This turned out to be 0.033". This value, they observed, appeared to be low. Repeating their calculations again with Hedgepeth's prediction of stress concentration factors, they obtained λ to be 0.1mm. This compared favourably with Mander and Bader's [116] experimental observation of λ. Finally Batdorf and Ghaffarian [20] noted that even though the theory predicts that the modulus m for composite strength distribution should tend to infinity (i.e., the variability should tend to zero), the experimental data seem to indicate that the modulus levels off to a finite value.

In conclusion, we may note that the value of ineffective length has been assumed to remain the same, irrespective of the order of the multiplet. Even though the agreement between theory and experiment appears possible, many parameters crucial in getting a quantitative prediction are not experimentally measured values but are only assumed values. Further even these agreements were seen only for one experimental data set, and experimental data in this area are scarce. Thus the agreement between theory and experiment appears only tentative at this point of time.

2.7.12. Monte-Carlo simulation: An alternative approach to the direct statistical strength prediction is the Monte carlo simulation of the failure process. This technique has been used by several authors [26,62,64,103,117], and of these, Manders et. al., [117] made a more detailed study. They assumed a two parameter Weibull strength distribution for the fibers and used the chain of bundles model and considered a bundle whose cross section was square with 10 fibers in each direction. The bundle length was equal to 2δ where δ , the ineffective length, was assumed to be equal to 100 micrometers for carbon epoxy. Strength distribution was determined for both the local load sharing rule as well as the equal load sharing rule. Each of these computer simulations involved assigning random values of strength for each fiber segment, within the Weibull probability distribution and the load on the bundle was gradually increased, constantly checking if any fiber had broken . If fibers did break, the load from the broken fiber was redistributed according to the load sharing rule and the load increase resumed. The load at which the fiber breaks become unstable due to the load redistribution is the strength of the bundle. This simulation was repeated 100 times, each time reassigning the random strength values for the individual fibers. Thus, failure probability from 0.01 to 0.99 was obtained for the mini bundle.

Manders investigated fibers with Weibull moduli of 3,5,7,11,15 and 30. The results indicated that the critical size of the fiber breaks, which trigger unstable fracture, ranges between 3 to 5. They also determined the percentage of broken fibers just before the unstable fracture and the efficiency with the fiber strength is used in the mini bundle, i.e., the ratio of the mean strength of the bundle to the mean strength of the fibers, termed as Coleman factor ε:

$$\varepsilon = [\Gamma(1 + m^{-1})\ m^{m-1} \exp(m - 1)]^{-1} \tag{2.39}$$

Some of the results of the Monte-Carlo simulation are shown in table VII.

The results indicated that the strength of minibundles was approximately Weibull. Manders et.al., [117] finally illustrated the effect of fiber Weibull modulus on composite strength. For

two otherwise identical fibers with shape parameters of 7 and 15, respectively, individual minibundles will have a mean strength of 0.63 and 0.75 (ratio = 1.19) and for a 1 meter long composite, strengths would be 0.17 and 0.41 (ratio = 2.4).

2.7.13. Prediction of optimum level of prestressing: Manders and Chou [118] theoretically evaluated the enhancement of strength in composites due to prestressing the fibers, before consolidation into the composite. Such prestressing would break the fibers at their weaker points and this prebreaking in effect reduces the overload on their neighbours, since the dynamic stress concentration would be replaced by a static stress concentration. They consider the "linear circular bundle" and evaluate the composite strength by assuming the occurrence of a doublet leads to composite failure, which is conservative. The objective was to determine the optimum level of prestressing depending on the ratio of static to dynamic SCF and fiber strength variability. They concluded that the optimum level of prestressing is a function of composite volume and fiber Weibull modulus. For a smaller volume of composite, the optimum level of prestressing is higher and a greater benefit is possible through prestressing. Fibers with higher Weibull modulus are more susceptible to dynamic stress concentration and are likely to have greater benefit from prestressing. However, they find only a marginal benefit in terms of increased composite strength, if the static stress concentration factor and dynamic stress concentration factor differ only by a small amount. For example if $k_{stat} = 1.33$ and $k_{dyn} = 1.5$, for fiber shape parameter $m = 5$, the benefit in terms of increased strength due to prestressing is only 2% and for $m = 15$ the benefit of prestressing is 4%. However if the dynamic stress concentration factor is assumed to be equal to 2.0 instead of 1.5 the corresponding strength increases would be 14% and 20% respectively. These may be compared with the experimentally observed values of strength increase due to prestressing by Chi and Chou (section 2.6.3).

Table VII: Results of Monte Carlo simulation from Manders [117]

Fiber Weibull modulus m	3	5	7	11	15	30
Percentage of fibers broken at ult. load (equal load sharing	28	18	13	9	6	3
Percentage of fibers broken at ult. load (local load sharing)	22	13	7	2.5	1	0.05
Coleman factor:						
Equal load sharing	0.556	0.646	0.702	0.769	0.809	0.880
Local load sharing	0.550	0.626	0.671	0.733	0.774	0.865
Weibull shape parameter for composite in local load sharing	--	22.4	22.8	22.4	22.2	27.7

2.8.0. Discussion

It is clear from the review of literature, presented in the previous sections, that the failure process in composites is complex and many different parameters influence this process. We may consider an individual failure mode as a continuous chain of dynamic events occurring within a very brief period of time at a given load level. For example, the failure mode for carbon/epoxy at low load levels may be single fiber breaks, which stably arrest at the interface, i.e., the only failure involved in this mode is that of the fiber. For glass/epoxy, the failure of a fiber is often followed by the debonding of the fiber matrix interface. Other failure modes may include failure of a fiber, failure followed by matrix shear failure or failure of a single fiber followed by a sequence of failures of neighbouring fibers as observed by Purslow (section 2.5.6). Thus in the failure of composites, many different failure modes can be operative. Of these, that failure mode which causes unstable damage growth, and the conditions under which this mode is promoted, is of primary concern.

The extensive literature which exists on this subject has provided valuable insight into the failure process. However, there are many gaps in our understanding of the evolution of failure. For example, the failure behaviour of different matrix materials at the microscopic level, have not been well characterized. The actual value of the stress concentration in the material around fiber breaks, in the presence of matrix yielding and failure are at present unknown. The extent and sequences of failure modes participating in the evolution of failure in composite systems having different combinations of fibers, matrices and interfaces have not been clearly established. While most theoretical models assume that the strength is exclusively determined by fiber strength statistics and the magnitude of stress concentration around the fiber breaks, some of the experimental results indicate that, at least in some composite systems, the final failure is caused by the onset of dynamic fracture. Hence, some of the important issues in the modelling of unidirectional composite failure are not settled. Information on these aspects is likely to be crucial in extending our understanding of the general com-

posite failure process not only under static load but also under more complex loading conditions such as fatigue and creep.

3.0: In-situ SEM Observations of Failure Process

3.1. Introduction

From the literature reviewed in chapter 2, it is clear that the strength of unidirectional composite materials is determined to a large extent by the micro-fracture events taking place on the scale of individual fiber diameter. The ability of the matrix material and the interphase to contain the damage due to individual fiber fractures and redistribute the load relieved by the broken fibers, would be important in determining the strength of composite materials. For the identification and measurement of these micro-level deformation and failure processes, a suitable experimental technique is essential. The present chapter describes the development such a technique.

In-situ scanning electron microscopy is the tool employed for this process. This technique offers the ability to continuously monitor the evolution of damage in composite materials with high resolution. Using SEM, the damage to the fibers whose diameters are in the range of 0.005 mm to 0.01 mm, and the microscopic damage to surrounding matrix could be studied in

detail. The deformation processes in five different composite systems were monitored. In addition, with a view towards measuring the strain distribution around broken fibers, a process by which speckle patterns, suitable for strain analysis at these microscopic scale has been developed.

3.2. Materials

The five composite systems studied by in-situ SEM are listed in table 8.
They represent a wide range of combinations of fiber and matrix materials. The matrix materials included a relatively brittle, standard epoxy (BASF's 5208), a toughened epoxy (Hexel's F584), and a thermoplastic (polyethersulphone). Of the five composite systems, AS6/F584, P75/ERLX1902 and G40-600/5245 were fabricated by autoclave molding, according to the vendor's recommended procedure, at the Virginia Tech autoclave facility. The other two laminates were supplied by outside vendors. All the laminates were 8 plies thick Samples for the SEM studies as well as the acoustic emission studies described in the next chapter were cut from the same series of laminates. The test coupons were machined from the laminates by a diamond parting wheel. SEM samples were 2.5″ long and 0.25″ wide.

3.3. Experimental Technique

The arrangement used for the scanning electron microscopy is shown in figure 1.
Here the specimen is subjected to 3 point bending inside the chamber of the scanning electron microscope. The electron beam scans the tensile surface of the specimen and produces an image. A JEOL JSM 35 scanning electron microscope was used for this purpose. A three point bend as well as a tensile fixture were fabricated for these in-situ studies. However, preliminary studies indicated that the three point bend fixture is better suited for the present

Table VIII
Description of the five composite systems used in the present study

Composite System	Manufacturer	Resin Strength (psi)	Resin Modulus (ksi)	Elongation percent	G_{IC} in-ib/sq. in	type
T300/5208	BASF Structural Materials Inc.	7300	560	1.4	0.41	modified epoxy
AS6/F584	Hexel	10600	600	2.9	0.82	modified epoxy
G40-600/5245	BASF Structural Materials Inc.	12000	480	2.9	0.9	modified bismaleimide
P75/1902	AMOCO	6800	650	1.8	N.A.	modified epoxy
G3500/PES	Richards Medical Co.	N.A.	N.A.	N.A.	N.A.	thermo-plastic

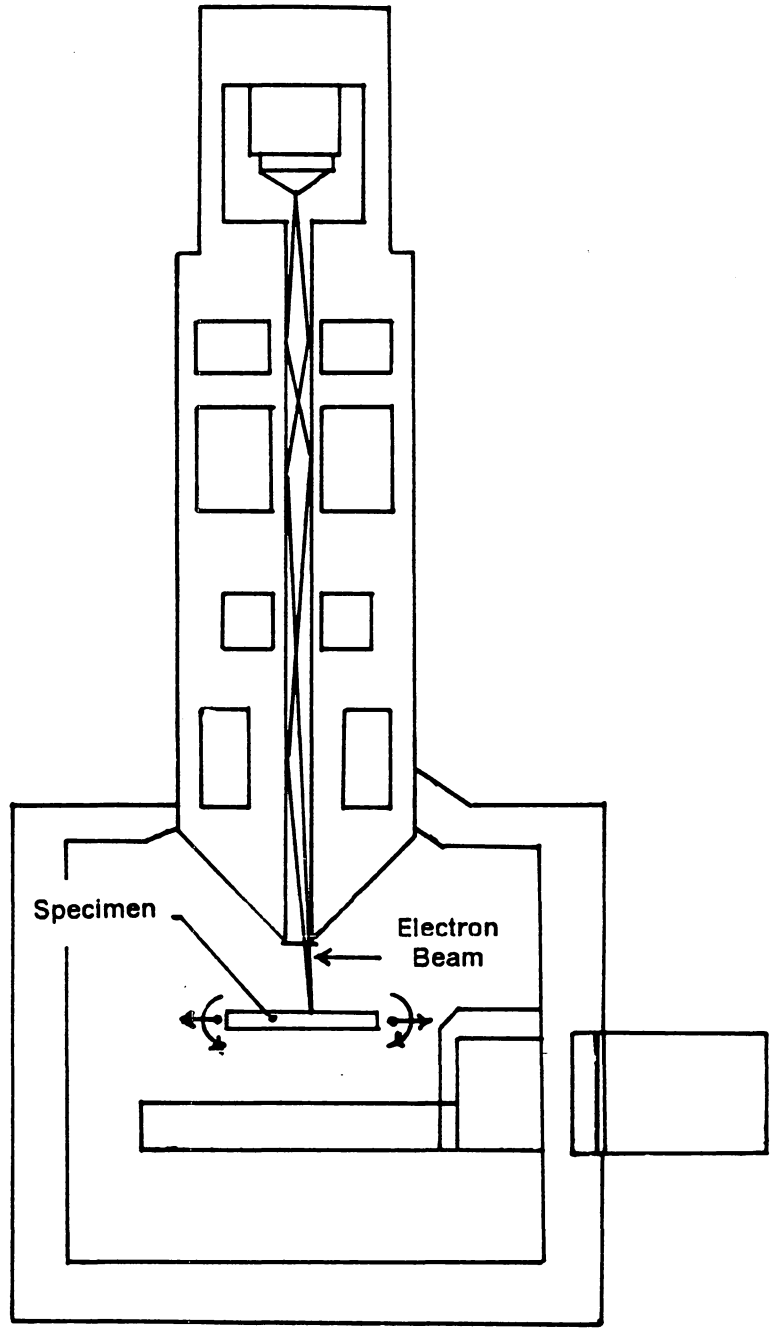

Fig. 1 Schematic of SEM test arrangement

application, since it produced a relatively stable damage development, and the region where the most critical damage developed was confined to a known area of small size.

3.4. Specimen preparation

The top surface of each SEM specimen was hand polished successively by aluminum oxide polishing powder of sizes 5, 3, 1, 0.3 and 0.05 micrometers. The final polishing with 0.05 micrometer aluminum oxide powder produced surfaces on which no scratch marks could be seen, even at high magnifications. These specimens were cleaned in an ultrasonic tank and coated with a thin layer of gold in a sputter coating apparatus. The specimens were mounted on the three point bend fixture and placed into the chamber of the scanning electron microscope. The central displacement of these specimens were gradually increased in steps and the failure modes at each displacement level were examined. The results reported in this chapter were obtained by in-situ SEM of over fifty different specimens, and the micrographs included here are a select number from a total exceeding 1500 frames.

3.5. Results

Static tensile tests were performed on all five composite systems as described in the next chapter. The strength and modulus determined for the five systems are given in table 9. AS6/F584 system

determined for the five systems are given in table 8. AS6/F584 system had the highest tensile strength and P75/ERLX 1902 had the lowest value.

Before presenting the SEM results, it should be mentioned that, in these SEM studies, one is concentrating on a very small sub-region of a large field over which damage is developing. There are local variations in the deformation and failure behaviour from point to point, even

Table IX: Measured properties of composite materials

Material	Strength (ksi)	Modulus (msi)
T300/5208	210.02	20.29
AS6/F584	371.47	22.56
G40-600/5245	329.58	24.66
P75/1902	111.78	44.90
G3500/PES	199.01	19.10

within a field having overall uniform strain. The results presented here are those which appeared to highlight the characteristics seen in individual composite systems. Care was taken to make sure that the individual trends illustrated indeed charaterize the average material behaviour. However, it should be emphasized that variations do exist in the failure behaviour for each system, even within the same specimen at any given load level.

Typical SEM micrographs corresponding to T300/5208 and AS6/F584 systems are shown in figure 2.

The central displacements of the 3 point bend specimen corresponding to these damage states were about 85 % of the respective displacements at failure. It may be noted in these figures that the fiber spacing is nonuniform and in some areas, the fibers are packed so closely as to touch each other and are contiguous for considerable distance along their length. In both the systems, distributed fiber fractures could be seen. In addition, in the micrographs corresponding to T300/5208 system, among those groups of fibers which were contiguous, several self-similar cracks appear to span the entire width of the groups. This mode of failure was frequently seen in T300/5208 system even at a relatively low strain level of 60 % of the ultimate. In all other composite systems with the exception of P75/ERLX1902 system, even though fiber contiguity existed, such grouped self-similar cracks were relatively rarely seen.

We begin the description of the individual failure modes, with the results corresponding to T300/5208 composite system. Higher magnification of one such self-similar crack is shown in figure 3. In this figure, a gradually widening pattern can be seen near the horizontal edges of broken fibers. Detailed examination of this region indicated that, due to the fracture process in these fibers, the gold coating near the crack edges seem to have disintegrated exposing the underlying fiber. The width of this disintegration, however, is non-uniform and the increase of width from one edge to the other edge appears to suggest the direction of crack propagation, in this figure from left to right. Such patterns were seen among fibers which failed at relatively high strain levels. The appearance of these river patterns on the coating leads one to speculate if the width of the coating disintegration may be indicative of the ve-

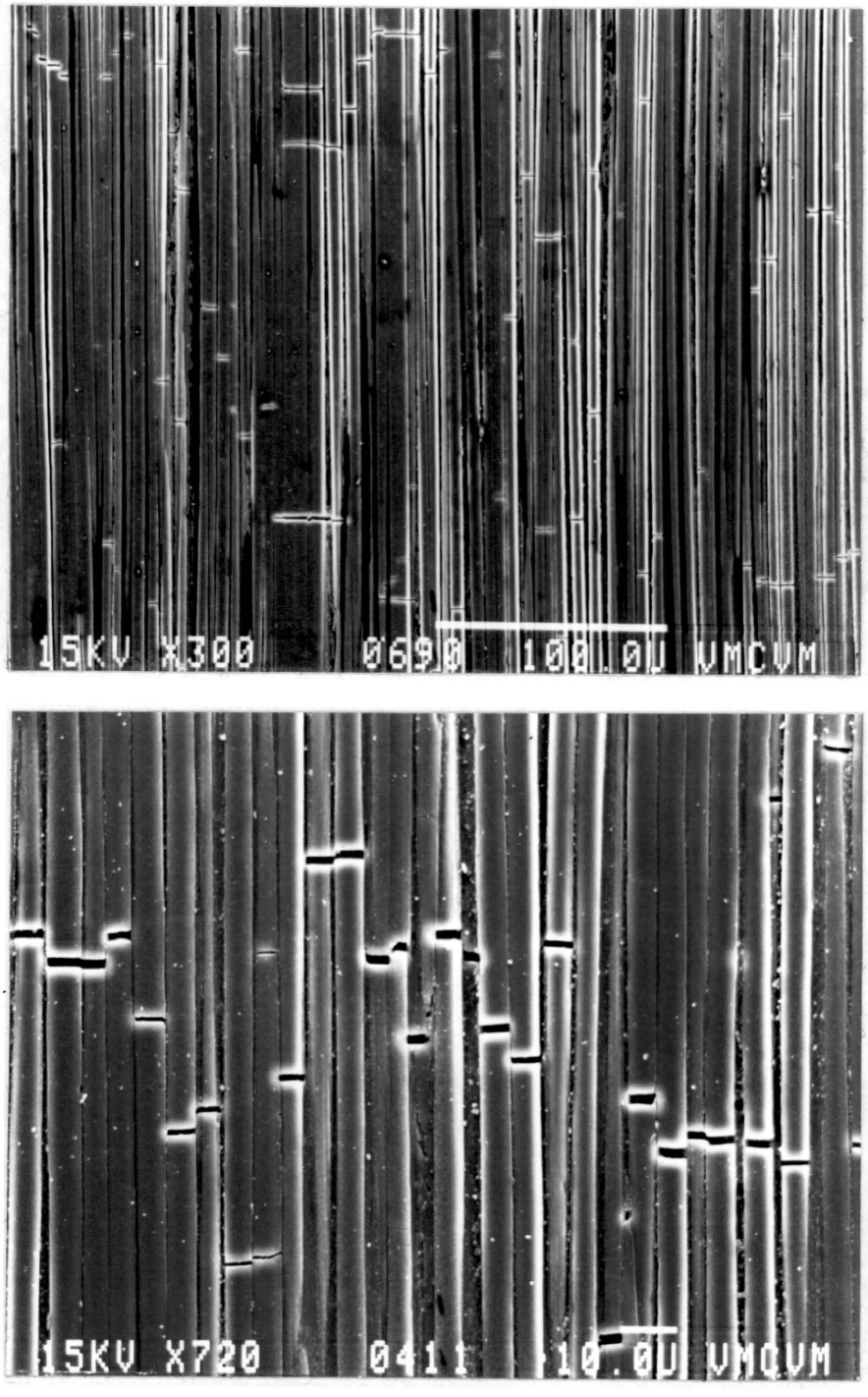

Fig. 2: Typical fiber failure distribution observed at about 85% of ultimate strain in polished three point bend specimens; (a) T300/5208 system (b) AS6/F584 system.

locity of crack propagation in individual fibers, and if the patterns in figure 3 is indicative of a momentary decelaration of the crack at the interphase between the two fibers, before accelerating in the second fiber. A similar pattern among a group of four fibers, not all of which are contiguous are shown figure 4. In rare cases crack branching within individual fibers is seen, as in figure 5. In this case, after branching, the crack has arrested at the interphase, without propagating into the next fiber, which is almost contiguous with the fractured fiber. In figure 6, the crack seems to have branched within the first fiber before proceeding on to cut the next contiguous fiber into five segments. Such events were seen only close to the ultimate failure.

Figure 7 shows the effect of fiber fracture on the matrix failure mode in a relatively resin-rich area.

Even though some interfacial separation is seen, the fiber fracture has continued into the surrounding matrix material to a considerable distance. This may be compared with figure 3 where the crack from the fiber fracture has arrested at the interphase. Self-similar extensions of fiber fracture into the matrix was seen in T300/5208 system towards the ultimate fracture, but was absent in other composite systems. Another failure mode observed only in T300/5208 system the matrix shear failure, shown figure 8.

In this case the interphase appears to be intact. The length of such shear failures varied from 0.5 fiber diameters to greater than 10 fiber diameters extending on either side of the broken ends of fibers.

The distribution of fiber fractures, seen at three different strain levels -- 77 %, 88 % and nearly 100 % of the ultimate are shown in figure 9.

This figure was constructed from a total of 27 micrographs taken at different displacement levels. The fractures seen at 77 % of ultimate strain are marked as dots (.), those which appeared between 77 % and 88 % of ultimate strain are marked as asteriks (*) and the remaining fiber breaks which appeared between 88 % of ultimate strain and near 100 % of ultimate strain are marked as plus signs (+). Self-similar among members of contiguous fiber

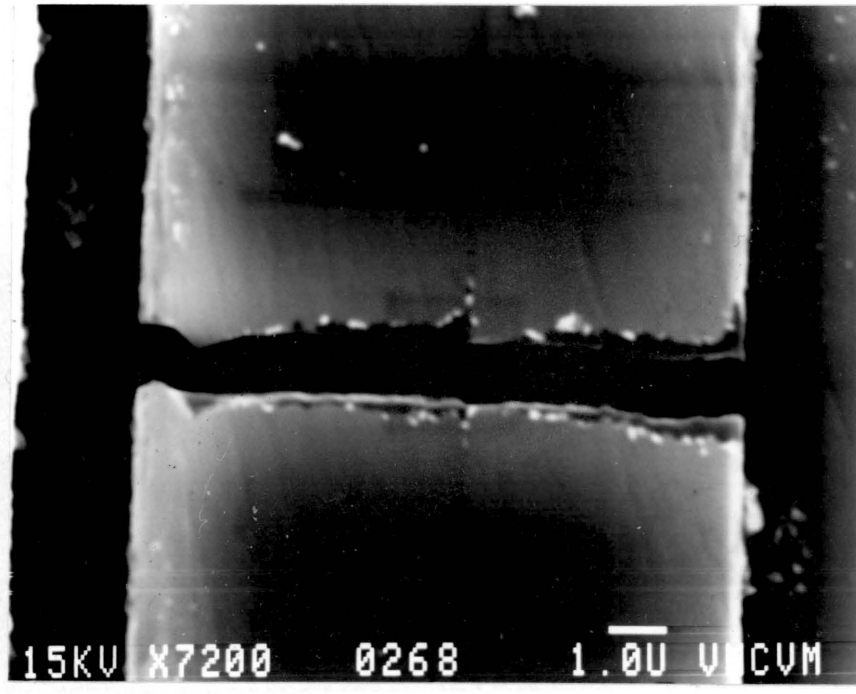

Fig. 3: Failure of two contiguous fibers seen in T300/5208 composite.

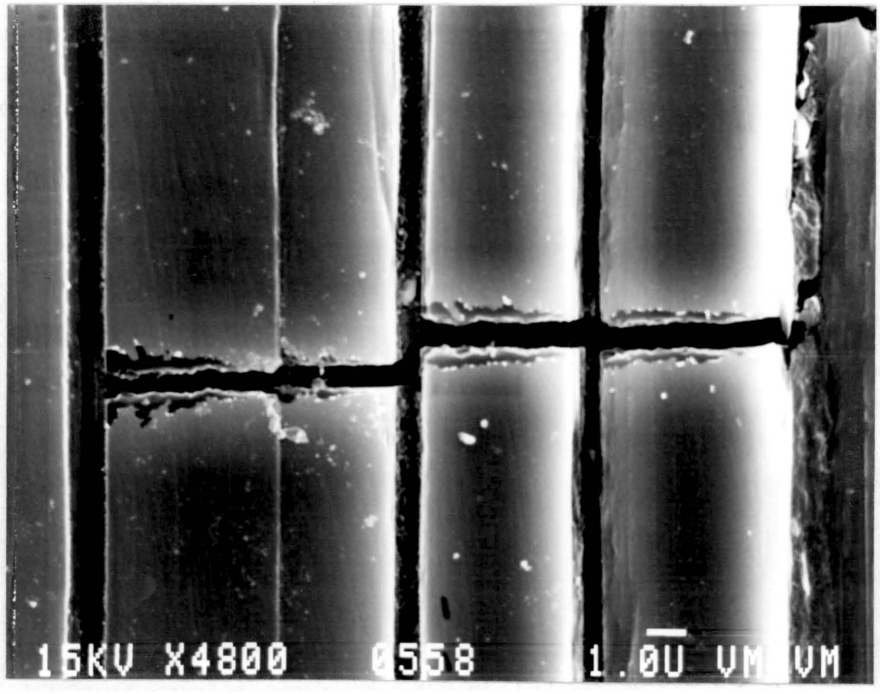

Fig. 4: Failure of a group of fibers in T300/5208 composite system.

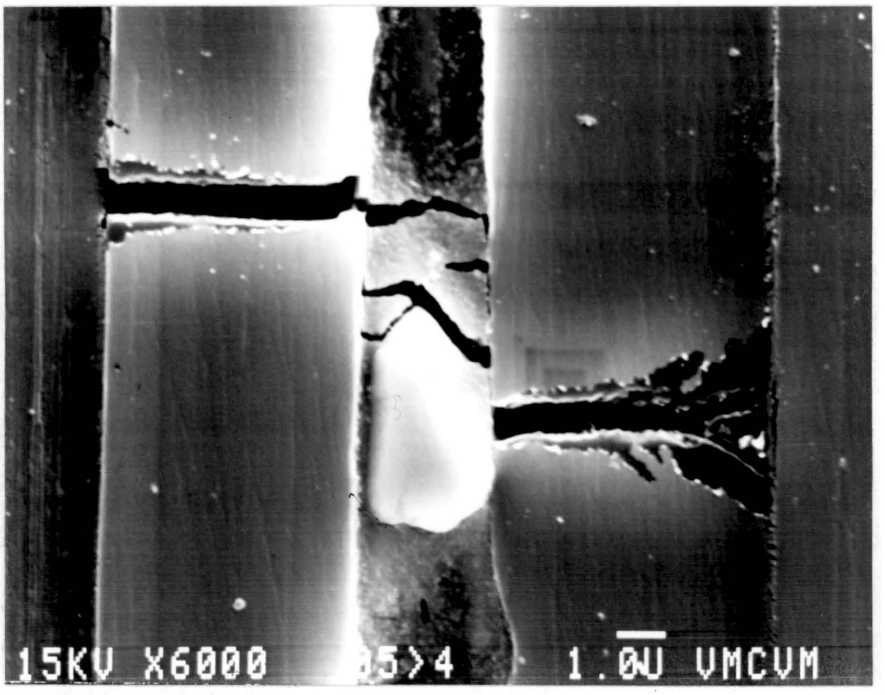

Fig. 5: Crack branching within a single fiber in T300/5208 system.

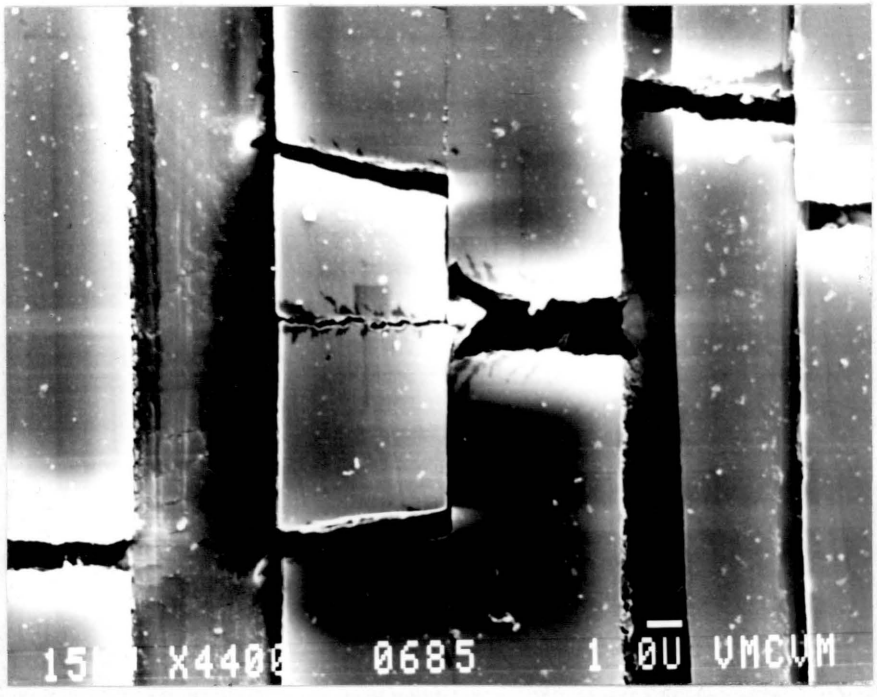

Fig. 6: Crack branching at the interfiber surface of contiguous fibers in T300/5208 system.

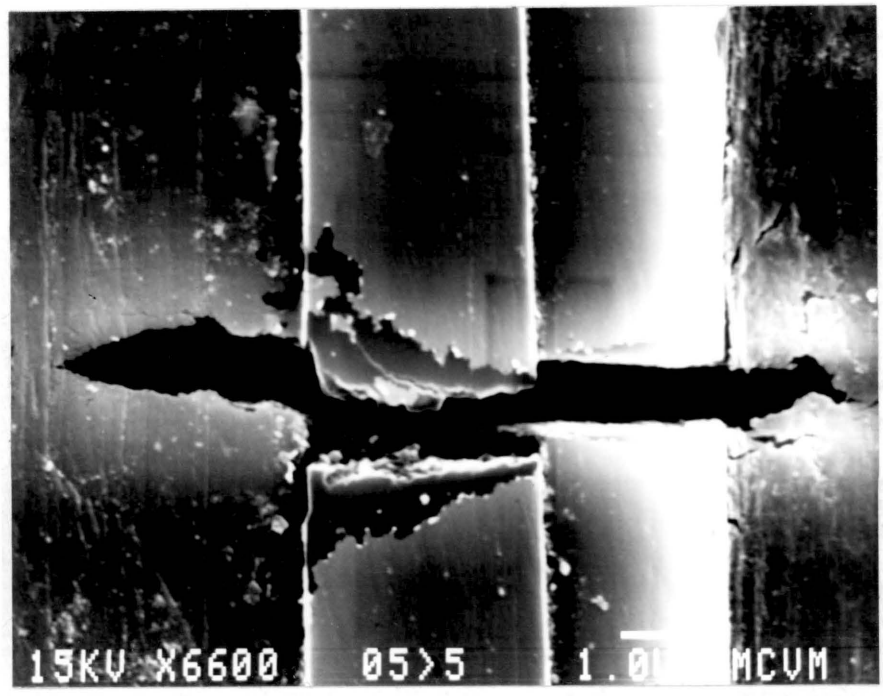

Fig. 7: Damage to the matrix around broken fibers in T300/5208, at near ultimate strain.

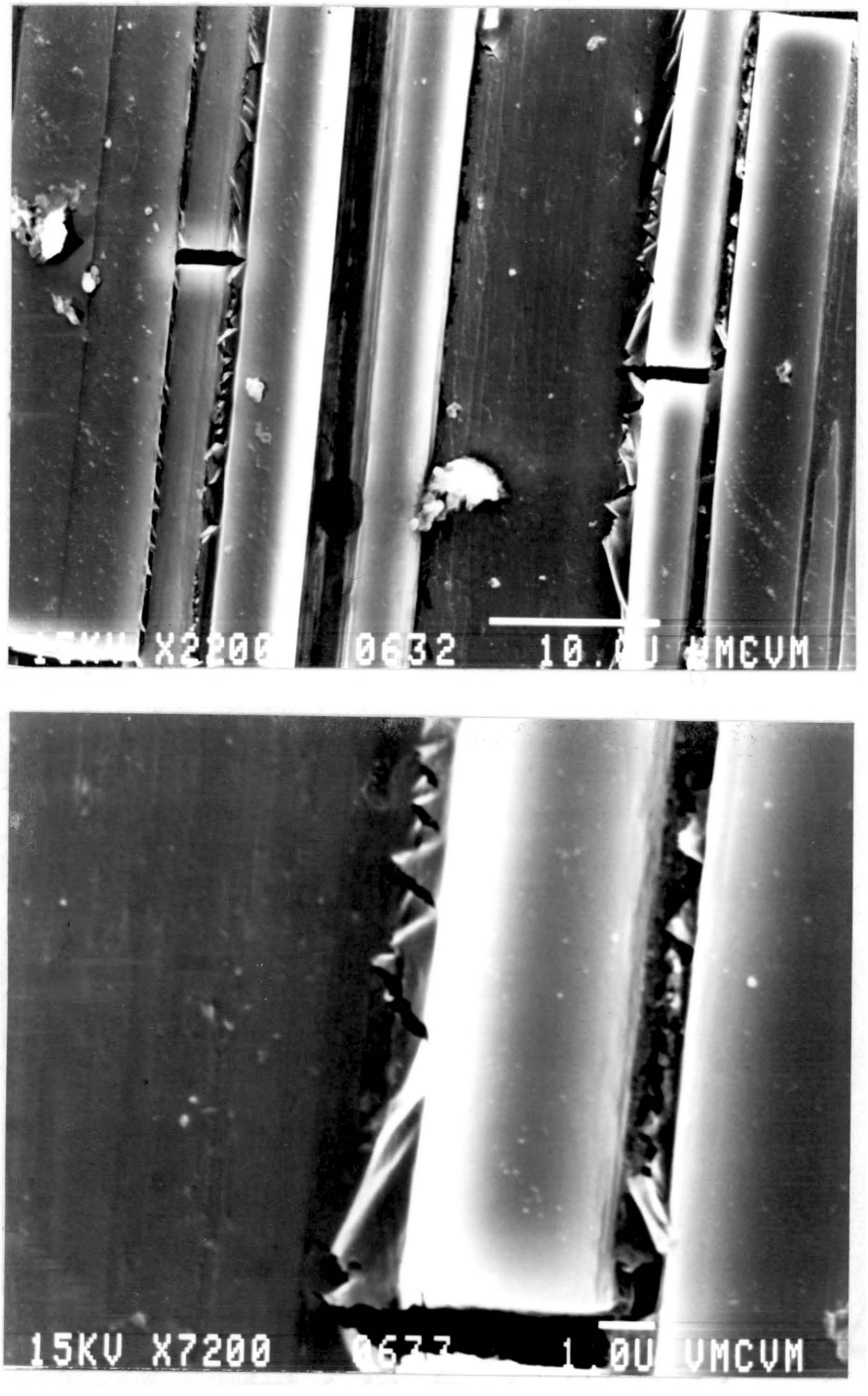

Fig. 8: Matrix shear failure seen in T300/5208 system, shown at two different magnifications.

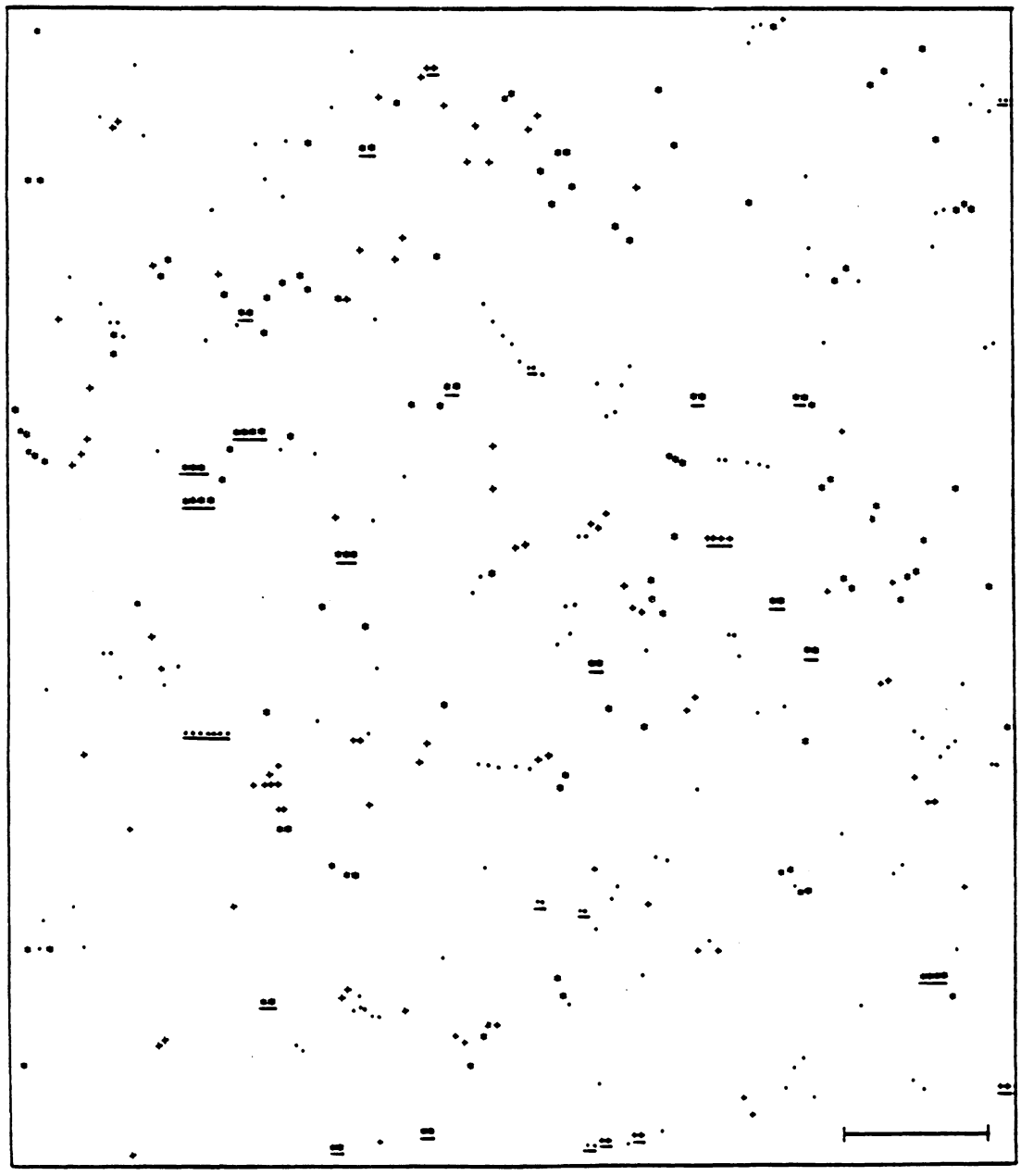

Fig. 9: Distribution of fiber fractures in T300/5208 system at different strain levels. The symbols dots (.), asteriks (*) and plus signs (+) respectively show the fiber fracture distributions observed at 77%, 88% and nearly 100% of the ultimate strain.

groups are indicated by a line drawn below the respective symbols. The fiber orientation was along the y-axis in this figure and the scale mark shown corresponds to approximately to twenty fiber diameters.

Self-similar fiber fractures were seen even at 77 % of the ultimate strain. But a greater number of them appeared between 77 % and 88 % of ultimate strain and a somewhat lesser number appeared in between 88 % and near 100 %. Most single fiber fractures appeared to form as closely spaced groups, and, as the strain is increased, the damage appears to spread laterally, but the individual fiber fractures are staggered in the vertical direction. There appears to be a somewhat reduced fiber fracture density above and below the locations of self-similar fiber fractures seen in contiguous fiber groups. Fiber fracture formation in AS6/F584 and G40/600/5245 were similar to that of T300/5208, but the number of self-similar fiber fractures were far fewer in number.

In AS6/F584 composite system the matrix did not appear to develop cracks around fiber fractures occuring at low stress levels. However, at strain levels of the order of 90 % of ultimate, the matrix developed extensive microcracking, fanning out from the point of fiber break, as in figure 10. The length of this network of microcracks extended to 10 to 15 times the fiber diameter, on either side of the fiber breaks. In addition to those cracks, other microcracks normal to the fiber direction but bridging adjacent fibers were also seen; these are barely visible in figure 10.

In the G40-600/5245 system a somewhat different failure mode of the matrix was seen. In this system some of the fiber fractures resulted in multiple matrix cracks, even at strain levels of the order of 50 % of the ultimate. However, around other fiber fractures at this strain level, no matrix damage could be observed. As the strain level increased, there was a greater tendency of occurance of multiple matrix cracks around the broken fibers. As can be seen in figure 11, the matrix cracks in this composite system are unlike those seen in AS6/F584 and are relatively straight. The matrix microcracks also appear to open up to a greater extent

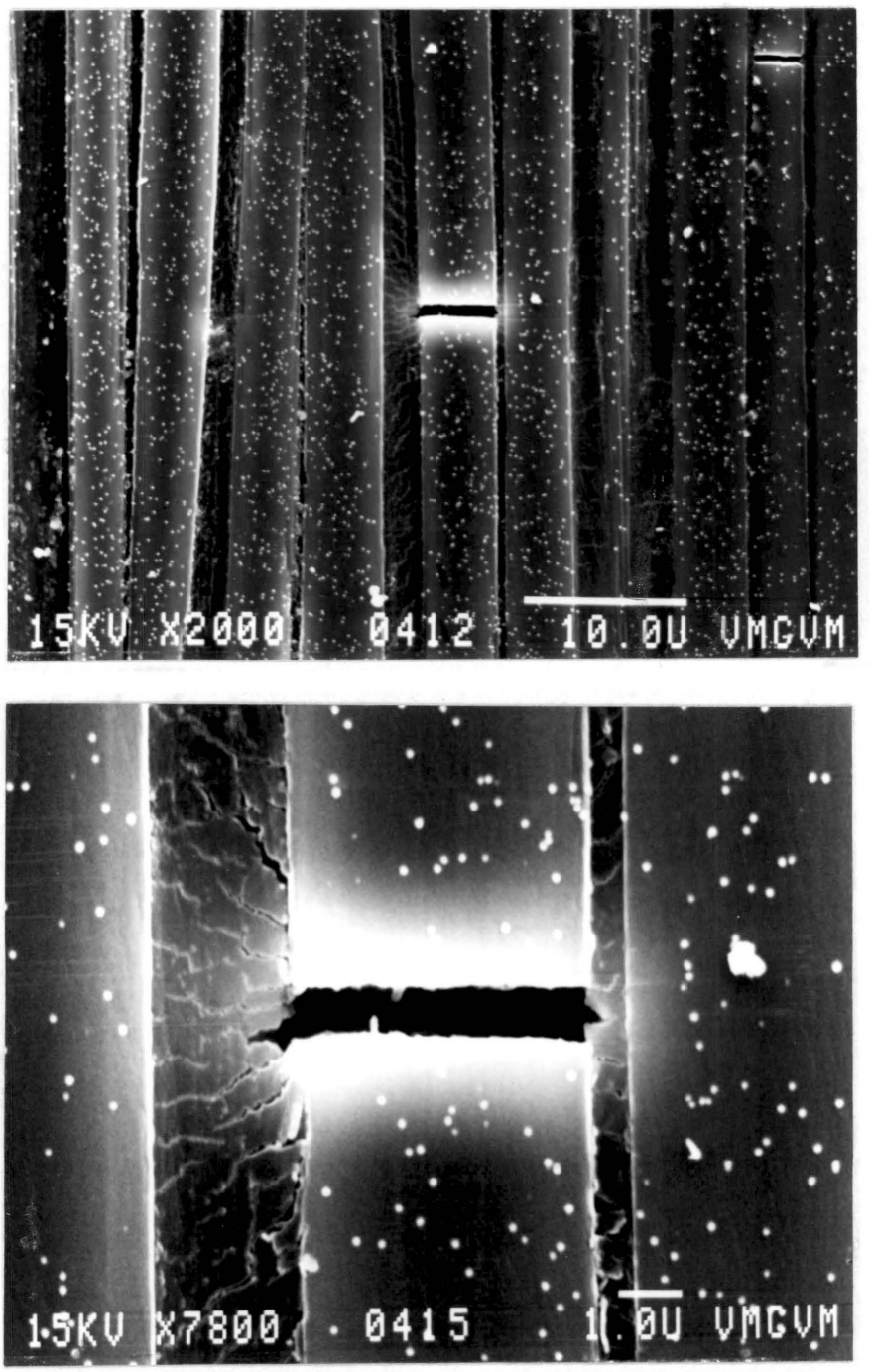

Fig. 10: Matrix microcracking in AS6/F584 composite system.

compared to those in AS6/F584. In rare instances crack branching within individual fibers was seen in G40-600/5245.

Figure 12 shows typical fracture surfaces of two of the composite systems after ultimate failure.

In the T300/5208 samples the final failure was by the fracture of a group of fibers in the surface layer and subsequent debonding from the rest of the materials. In all the remaining systems studied here, the failure appears to originate from the compression side and the specimens separated into two. The fracture surfaces showed that a larger portion of specimen thickness towards the lower surface was relatively flat, indicative of compression failure. A relatively smaller portion of the specimen thickness on the tensile side of the specimen, had irregular fiber pullout, typical of tensile failure. Figure 12(b) shows a small area of fracture surface including both these failure modes, corresponding to AS6/F584 system.

The failure process in high modulus composite P75/ERLX 1902 was found to be different from those of the other composite systems. Even while polishing these specimens, the fibers were found to be much more softer compared to the other fibers, and were easily abraded by the polishing dust. The individual fibers exhibited distinct fibrous texture, observable at high magnifications. Further they were not adversely affected by scratches, as seen in figure 13.

Such scratches were seen to result in continuous groups of fiber fractures in the other composite systems described earlier. In this system, the final catastrophic fracture, probably initiating from the compressive side, occurs very early and very few fiber breaks could be seen on the tensile side before this occurs. Figure 14 shows the rare cases of fiber fracture seen in these specimes.

It may be noted that the fiber fracture modes are different from those seen in the other composite systems. The cracks take convoluted paths across the fiber, and a split can also be seen on the left side of the figure 14(b).

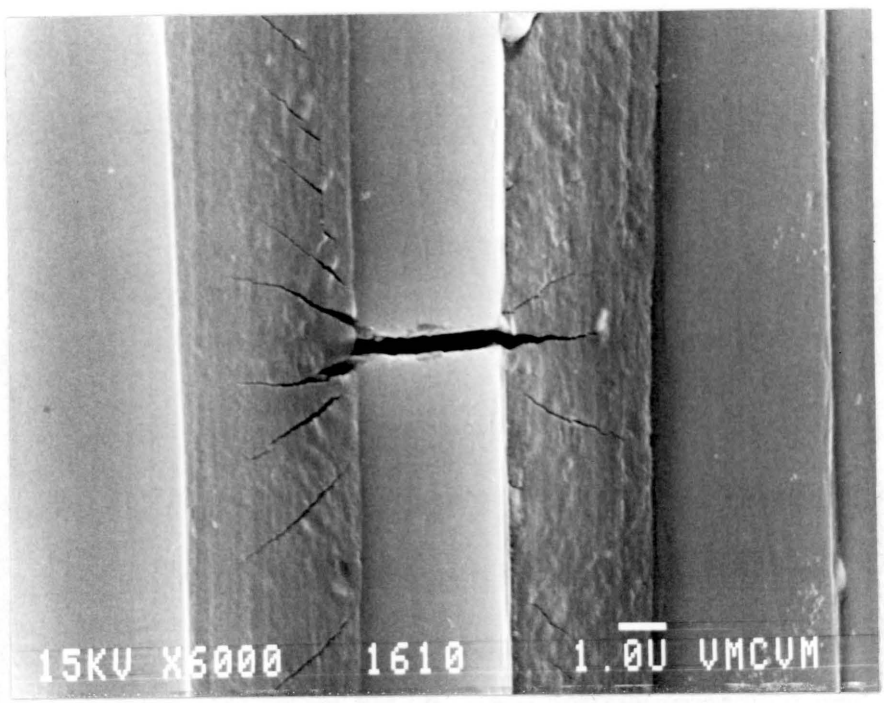

Fig. 11: Matrix micro-cracking in G40-600/5245 system.

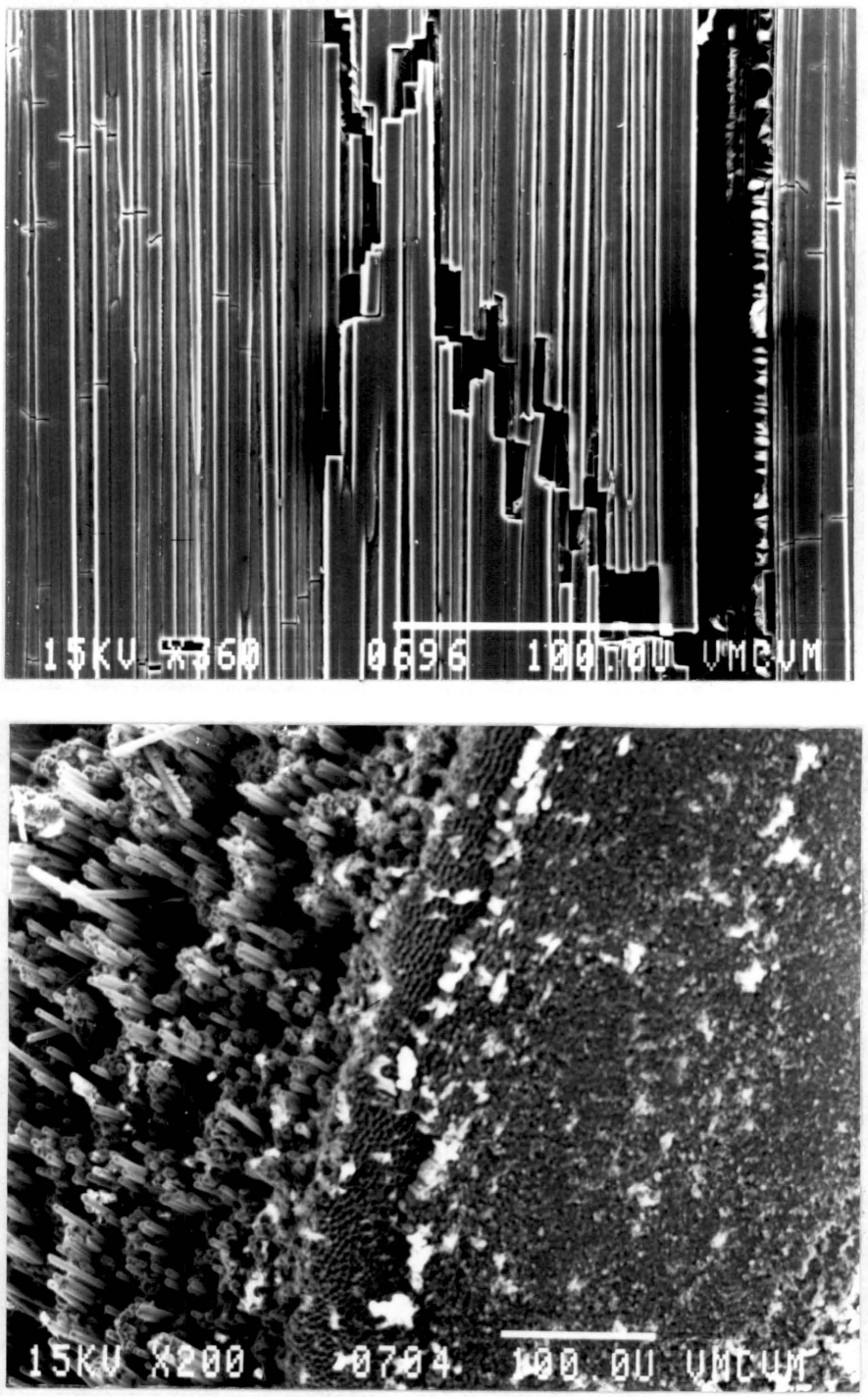

Fig. 12: Typical fracture surfaces of (a) T300/5208 system and (b) AS6/F584 system after the final fracture.

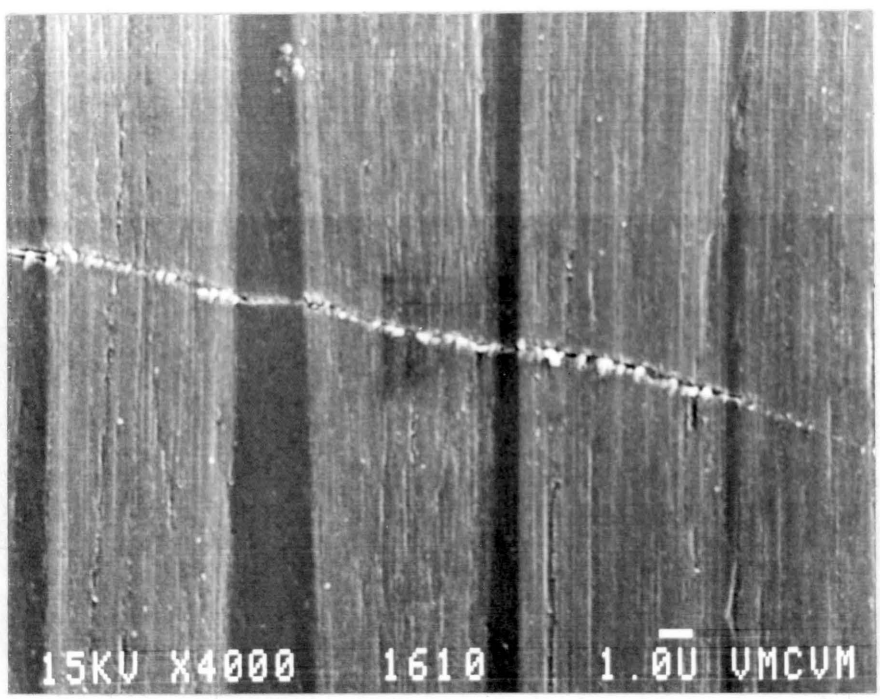

Fig. 13: Micrograph illustrating fibrous texture of individual P75 fibers and their relative insensitivity to surface scratches.

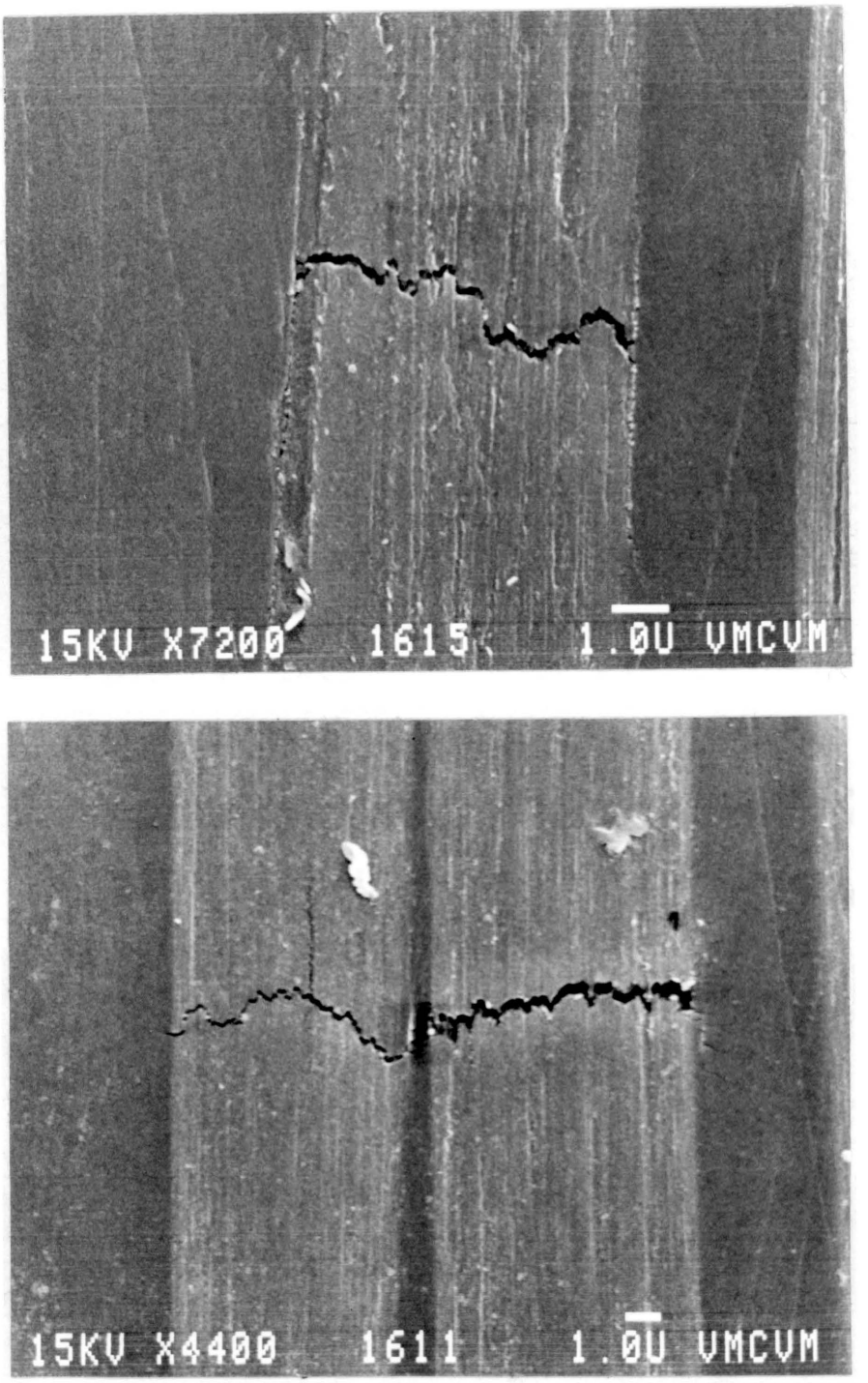

Fig. 14: Fiber fractures in P75/ERLX 1902 composite system

The last composite system studied under this investigation was G3500/PES, having a thermoplastic matrix polyethersulphone. In the samples used in this study, bands of fiber waviness, with the wave length in the range of 1 to 2 mm, could be seen at several locations. These wavy fiber bands could be easily located by naked eye. One such wavy fiber band is shown in figure 15.
As mentioned in chapter 2, there is a considerable difference between the thermal expansion coefficients of carbon fibers and some of the thermoplastic matrix materials. Apparently, the above bands were caused by such a thermal expansion coefficient mismatch.

When specimens from this composite system was strained, fiber fractures preferentially occured within these fiber bands. One such area is shown in figure 15.
It may be seen that there is a larger density of fiber fractures at the middle as well as towards the ends of these waves. There seem to be little fiber/matrix adhesion in this system, since in a number of areas, even without fiber fractures, the fibers appeared to debond from the matrix as indicated in figure 17.

3.6. Speckle pattern for strain measurement around broken fibers

As discussed in chapter 2, the nature of the strain field around broken fibers, determine the rate of the spread of damage into the neighbouring fibers. Hence, actual measured values of strain distribution around broken fibers, in the presence of matrix yielding and failure, is of considerable practical interest. However, no such results for actual composite materials appear to be available at the present time.

In the present investigation, a procedure for producing speckle pattern on the microscopic scale, suitable for strain measurement, has been developed. Once speckle patterns are developed, the procedure for strain measurement around broken fibers would be as follows: SEM micrographs containing speckle patterns, corresponding to undeformed as well as de-

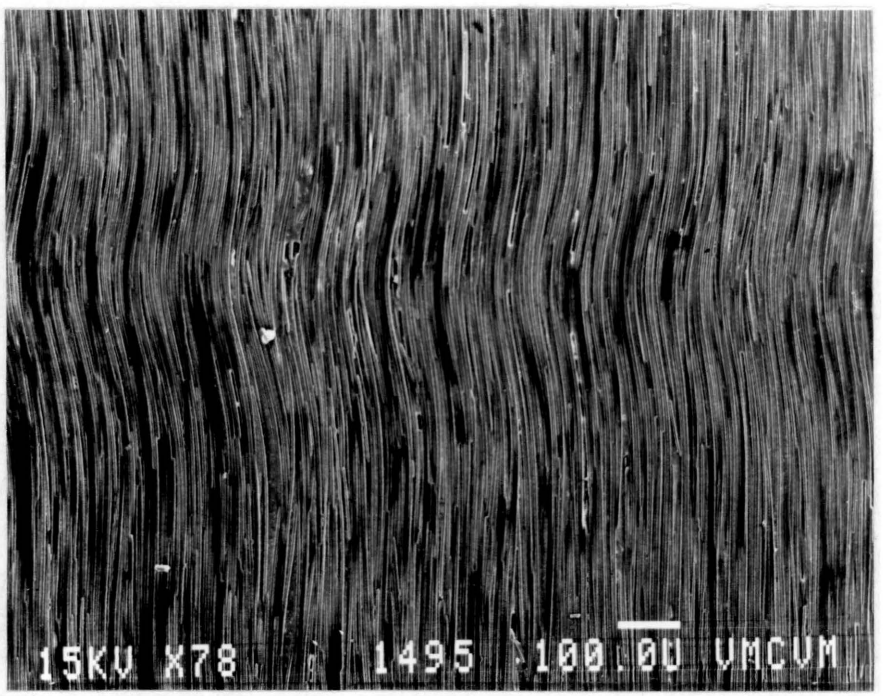

Fig. 15: Fiber waviness present in G3500/PES composite system.

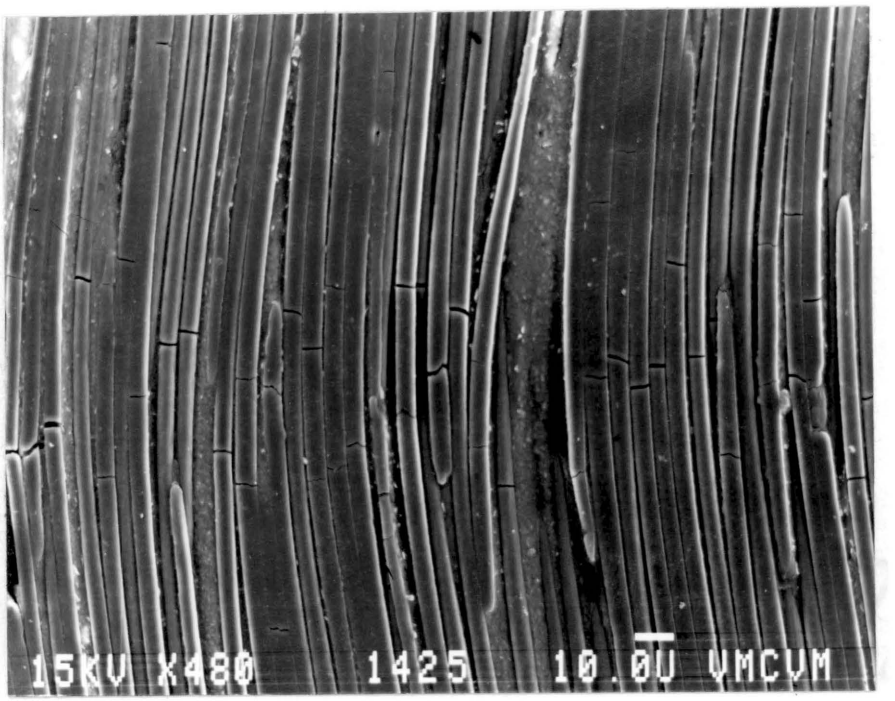

Fig. 16: Fiber fracture distribution in G3500/PES system.

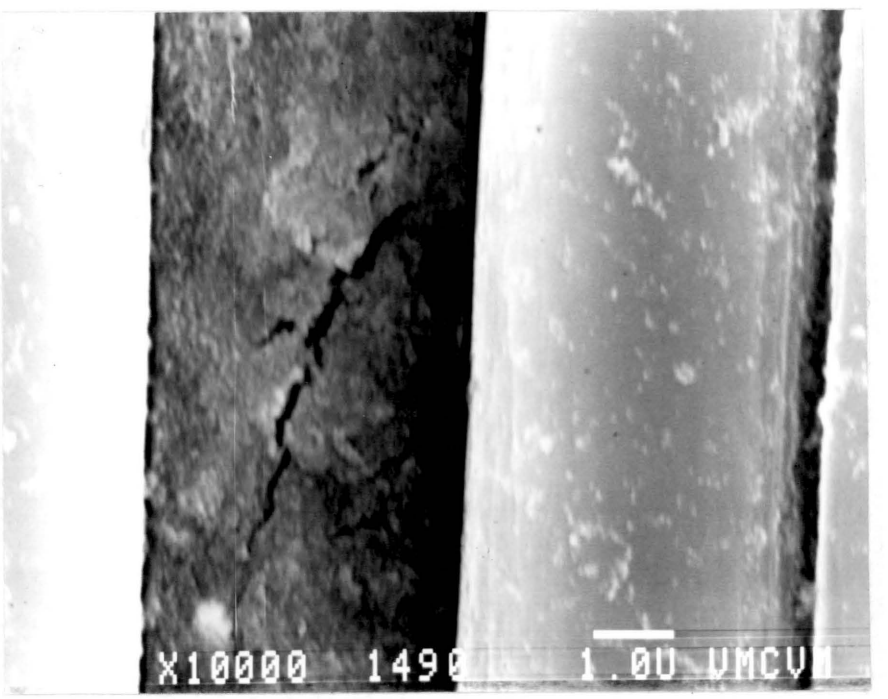

Fig. 17: Interfacial debond in G3500/PES system.

formed states, are produced. These micrographs are scanned by a high resolution video camera and digitized into 512 x 480 pixels. The light intensity at each of these pixels is recorded with a 8 bit resolution - i. e., 256 levels. Peters and Ranson [136] provide the procedure for correlating the speckle patterns corresponding to undeformed and deformed states and extracting values of displacement and strain. Briefly, this procedure involves dividing the field into subsets, typically of 10 x 10 pixels and the light intensity patterns in each subset is fitted with a polynomial surface. Thus, light intensity surface corresponding to undeformed and deformed states are constructed and stored in the computer. From these light intensity surfaces, the translation and rotation of each subset can be tracked. Further, using digital correlation techniques, the strain tensor over the image field can be obtained. Chu et. al., [40] have demonstrated that displacements can be measured to a resolution of 0.1 pixel width and strain measurement to an accuracy of order of 10 % can be attained in the moderate strain regime, i. e., where the strain magnitudes are of the order of 2 to 3 %. Since the local strains in the matrix around broken fibers appear to be of this order of magnitude, the image processing procedure, appears suitable for this application.

As a part of a collaborative effort with Dr. Sam Russell of University of South Carolina, a procedure for developing the speckle pattern required on this micrscopic scale was developed. For the image processing application, the micrographs should have a sufficiently high speckle density, and the individual speckle size in the order of 0.1 micrometers is required.

Several procedures were investigated for producing such a speckle pattern. These included deposition of fine carbon particles on the specimen surface by a vapour deposition procedure, leaching of a thin layer of gold coating on specimen surface by a fine mist of aqua regia, dispersion of gold and silver colloidal particles on the surface and spraying solutions containing particles of the required size. However, none of these procedures produced the type of speckle pattern required for this application. Finally, coating the specimen surface with microspheres of the required size was found to be satisfactory. Micrographs with speckle patterns, corresponding to undeformed and deformed states are shown in figure 18.

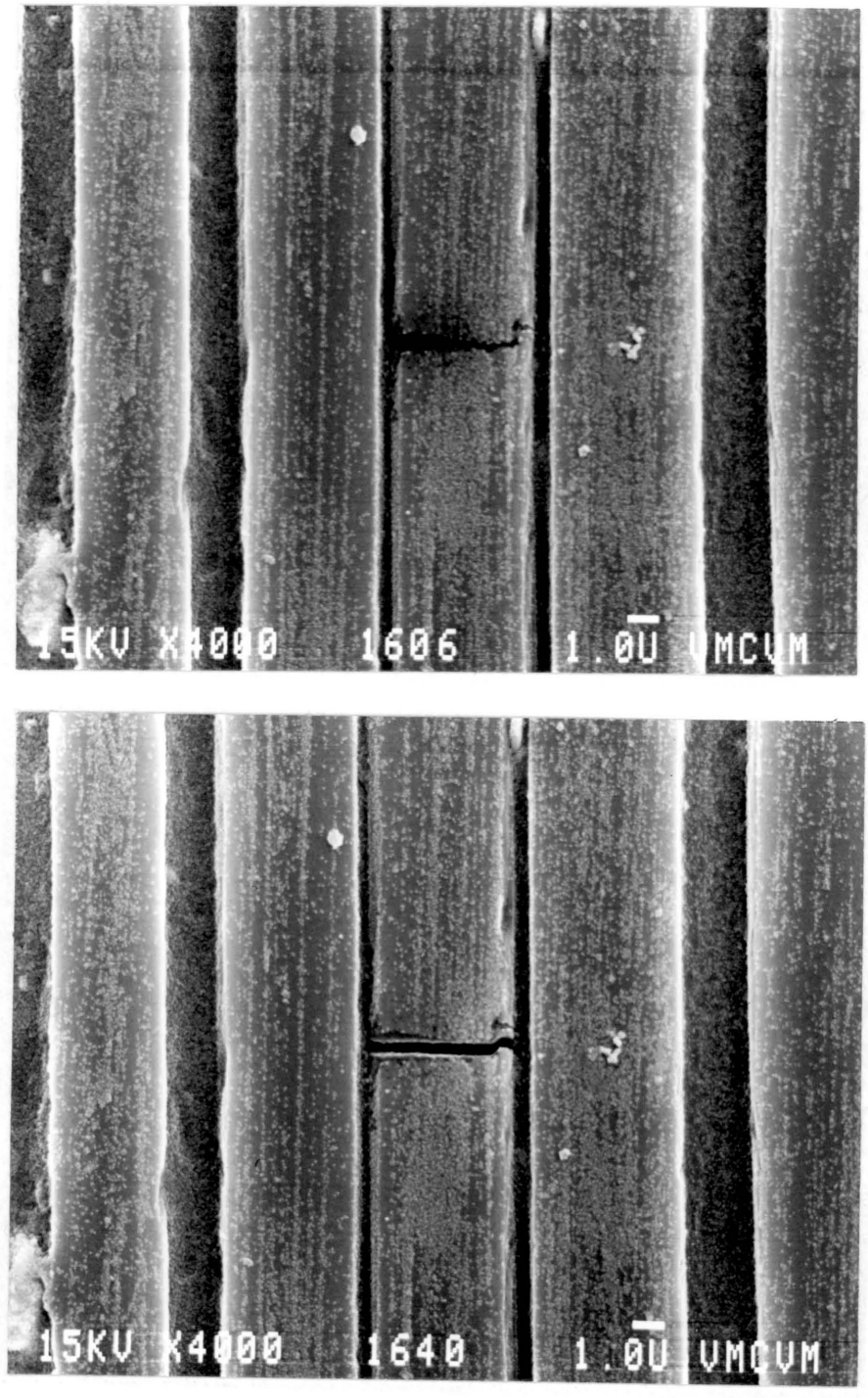

Fig. 18: Speckle patterns deposited on specimen surface.

By this procedure speckle micrographs corresponding to different compositesystems at various strain levels were prduced, and these are expected to be useful in measuring the strain field in the presence of matrix yielding and microcracking, discussed earlier.

3.7. Discussions

There are two important factors concerning the present three point bend specimens which need to be taken into account in interpreting the results. The first one is the probable introduction of additional flaws into the fibers during the polishing operation. As a result, there is likely to be greater density of fiber fractures appearing at lower stress levels, compared to unpolished specimens. Secondly the three point bend configuration provides a stable failure process, since the gradient of stress across the beam thickness is conducive to the arrest of cracks from the surface layer. These two effects together can explain the higher fiber fracture density seen in the present investigation compared to the results of Jamison [91], for example, in which the fiber fracture density was measured by deplying tensile coupons. Because of the same reason the catastrophic failure is likely to be delayed in the three point bend specimens, inspite of the extensive damage occurring to the fibers. This stable failure pattern enables one to examine the evolution of failure in greater deail. In an unpolished tensile coupon, however, there is a likelihood that some of the crack arrests such as the one seen in figure 5 may not be favoured, because of the higher stress levels at which fractures may be occurring.

From the results presented in the earlier sections, several differences in the failure modes among the five composite systems are apparent. Further, some of the failure processes have come to light for the first time. One such failure mode is the occurrence of the self- similar crack growth within contiguous fiber bundles seen in T300/5208 system. In such fiber groups, the fracture originating in any one of the fibers appears to spread across the entire group with very little resistance. However, in the three composite systems AS6/F584, G40-600/5245 and G3500/PES, the interphase and the matrix appear to able to prevent such crack growths. It

may be visualized that as the spacing between adjacent fibers decrease, the value of stress concentration in the fiber next to the broken fiber increases and in the limit when the fibers are contiguous, the stress concentration factor turns into stress intensity factor. Under such conditions, the presence of strong fiber-matrix bond and brittle matrix in the composite, encourages the fracture of the first fiber in a contiguous bundle to spread to the rest of the members in that group, just as in brittle homogeneous materials.

The appearance of dynamic crack propagation and branching in T300/5208 and G40-600/5245 systems at strain levels close to failure is another failure mode of interest. These dynamic fractures may be compared with the results of Herring et. al., [86], who observed dynamic fracture in boron/aluminum composite. Similar branching phenomena were also seen by Theocaris et. al., [179], in model composites. Because of the reasons discussed in the first paragraph of this section, there are likely to be higher incidences of such dynamic fractures in uniaxial tensile coupons. However, it remains to be established if the appearance of the dynamic crack growth behaviour near the ultimate failure, indeed is responsible for the transition of the composite failure process from the gradually evolving distributed fiber fracture to an unstable, catastrophic crack propagation across the entire specimen.

The type of deformation and failure seen in the matrix materials surrounding the broken fiber was found to be a function of the stress level at which the fracture was occurring as well as the matrix material. These differences in the deformation and failure mode of the matrix material around individual broken fiber, would alter the length over which the stress diffusion is taking place, from the broken fiber into the surrounding material. Two extremes in these stress diffusion from a broken fiber into the neighbouring fibers can be visualized. The first case would be that of a matrix which is completely elastic and brittle, which allows a fiber crack to extend in a self-similar manner upto the neighbouring fiber surface. This is likely to result in a relatively high stress concentration in the neighbouring fiber, but the stress diffusion would take place in a relatively short distance along the fiber length. In the second case the matrix is assumed to undergo plastic deformation and microcracking, by which the

length of stress diffusion is considerably increased, but the magnitude of stress concentration is reduced. In addition such deformation would be capable of absorbing a relatively larger amount of strain energy from fiber fractures. Matrix deformations observed in the earlier results fall between these two extremes. The value of the stress concentration factors resulting from the above failure modes and the ineffective lengths are of practical interest. In this respect, the strain measurement procedure outlined in section 3.6 is likely to be useful.

4.0: Acoustic Emission Monitoring of the Failure Process

4.1. Introduction

The SEM observations presented in chapter 3 provide information about the deformation and failure occurring at the microscopic level. However, this technique does not provide information on how the gradually evolving failure turns into an unstable fracture propagation. Acoustic emission technique appears to have the potential to address this aspect of the failure in composites, since it can detect damage taking place anywhere within the specimen. However, one of the main limitations of the acoustic emission technique has been its inability to quantify the rate of damage growth. In this chapter efforts towards improving the accuracy of acoustic emission measurements and subsequent use of this technique to monitor the development of damage in unidirectional composite test coupons are described. As a part of these tests, the strength and moduli of the five composite systems were also determined.

4.2. Specimen Geometry and Loading

The five carbon fiber / polymer matrix composite systems studied are listed in table 7 of chapter 3. All specimens used for AE measurements were eight ply thick and of half inch width. AS6/F584, G40-600/5245, P75/ERLX1902 and G3500/PES specimens were eight inches long and T300/5208 specimens were six inches long. Of these the edges of the relatively brittle systems, namely T300/5208 and P75/ERL1902 were polished with a 600 grit emery, to remove a layer of material likely to contain machining induced damage. Preliminary test results indicated that such polishing was unnecessary for the other systems, which were relatively tougher. The specimen ends were covered with layers of 180 grit emery cloth and were gripped in hydraulic wedge grips. However, for a satisfactory gripping of the specimen, without premature failure at the grips or specimen slippage, appropriate grip pressure and emery cloth layer arrangements had to be determined through several trials. The arrangement of emery cloth layers shown in figure 19, and a grip pressure of 900 psi worked satisfactorily.

Strain measurement was done by means of a one inch gage length extensometer. The extensometer knife edges were placed inside the V-shaped grooves of aluminium tabs bonded to the specimen. The elastic moduli were calculated from the slope of the stress strain curve between 60 % and 80 % of ultimate stress. All the quasi-static tensile tests were done on a MTS 880 servo-hydraulic testing machine at a nominal strain rate of 0.000,005 per second. The strength and moduli values are given in table 8 of chapter 3.

4.3. Specimen acoustics

Simple stress wave propagation studies were done on the unidirectional test coupons to understand the way in which these waves propagate. Such a study can aid in the selection of appropriate instrumentation. Simulated AE signals were introduced at one end of the

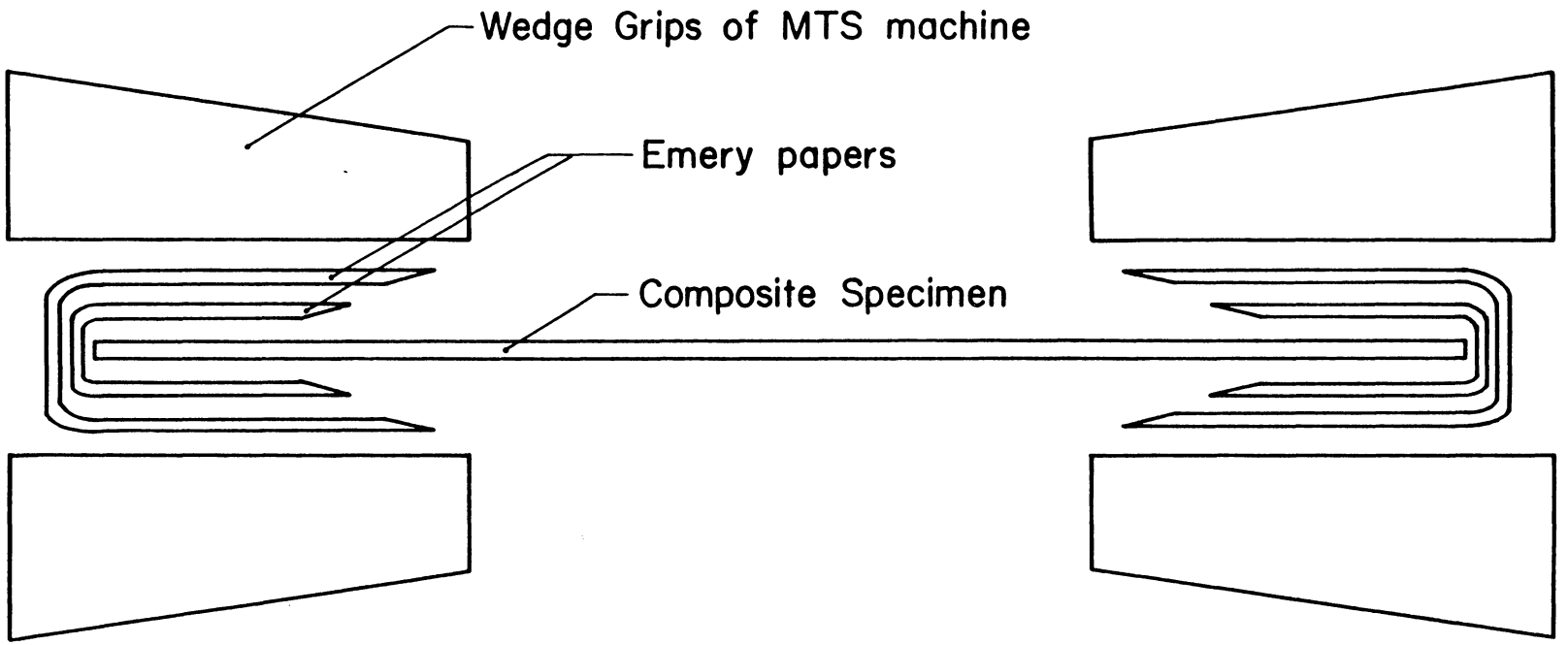

Fig. 19: Grip arrangement used for the tensile tests.

specimen as shown in figure 20 and the signals were picked up by a sensor, after propagating for some distance.

To introduce the stress waves into the specimen a highly damped ultrasonic transducer with a central frequency of 5 MHz - Panametric V110, was pulsed by single pulses in the shape of a half sine wave, of frequencies ranging from 1 MHz to 10 MHz. Pencil lead breaks were also used to the simulate an AE source. These tests were done on laminates having different stacking sequences. The results corresponding to three different laminates are shown in figure 21.

A 5 MHz pulse was used for pulsing the transmitting transducer, for these cases. It can be noted that the frequency content of the propagating signal is affected to a considerable extent by the laminate thickness. In the eight layer specimen the dominant frequency is approximately 0.9 MHz. When the thickness is reduced to four layers, the frequency appears to increase to nearly twice this value. In the seven layer cross-ply specimen, the dominant frequency was seen to be about 0.9 MHz. Hence the specimen acoustics considered before selecting the bandwidth of the AE instrumentation. These stress waves bounce back and forth as shown in figure 22(a) and the level of attenuation does not appear to be excessive.

Hence, the AE source to transducer distance, in actual AE tests on this coupons is not likely drastically to affect the signal amplitudes.

4.4. Selection of AE Sensor

The sensor is the most critical part of the acoustic emission instrumentation. In the present study, the micro-fracture size is estimated from the amplitude and energy content of the signals as detected by the AE sensors. Hence, it is important that the sensor reproduces with high fidelity, both in terms of amplitude and frequency content, the stress waves created by the failure event. From considerations of failure event duration, it is possible to estimate the frequency content of the AE signal caused by this event. In the present case, since the

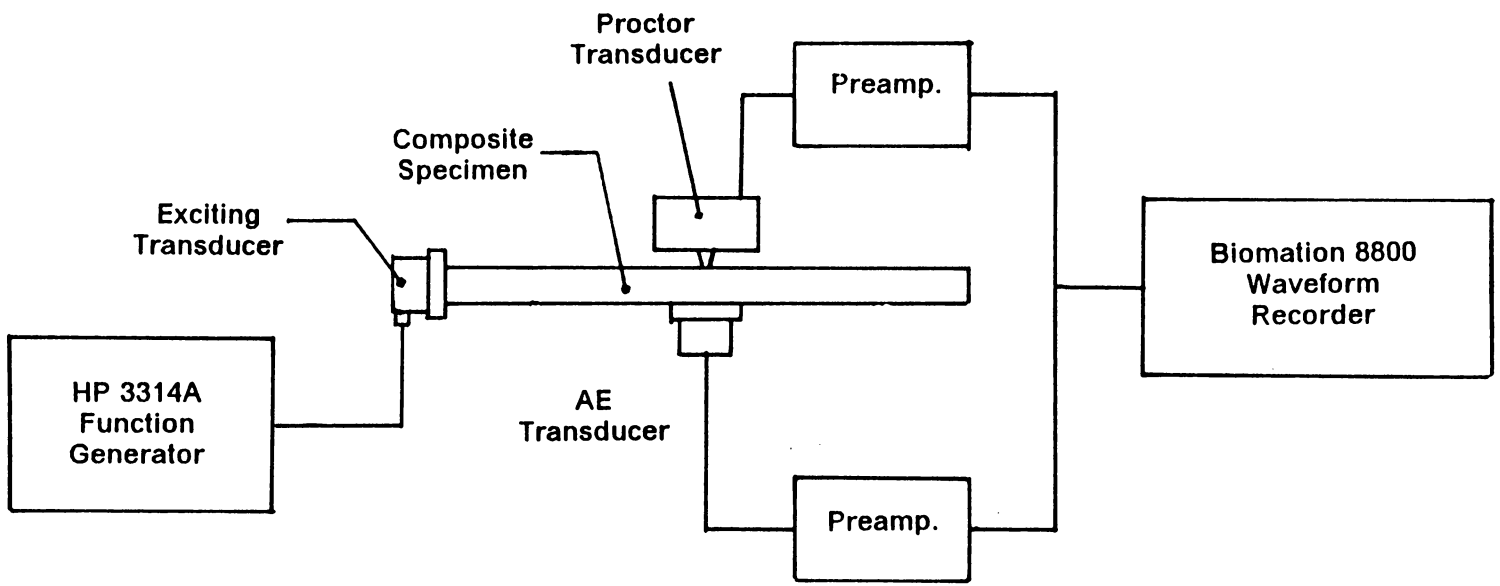

Fig. 20: Experimental setup to study the wave propagation in composite specimens.

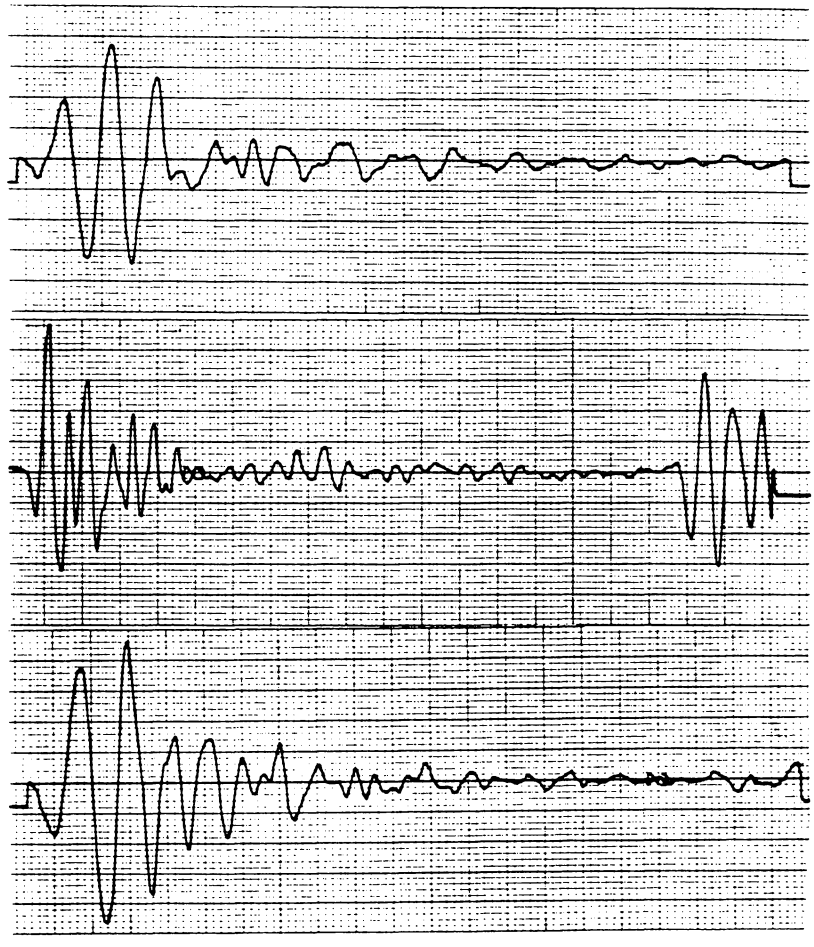

Fig: 21: Comparison of responses of different laminates as waveguides: (a) 8-ply unidir. (b) 4-ply unidir. (c) 7-ply cross ply

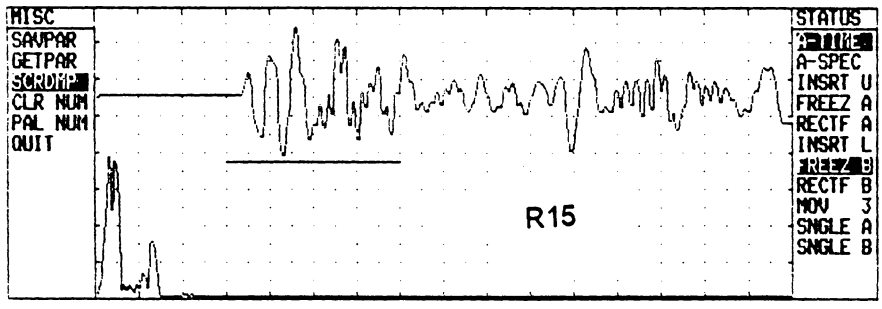

A-Ti Start (us):	0.000	A-Horz Res(us/d):	5.120	A-Vert Res(v/d):	0.250
A-Ga Start (us):	15.360	A-Ga Length (us):	20.480	A-Gate Len (pt):	512
A-Fr Start (Mhz):	0.000	A-Hor Res(Mhz/d):	0.7813	A-Ver Res(/d):	0.250
A-Decibels:	Off	A-dB Range:	24.0	A-FFT Length:	512
Sample Rate(Mhz):	25.000	Color Number:	0	Pallette Number:	0

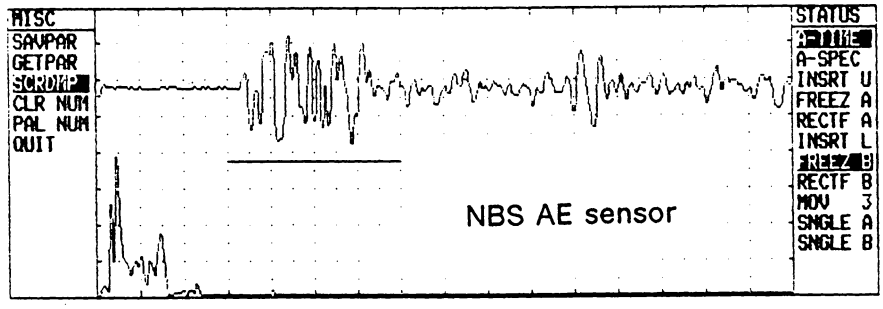

A-Ti Start (us):	0.000	A-Horz Res(us/d):	5.120	A-Vert Res(v/d):	0.063
A-Ga Start (us):	15.360	A-Ga Length (us):	20.480	A-Gate Len (pt):	512
A-Fr Start (Mhz):	0.000	A-Hor Res(Mhz/d):	0.7813	A-Ver Res(/d):	0.250
A-Decibels:	Off	A-dB Range:	24.0	A-FFT Length:	512
Sample Rate(Mhz):	25.000	Color Number:	0	Pallette Number:	0

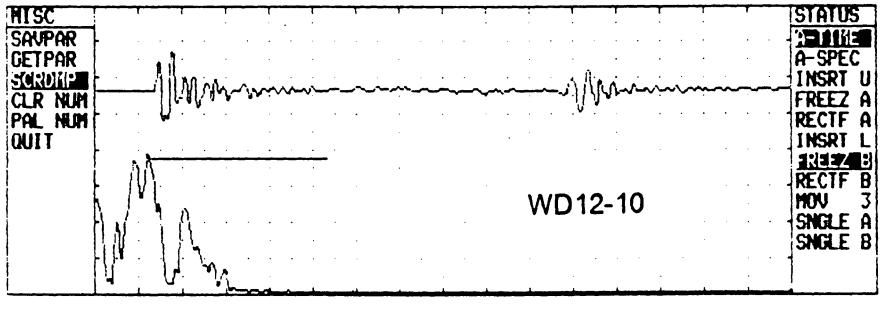

A-Ti Start (us):	-5.120	A-Horz Res(us/d):	3.340	A-Vert Res(v/d):	0.125
A-Ga Start (us):	0.000	A-Ga Length (us):	15.360	A-Gate Len (pt):	384
A-Fr Start (Mhz):	0.000	A-Hor Res(Mhz/d):	0.7813	A-Ver Res(/d):	0.250
A-Decibels:	Off	A-dB Range:	24.0	A-FFT Length:	512
Sample Rate(Mhz):	25.000	Color Number:	0	Pallette Number:	0

Fig. 22(a): Responses of the three sensors to 1 MHz pulse excitation.

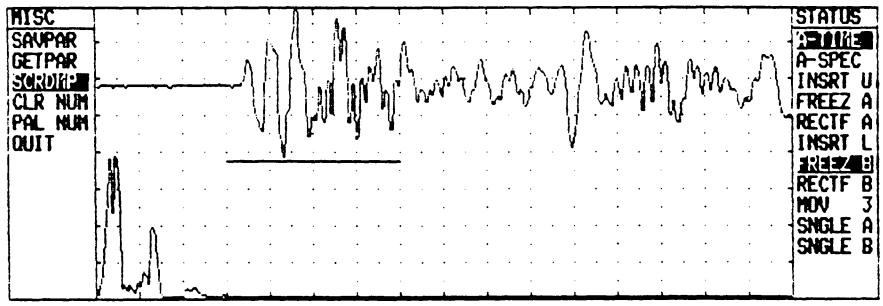

A-Ti Start (us):	0.000	A-Horz Res(us/d):	5.120	A-Vert Res(v/d):	0.063
A-Ga Start (us):	15.360	A-Ga Length (us):	20.480	A-Gate Len (pt):	512
A-Fr Start (Mhz):	0.000	A-Hor Res(Mhz/d):	0.7813	A-Ver Res(/d):	0.250
A-Decibels:	Off	A-dB Range:	24.0	A-FFT Length:	512
Sample Rate(Mhz):	25.000	Color Number:	0	Pallette Number:	0

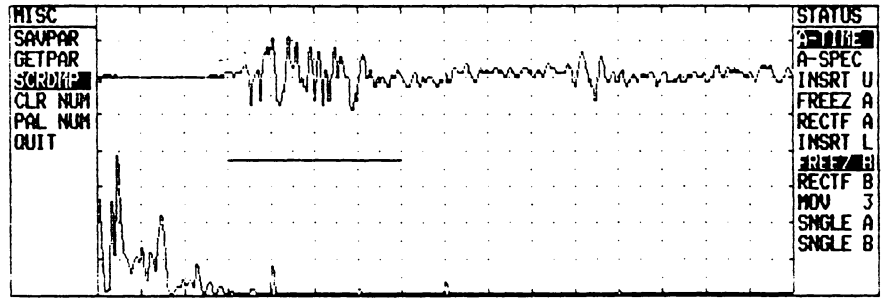

A-Ti Start (us):	0.000	A-Horz Res(us/d):	5.120	A-Vert Res(v/d):	0.031
A-Ga Start (us):	15.360	A-Ga Length (us):	20.480	A-Gate Len (pt):	512
A-Fr Start (Mhz):	0.000	A-Hor Res(Mhz/d):	0.7813	A-Ver Res(/d):	0.250
A-Decibels:	Off	A-dB Range:	24.0	A-FFT Length:	512
Sample Rate(Mhz):	25.000	Color Number:	0	Pallette Number:	0

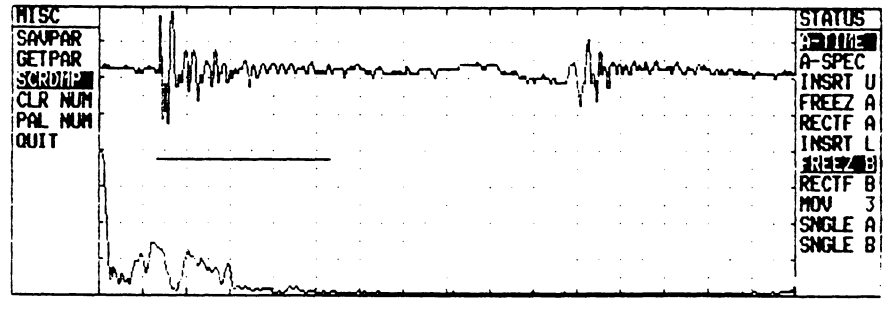

A-Ti Start (us):	-5.120	A-Horz Res(us/d):	3.840	A-Vert Res(v/d):	0.031
A-Ga Start (us):	0.000	A-Ga Length (us):	15.360	A-Gate Len (pt):	384
A-Fr Start (Mhz):	0.000	A-Hor Res(Mhz/d):	0.7813	A-Ver Res(/d):	0.250
A-Decibels:	Off	A-dB Range:	24.0	A-FFT Length:	512
Sample Rate(Mhz):	25.000	Color Number:	0	Pallette Number:	0

Fig. 22(b): Responses of the three sensors to 5 MHz pulse excitation.

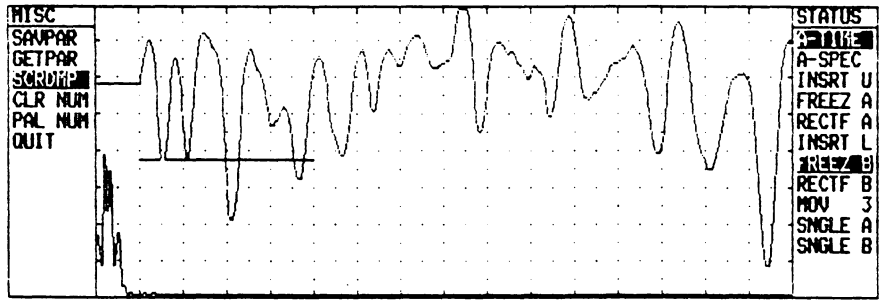

A-Ti Start (us):	-5.120	A-Horz Res(us/d):	5.120	A-Vert Res(v/d):	0.063
A-Ga Start (us):	0.000	A-Ga Length (us):	20.480	A-Gate Len (pt):	512
A-Fr Start (Mhz):	0.000	A-Hor Res(Mhz/d):	0.7813	A-Ver Res(/d):	0.250
A-Decibels:	Off	A-dB Range:	24.0	A-FFT Length:	512
Sample Rate(Mhz):	25.000	Color Number:	0	Pallette Number:	0

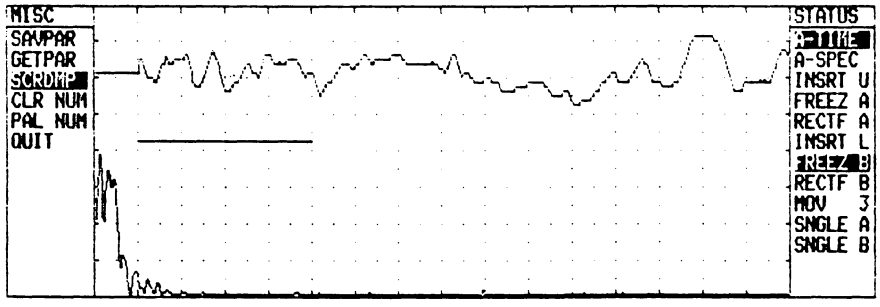

A-Ti Start (us):	-5.120	A-Horz Res(us/d):	5.120	A-Vert Res(v/d):	0.031
A-Ga Start (us):	0.000	A-Ga Length (us):	20.480	A-Gate Len (pt):	512
A-Fr Start (Mhz):	0.000	A-Hor Res(Mhz/d):	0.7813	A-Ver Res(/d):	0.250
A-Decibels:	Off	A-dB Range:	24.0	A-FFT Length:	512
Sample Rate(Mhz):	25.000	Color Number:	0	Pallette Number:	0

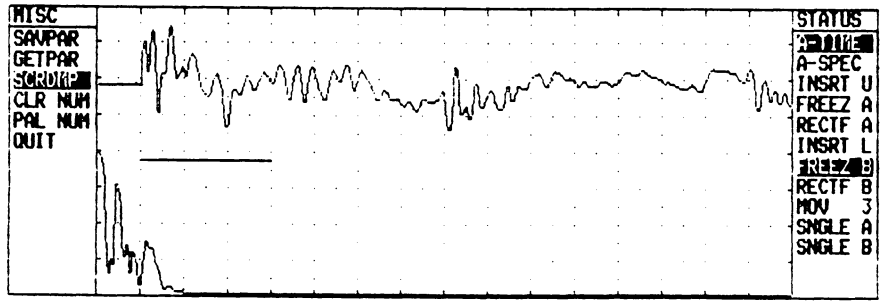

A-Ti Start (us):	-5.120	A-Horz Res(us/d):	5.120	A-Vert Res(v/d):	0.063
A-Ga Start (us):	0.000	A-Ga Length (us):	15.360	A-Gate Len (pt):	384
A-Fr Start (Mhz):	0.000	A-Hor Res(Mhz/d):	0.7813	A-Ver Res(/d):	0.250
A-Decibels:	Off	A-dB Range:	24.0	A-FFT Length:	512
Sample Rate(Mhz):	25.000	Color Number:	0	Pallette Number:	0

Fig. 22(c): Responses of the three sensors corresponding to lead break.

failure of individual fibers or groups of fibers is dynamic fracture, the duration of such an event is likely to be in the range of a few tens of nanoseconds, i.e., of order of 10^{-8} to 10^{-7} second. Hence the resulting stress waves are expected to have substantial frequency components in the MHz range. Further, the amplitudes are distributed over a very wide range. Failure of single fibers at low stress levels and large groups of fibers at near ultimate stress levels would form the extremes of the amplitude range. From these considerations a transducer having sufficiently wide frequency bandwidth and an appropriate sensitivity level is required to be selected.

The AE sensor diameter should be small compared to half the wave length of the highest frequency component present in the stress wave being measured. When the transducer diameter is larger than this length, there is a distortion in the ouput signal termed "aperture effect", [ ]. In such a case, as the packet of stress waves travel across the surface of the piezoelectric sensor, a portion of the surface is subjected to positive pressure while the remaining portion is subjected to negative pressure. Correspondingly these two portions of the sensor element develop mutually opposing electrical potentials and the algebraic sum of the signal due to the two portions appear as the sensor output. Hence, this output signal does not represent the actual stress wave, both in terms of amplitude as well as the frequency content.

For the selection of an appropriate sensor for the present application, a number of transducers were evaluated, regarding their suitability with respect to frequency as well as sensitivity. These included general purpose acoustic emission transducers such as PAC R-15 and Dunegan Corporation S-140A, wide band acoustic emission sensors such as Dunegan Corporation S9208, U30S, PAC WD transducers, the National Bureu of Standards conical transducer [145], pinducer as well as several ultrasonic transducers.

The response of three of the sensors to different excitations are compared in figure 22. The sensors were R-15, NBS conical transducer and a 0.125 inch diameter, 10 MHz, highly

damped ultrasonic transducer (Ultran Laboratories WD12-10). Figure 22(a) shows corresponds to excitation by a half sine wave of 1 MHz frequency. In all three cases, the amplifier bandwidth was from 50 KHz to 5 MHz. Of the three transducers, the R-15 transducer oscillates for the longest period of time and the WD12-10 transducer for the shortest period of time. In the output signal of WD12-10 transducer the initial packet of waves and the reflected one are clearly separated. The response of the NBS conical transducer lies between those of the other two transducers. In this connection, it may be noted that the NBS conical transducer has a flat frequency bandwidth of upto 1 MHz. The output amplitude of R-15 is about four times that of WD12-10.

A similar comparison of the response of the three transducers corresponding to 5 MHz exciting pulse is shown in figure 22(b). In this case there are larger differences in the three output signals. The frequency content of signal from WD12-10 extends upto 2.5 MHz whereas the output of R-15 is confined to much lower frequencies. The output amplitude of R-15 is nearly 2.5 times that of WD12-10. Figure 22(c) shows the response of the three transducers, when the excitation was by lead break at one end of the specimen. In this case the transducer outputs differ significantly both in terms of the amplitude as well as frequency content. In these experiments R-15 transducer signal was amplified by only 15 dB while NBS and WD12-10 transducers' outputs were amplified by 40 dB gain. Taking into account this difference in gain, R-15 output's peak amplitude is nearly 40 times that of WD12-10. Further, the frequency contents of the three outputs display much greater differences.

The above comparison has shown some of the differences in the three sensor performances relevant to the present study. Before selecting the appropriate sensor, we should note that, in any specimen, a pulse excitation with broad band frequency content, such as that of lead break or fiber break, is likely to excite a number of mode shapes, including longitudinal as well as shear modes. In addition, as shown in acoustic emission waveforms, to be discussed in section 4.5, higher harmonics of structural vibrations are also likely to be present. Further, the piezoelectric sensors such as the ones used in the present study, introduce ad-

ditional modifications in the detected signal because of their own internal resonance characteristics. In particular the general purpose AE transducers are sensitive to both longitudinal waves and shear waves. This appears to be part of the reason for the relatively complex waveform corresponding to R-15 in figure 22(b). The longitudinal and shear components present in the sensor outputs interfere or overlap with each other to various extents depending on the source to sensor separation. Ultrasonic longitudinal transducers, however, are primarily sensitive to compressional waves and are relatively insensitive to shear waves. Thus they can effectively separate the longitudinal modes from shear modes. Another way in which the detected signal can be distorted is through the so called "aperture effect", which results if the transducer diameter is greater than half the wave length of the highest frequency component present in the signal.

Considering these factors, the WD12-10 transducer appeared to present signals which were relatively simple in terms of waveforms still preserving the frequency components of the original signal. It also had the required sensitivity level, so that the preamplifiers were not saturated by high amplitude signals. Hence this transducer was selected for sensing the acoustic emission signals in the present study.

4.5. Acoustic Emission Instrumentation

The acoustic emission signals from unidirectional composite coupons were processed by a six channel, micro-computer based AE monitoring system - Physical Acoustics Corporation SPARTAN system. The specifications of this system are given in table 9. The full bandwidth of 50 KHz to 1.2 MHz of the system was used for processing the AE signals. The acoustic emission sensor was located at the center of the gage length of the specimens. The output of the sensor was fed to all the six channels of the SPARTAN system, in parallel. It was found that such a parallel connection results in the drop of the detected AE signal amplitude by about 5 dB, compared to the case in which the sensor output is fed to only one channel of the

SPARTAN unit. With this configuration, however, it is possible to process the acoustic emission signal simultaneously at six different threshold levels. The threshold levels chosen were 35 dB, 45 dB, 55 dB, 65 dB, 75 dB and 85 dB. Here 0 dB refers to a 1 microvolt signal at the transducer output point. Acoustic emission waveforms were also recorded using a PC based waveform recorder. This instrument had the capacity to store a total of 2000 AE events, with a sampling resolution of 1000 points per event. Sampling speeds upto 25 MHz were available on this instruments. For recording these waveforms a wide band amplifier with frequency bandwidth of 50 KHz to 5 Mhz was used.

For each of the composite systems studied in this program, a sufficiently large number of test results were available. For G3500/PES system ten individual tests to failure accompanied by acoustic emission monitoring were done. For each of the remaining four composite systems, a minimum of 15 individual tests were performed.

4.6. Results

There were significant differences in the failure modes of the five composite systems. Specimens of the P75/ERLX 1902 system failed by almost a straight failure surface across the specimen width. T300/5208 also failed due to a single crack across the specimen width in most specimens. However, these cracks were uneven and indicated a considerable amount of fiber pullout. These failure modes are shown in figure 23.
G3500/PES specimens splintered into ligaments, typically forming about ten to fifteen individual ligaments per specimen. The two relatively high strength composite systems, AS6/F584 and G40-600/5245 failed by the failure mode commonly referred to as "brooming" or "paint brush" failure mode, in which the failed specimen exhibited numerous fiber bundles separated from each other and each end of the failed specimen gave the appearance of a paint brush.

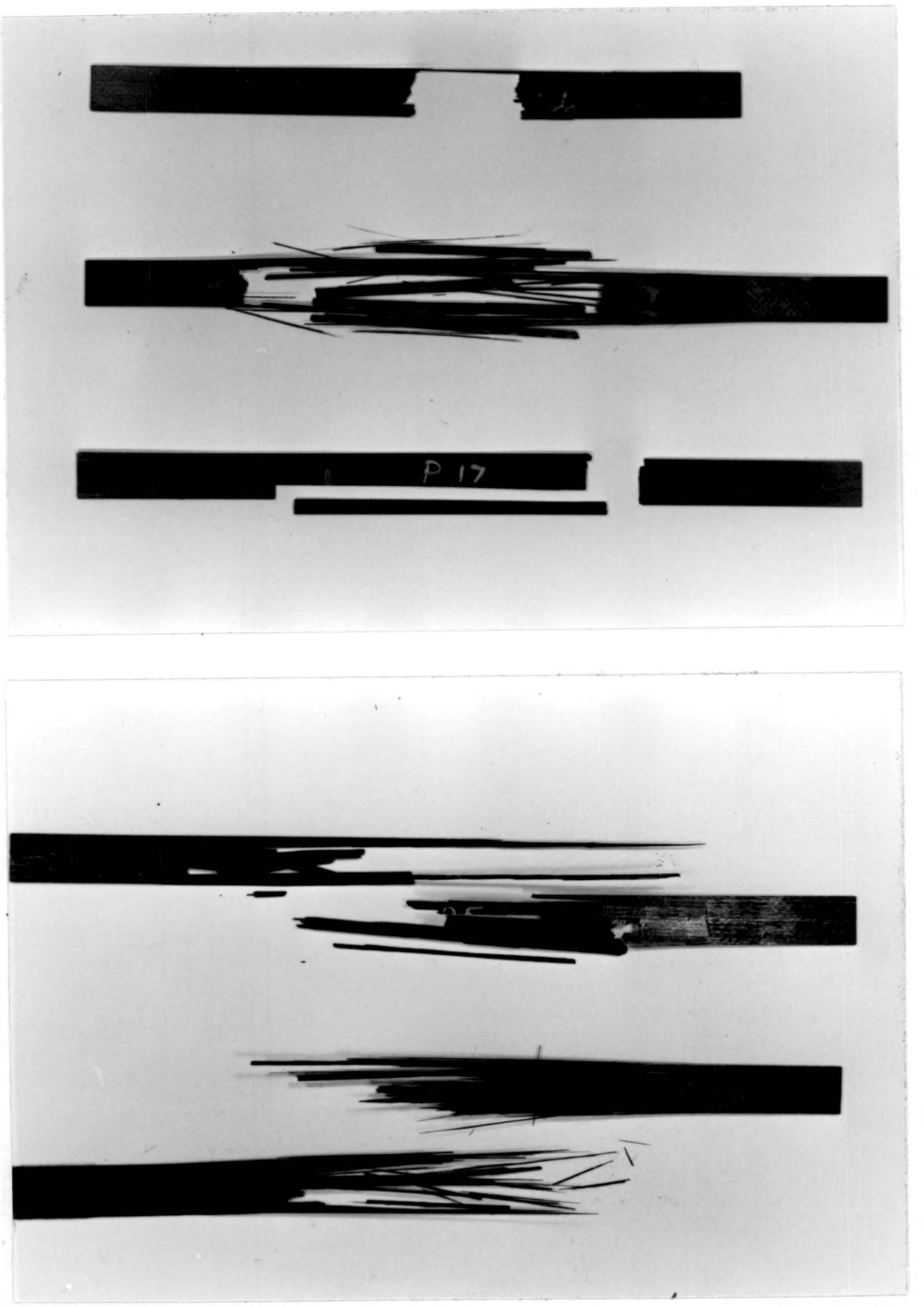

Fig. 23: Failure modes in the five composite systems; top to bottom: T300/5208, AS6/F584, P75/ERLX 1902, G3500/PES and G40-600/5245.

Of the five composite systems studied, G40-600/5245 showed the highest level of acoustic emission activity and P75/ERLX 1902 showed the least amount of acoustic emission activity. Typical results corresponding to each of the five systems are presented in the following paragraphs. The cumulative event counts of the five systems are compared in figure 24.
We can see that there is almost an order of magnitude difference in the total number of events registered at 35 dB threshold level, between these systems. G40-600/5245, T300/5208 and G3500/PES gave rise to a comparable number of acoustic emission events at this threshold level. AS6/F584 and P75/ERLX 1902 systems gave rise to a much lesser number of AE events.

In figure 25 the cumulative counts corresponding to the six threshold levels ranging from 35 dB to 85 dB are shown.
The energy content in each of those counts registered at the 85 dB threshold level is nearly 330 times as large in terms of amplitude in volts in comparison to the one registered at 35 dB threshold level. Hence the very large difference in the energy content corresponding to the counts at the six threshold levels should be taken into account interpreting these cumulative counts. From these figures we may note that G40-600/5245 and AS6/F584 composite systems give rise to very high energy events well before the ultimate stress level. However, in the other three composite systems, relatively low level AE signals were seen. In G3500/PES system, very close to the final failure, signals exceeding 85 dB, coinciding with the start of splintering were seen.

The amplitude distributions of the acoustic emission signals are given in figure 26.
In this three dimensional representation, the X,Y and Z axes correspond to amplitude, number of events and the load, respectively. Each of the horizontal lines drawn across the Z-axis represent an increment in load and the value of the increment is indicated in each of these figures. Thus, the cumulative amplitude distribution at various load levels can be seen in these figures. The amplitude range of 35 dB to 100 dB may be subdivided into three smaller ranges, for convenience of discussion. 35 dB to 55 dB, 55 dB to 75 dB and 75 dB to 100 dB intervals are, respectively, termed low amplitude, intermediate amplitude and high amplitude

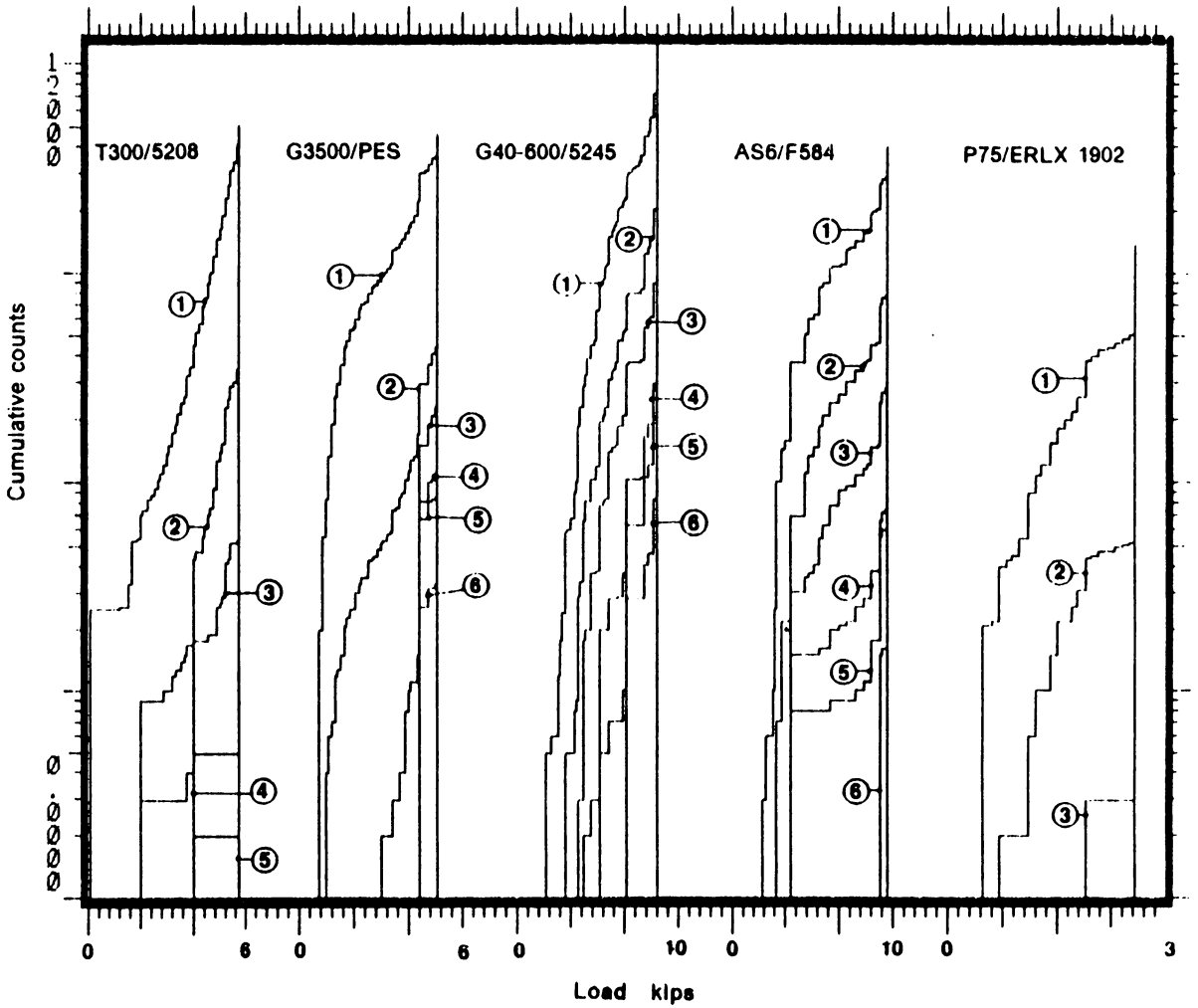

Fig. 25: A comparison of the cumulative counts corresponding to the five composite systems; threshold levels: ① : 35 dB ② : 45 dB ③ : 55 dB ④ : 65 dB ⑤ : 75 dB ⑥ : 85 dB

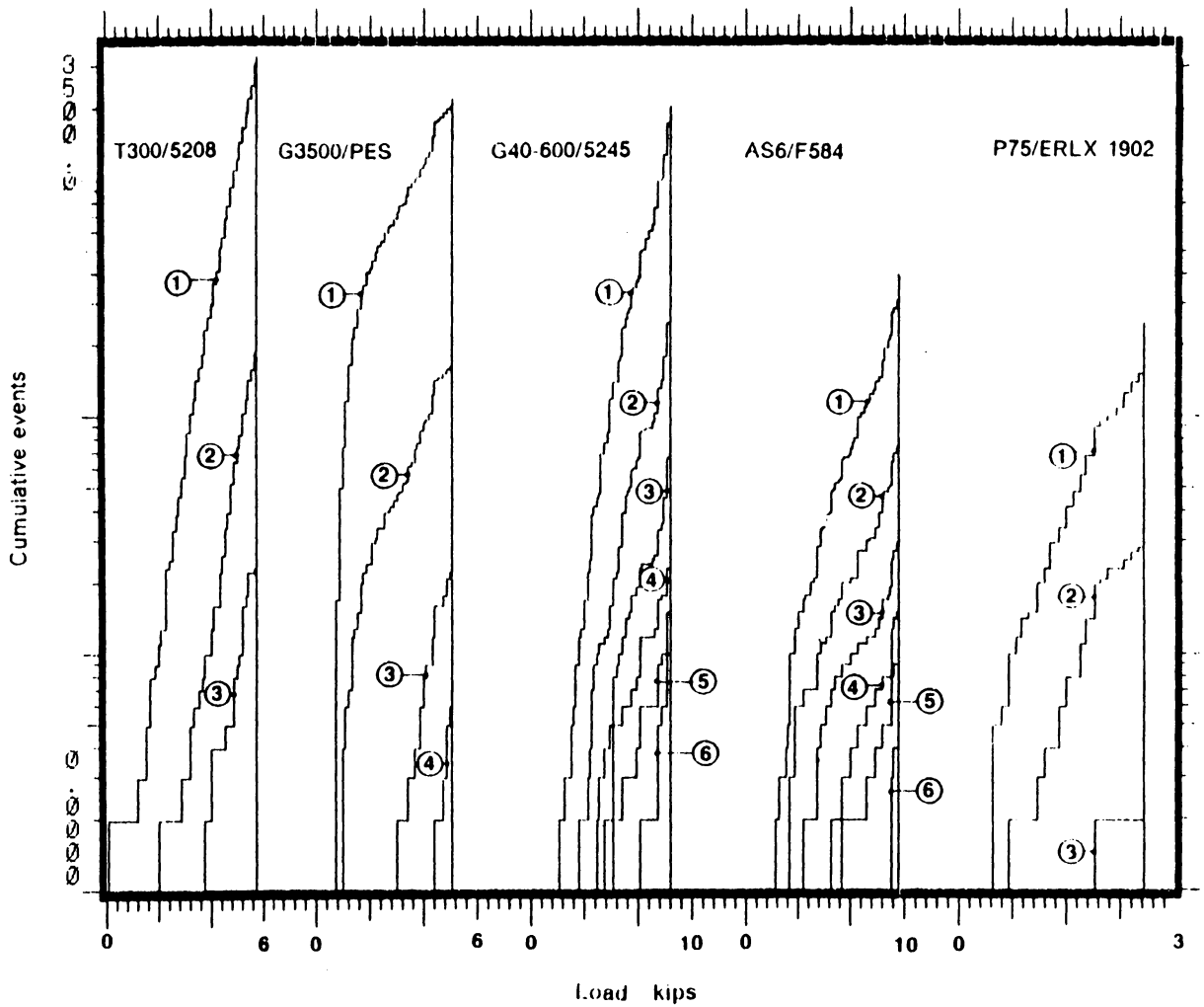

Fig. 24: A comparison of the AE events corresponding to the five composite systems; threshold levels: ① : 35 dB ② : 45 dB ③ : 55 dB ④ : 65 dB ⑤ : 75 dB ⑥ 85 dB

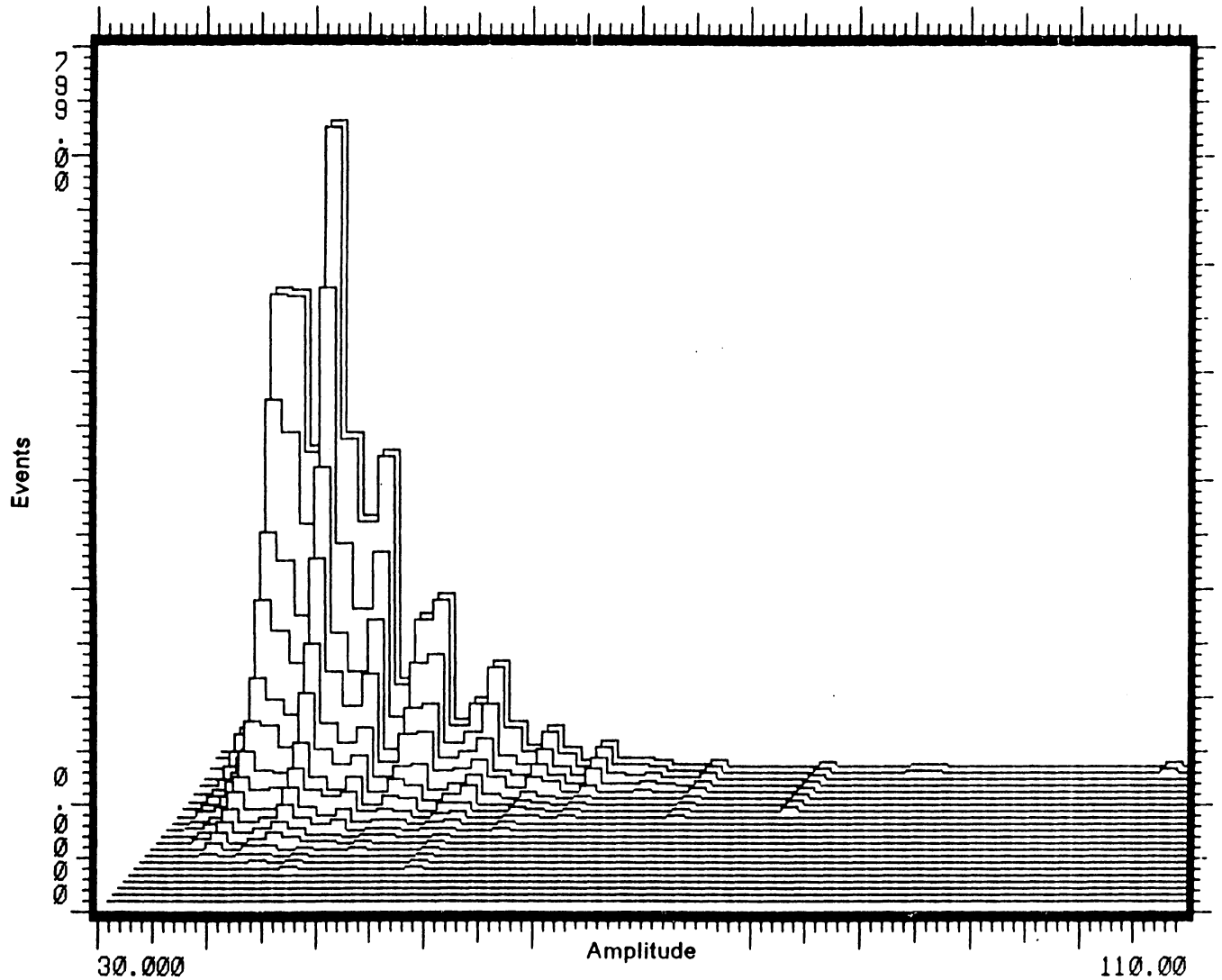

Fig. 26(a): Amplitude distribution of AE events corresponding to T300/5208 system

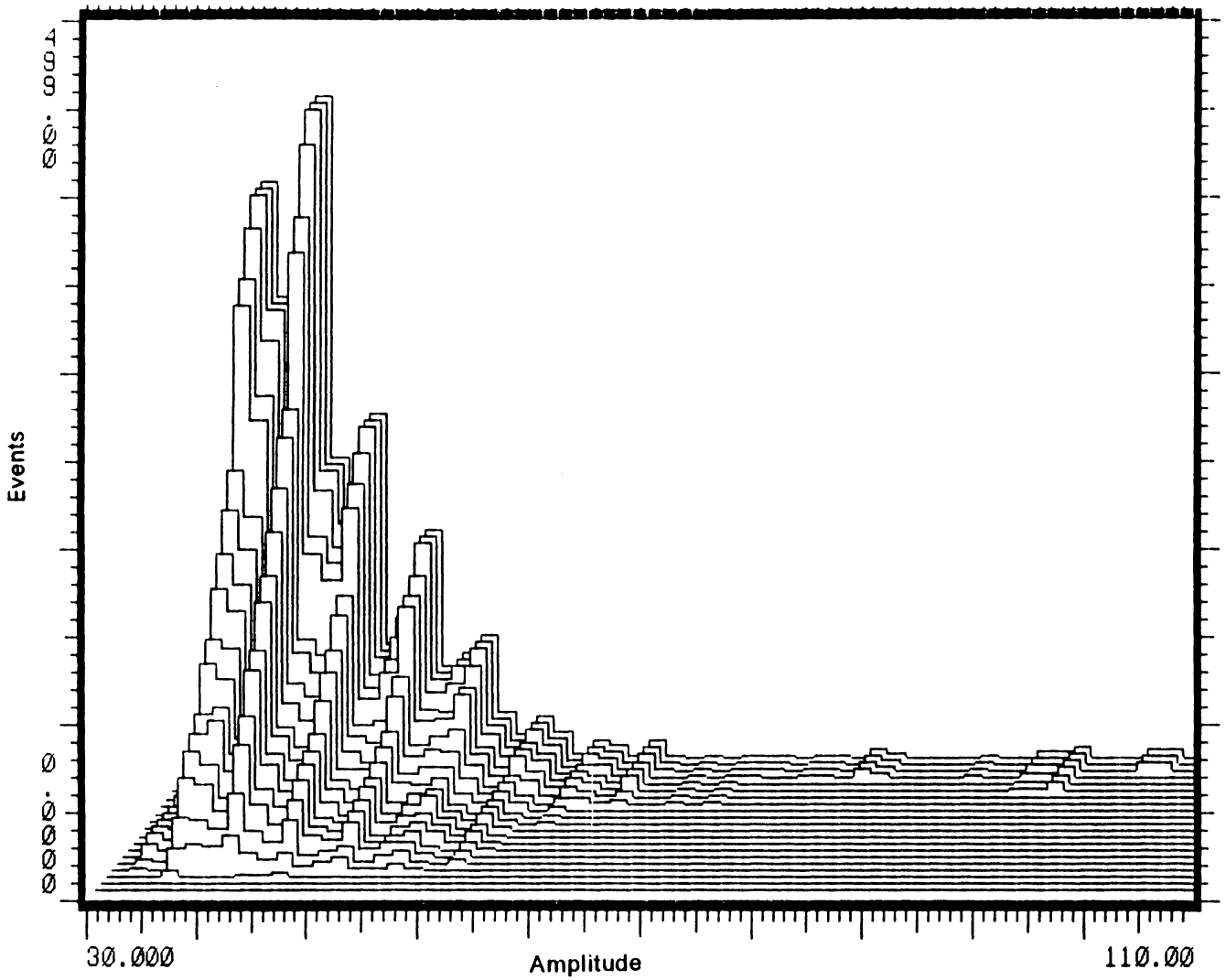

Fig. 26(b): Amplitude distribution of AE events corresponding to G3500/PES system.

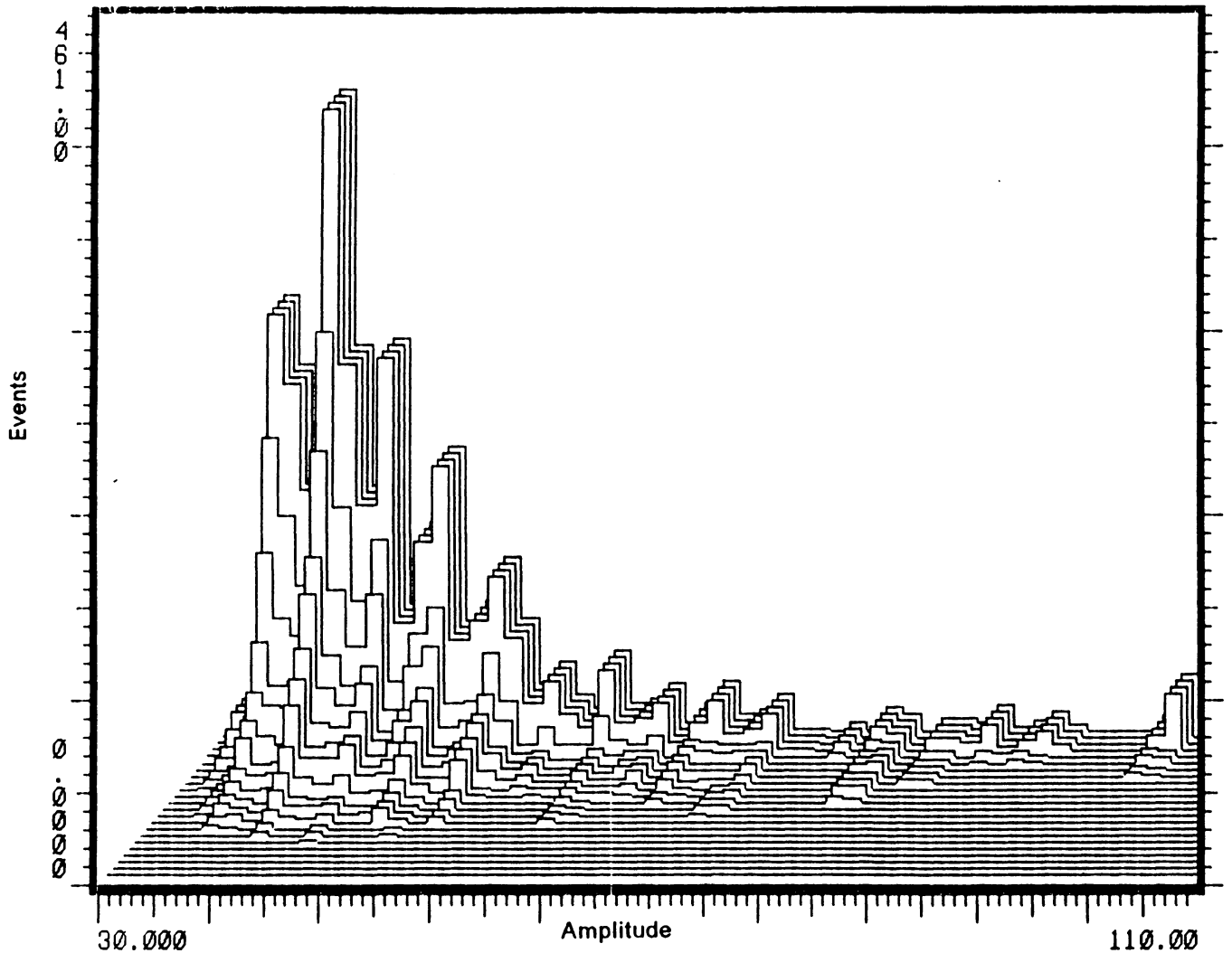

Fig. 26(c): Amplitude distribution of AE events corresponding to G40-600/5245 system.

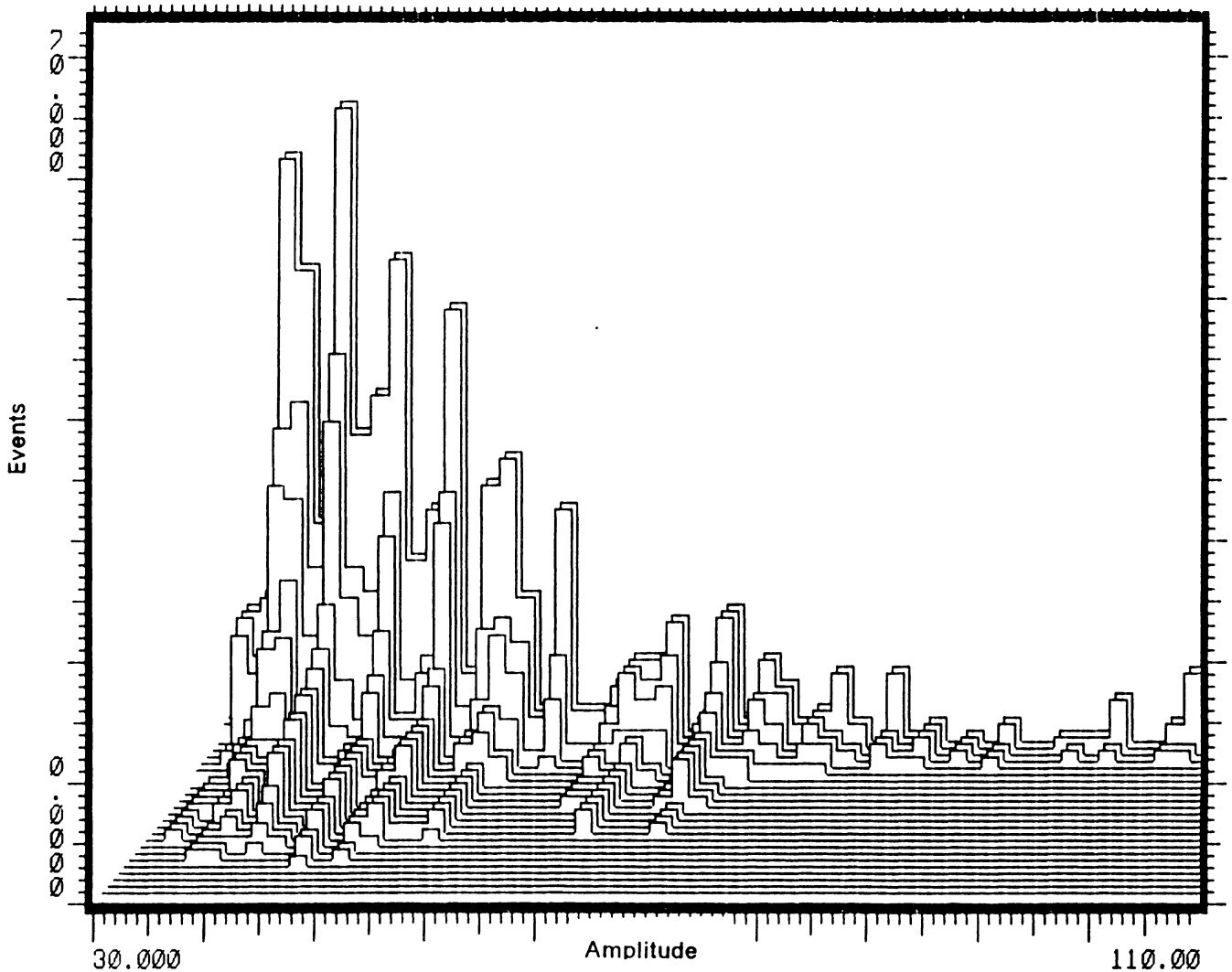

Fig. 26(d): Amplitude distribution of AE events corresponding to AS6/F584 system.

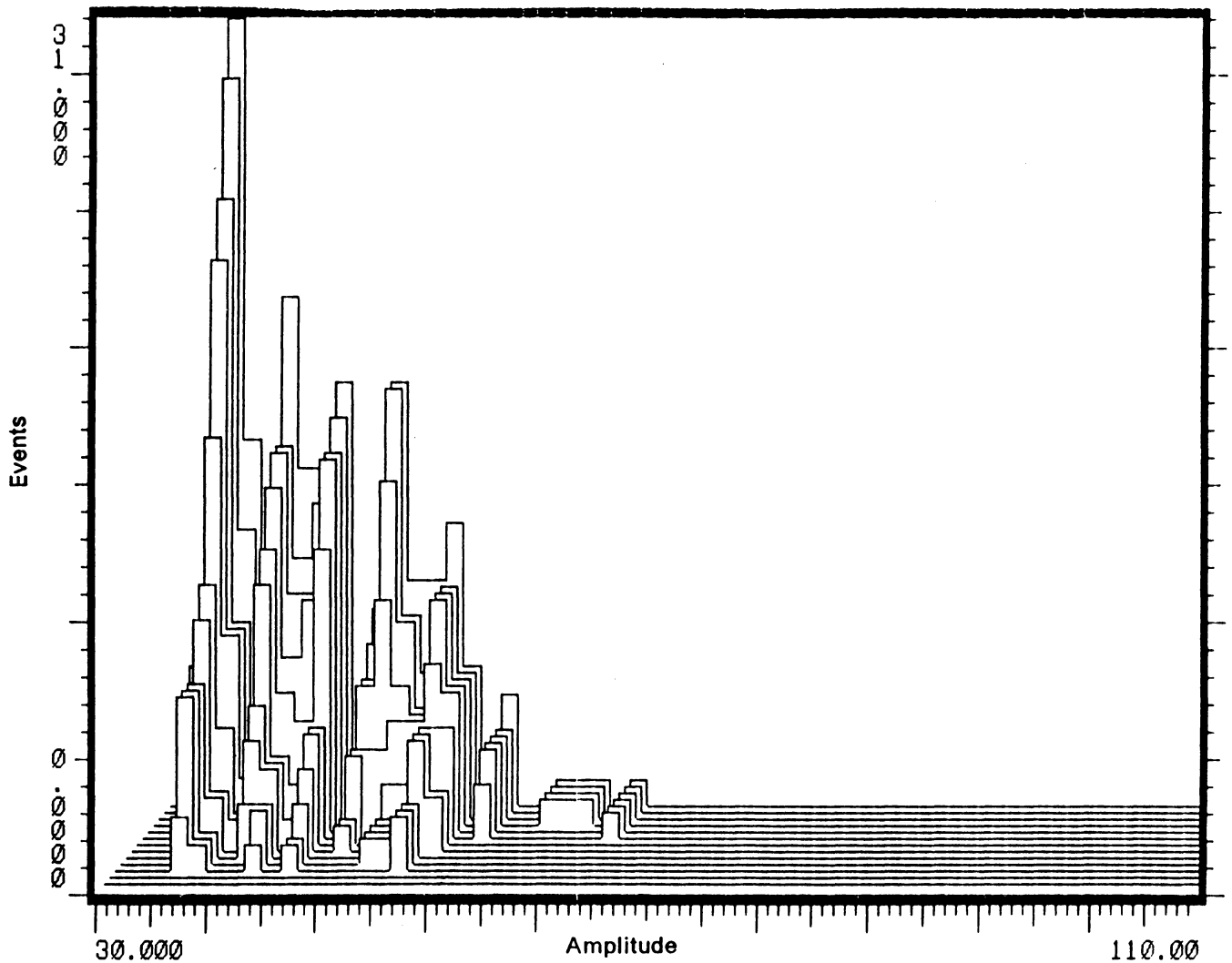

Fig. 26(e): Amplitude distribution of AE events corresponding to P75/ ERLX 1902 system.

ranges. Within each of these ranges, AE amplitudes vary over an order of magnitude, and hence the total variation across the amplitude distribution diagram is greater than three orders of magnitude. Since the energy content is proportional to the square of the amplitudes, the very large range of variation energy between release of different failure events is evident.

In both P75/ERLX 1902 and G3500/PES systems, AE activity began quite early - at about 20 % of the ultimate stress. in P75/ERLX 1902 all the AE activity were confined to the low amplitude range. In G3500/PES, the AE activity extended to the intermediate amplitude range after about 50 % of the ultimate stress, and high amplitude events appeared close the ultimate failure. In T300/5208, significant AE activity started appearing at about 40 % of ultimate stress. Though initially the activity was in the low amplitude range, it quickly spread into the mid levels of the intermediate amplitude range. However, the failure occurred without showing any significant level of high amplitude events. In both AS6/F584 and G40-600/5245, AE activity began at about 30 % of ultimate stress. Before 50 % of the ultimate stress, the activity extended to the intermediate amplitude range in the case of AS6/F584 and into the lower levels of the high amplitude range in G40-600/5245. In the last 20 % of the loading cycle, in both these systems, a significant number of high amplitude signals was seen. G40-600/5245 was, however, producing a much greater number of AE events throughout the 35 dB to 100 dB amplitude range.

The acoustic emission waveforms seen in AS6/F584, are shown in figure 27.
The presence of high frequency components of about 1 MHz, can be seen in this figure. Even though all these waveforms were likely to have been caused by fiber fractures, we see considerable differences in their shapes. In some of these waveforms, low frequency compponents seem to develop after about 15 microseconds beyond the initiation instant. It was found that this was approximately the time taken by simulated AE pulses to travel the length of the specimen.

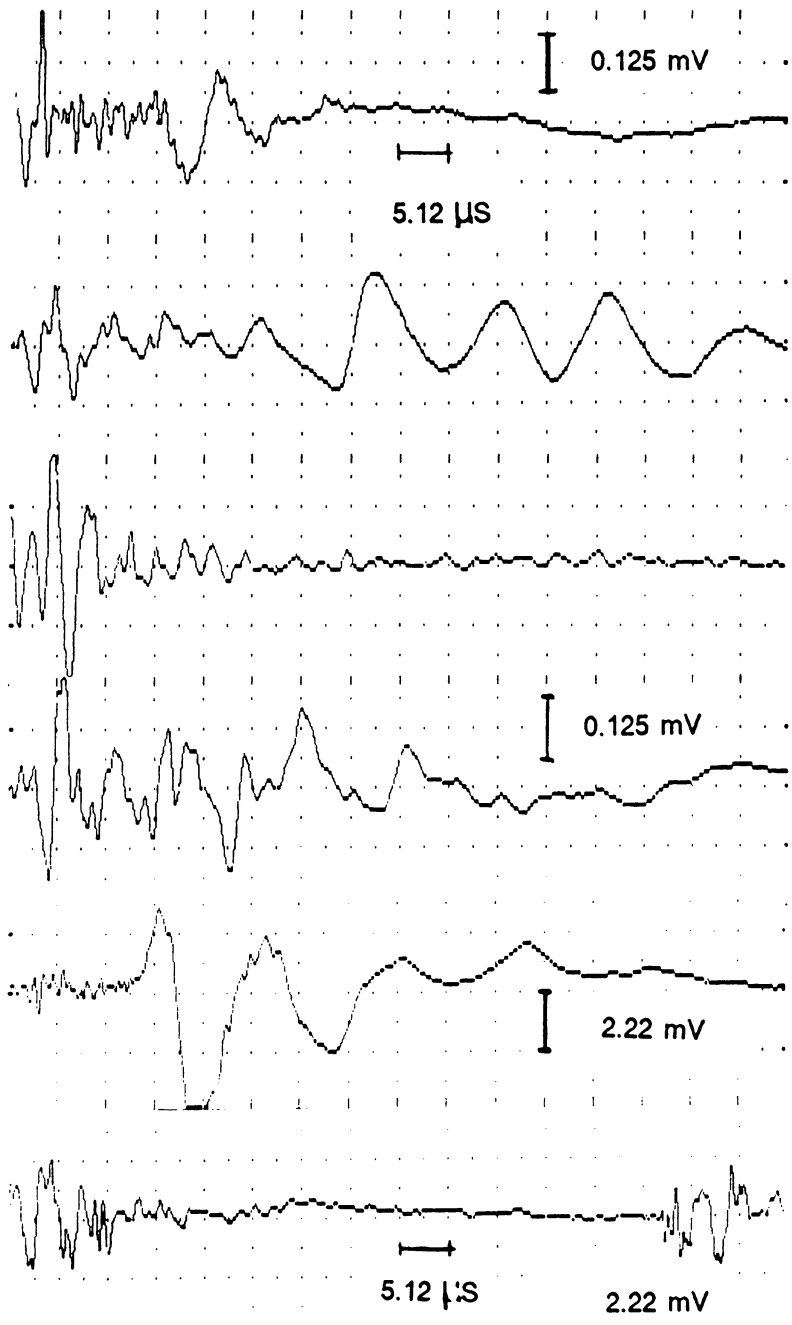

Fig. 27: Acoustic emission waveforms from tensile tests on AS6/F584 composite materials.

4.7. Discussion

A knowledge of the nature of the failure process in unidirectional composite materials can help in interpreting acoustic emission test results. The SEM results presented in chapter 3 provide some information about the initiation and rate of growth of damage and the nature of damage around fiber fractures. However, results in the form of direct observations about the failure taking place very near the ultimate failure are limited. Hence, it is necessary to interpret the acoustic emission results based on the probable event attributes to be expected from the failure modes, coupled with the limited amount of direct evidences available.

The discrete failure events present in unidirectional composites loaded along the fiber direction are random single fiber fractures, failure of groups of fibers as seen in T300/5208, development of microcracks in between the fibers, but normal to the fiber axes as the ones seen AS6/F584, the debonding of individual or groups of broken fibers from the surrounding material and the development of macroscopic splits across the specimen length. The relative magnitudes of energy from each of the failure modes can be estimated. The energy released from matrix cracks is expected to be orders of magnitude smaller than the energy released from fiber breaks because of the smaller strain energy stored in the matrix material at the point of failure. Since the total number of events seen in the present AE results are only of the order of 3000 or less, even at the 35 dB threshold level, it is likely that no acoustic emission from matrix cracking was included in the AE data. The energy released by the fracture of fiber groups would be a function of a number of parameters. They include the size of the group, the stress at the formation of fracture and the energy absorbed in the plastic deformation and creation of fracture surfaces in the matrix. The matrices present AS6/F584 and G40-600/5245 appeared to undergo more extensive damage around broken fibers. This damage is likely to absorb a greater fraction of the strain energy released compared to the brittle cracking of the matrix in the T300/5208 system. SEM studies indicated that no significant amount of fiber matrix interfacial failure present in the composite systems, except for

G3500/PES. No macroscopic splits are seen in the tensile coupons. Hence the most probable source of the majority of acoutic emission events appear to be failure of individual or groups of fibers.

The SEM studies indicated that in terms of the fiber fracture densities, the five composite systems can be ranked, from the least number of fiber fractures to the greatest number of fiber fractures per unit surface area in the following manner: P75/ERLX 1902, G3500/PES, T300/5208, AS6/F584 and G40-600/5245. The last two systems appeared to have similar fracture densities before failure. However, the number of AE events registered at 35 dB threshold level from these five composite systems did not follow the same trend as the one indicated by the SEM study, even though the volume of material in the AE specimens were comparable. The number of AE events registered for AS6/F584 was much less than that found in three of the other four systems. The G40-600/5245 sytem also did not give rise to significantly larger number of acoustic emission events compared to T300/5208. Possible explanation for these seemingly inconsistent results is offered in the next paragraph.

Provided the energy absorption in the surrounding materials is same, the acoustic emission energy registered by the transducer, corresponding to the formation of unit crack surface, at any given stress level should be same for all the five composite systems. Further, the amplitude of the AE signal is related linearly to the stress at which these cracks form. Hence a single fiber fracture occurring at near ultimate stress is expected to release AE signals twice in amplitude compared to that of another fiber failing at 50 % of ultimate stress. Taking into consideration these aspects we may attempt to interpret the acoustic emission data. As indicated by the SEM results, a larger portion of strain energy released by fiber fracture is absorbed by either plastic deformation or by the formation of microcracks in the tougher matrices present in AS6/F584 and G40-600/5245, and as a result AE events corresponding to fiber fractures in these composite systems are lower in amplitude compared to a similar failure in T300/5208.

In T300/5208, SEM micrographs showed the presence of fiber group fractures of sizes up to five fiber diameters wide, by self-similar crack propagation. We can expect the presence of such grouped fiber fractures in tensile coupons also. The acoustic emission signals in the intermediate amplitude range, in this system, probably correspond to such grouped fiber fractures. Compared to T300/5208, the AS6/F584 and G40-600/5245 systems give rise to almost two orders of magnitude higher AE signal levels. The higher stress levels at which the events in the latter two systems can only produce moderate increase in the amplitudes of the AE signals. Hence, it appears likely that the failure processes in AS6/F584 and G40-600/5245 include fracture of much larger fiber bundles well before the ultimate stress levels. However, these composite systems are able to survive such large failure events. The "paint brush" failure mode found in AS6/F584 and G40-600/5245 systems appears to support this contention. The failure process in P75/ERLX 1902, on the other hand, probably becomes unstable with the failure of much smaller fiber bundles compared to T300/5208. Thus, in conclusion, for the composites AS6/F584 and G40-600/5245 the size of micro-fractures which lead to unstable failure growth appears much larger compared to those found in T300/5208 and P75/ERLX 1902 systems.

Examination of the waveforms in figure 27 show that, even among the events belonging to a single failure mode considerable differences can be present. The above waveforms are likely to have been produced by fiber fractures. It appears that because of the differences in the location of the source events, different modes or combination of modes are excited. The presence of dominant low frequency modes which appear late indicates that higher harmonics of the structural modes are also likely to be present in these signals. The presence of such modes may make the estimation of source sizes merely from the magnitudes inaccurate.

5.0: Summary and Conclusions

The objective of this investigation was to understand the failure process in unidirectional composite materials subjected to quasi-static tensile load along the fiber direction. Emphasis was placed on identifying the physical processes operative during the evolution of failure. In-situ scanning electron microscopy and the acoustic emission technique were the tools employed for this purpose. SEM results provided the details of microscopic failure events taking place during the evolution of failure, while AET provided information useful for determining the rate of damage growth and estimating the sizes of individual micro-fracture events. Thus the results from these two techniques are mutually complementary. In addition to these studies, an extensive literature survey was also conducted and an attempt was made to assemble the information relevant to the failure in unidirectional composite materials and present this information in a coherent manner.

In this experimental study, five different commercially available composite systems, currently in use in the aerospace industry, were used. Hence the failure processes studied are representative of those taking place in actual structures.

The in-situ SEM study performed on three point bend specimens revealed several hitherto unreported failure modes occurring at the microscopic scale. Considerable differences were

present in the nature of the deformation in the matrix material around broken fibers. These included differences found in the same system as a function of load as well as differences between different composite systems. All the systems with the exception of G40-600/5245 exhibited no observable failure in the matrix at relatively low load levels. In G40-600/5345, even at 50 % of ultimate strain, multiple cracking of the matrix was present around broken fibers. As the strain level increased, the tendency for such multiple cracking increased. At strain levels close to the ultimate, T300/5208 exhibited self-similar crack extensions of the fiber fractures into the matrix. In AS6/F584, extensive microcracking of the matrix was found near ultimate strain levels. Further, these microcracks gave the appearance of a relatively ductile failure compared to those present in G40-600/5245. From the matrix failure modes observed in this study, it appears that in AS6/F584 and G40-600/5245 systems, the matrix deformation and failure absorbs a greater amount of strain energy released by the fracture of fibers, compared to T300/5208. Acoustic emission test results also support the above inference, since considerably smaller amplitude AE signals appear to result from single fiber fractures in AS6/F584 and G40-600/5245 systems compared to those in T300/5208 system. The extent of plastic deformation of the matrices in these systems, however, is unknown at the present time.

In this connection, efforts were made for developing a technique for measuring the strain distribution within microscopically small regions, as in the above case. A procedure for depositing speckle patterns within such areas, suitable for strain measurements by an image processing technique, has been developed.

In the T300/5208 system, fiber contiguity seems to accelerate the failure process. Even at relatively low strain levels, the failure of any one of the fibers in a contiguous fiber bundle propagated into the rest of the fibers in this group in a self-similar manner. Further, characteristics of dynamic crack growth, such as crack branching within individual fibers, as well as among adjacent fibers, were seen. These phenomena, together with the self-similar extensions of fiber fractures into the matrix, appear to indicate that the interphase and the matrix

of this system have relatively lesser capacity for arresting dynamically propagating cracks. Further, the AE analysis showed that acoustic emission amplitudes varied by more than an order of magnitude in T300/5208 system and those events having higher amplitudes are likely to have originated from fracture of fiber bundles rather than from fracture of single fibers. By combining these observations, it appears reasonable to hypothesize that a dynamic fracture mode participates to a significant extent in the overall failure process. As the stress level increases, dynamically propagating cracks acquire greater ability to overcome barriers such as interphase or layers of matrix. And, of the numerous dynamic cracks which initiate, one crack is able either to propagate across the entire specimen or propagate across a sufficiently large area to bring about the specimen failure. Direct evidence of such dynamic crack propagation in boron/aluminum is available from the work of Herring et. al., [86]. Further, fractographic results of a number of researchers (Purslow [147], Miller and Wingert [125] and Clements [43]) display regions of carbon/epoxy fracture surfaces showing planar crack propagation over large groups of fibers. These results support the above hypothesis about the dynamic fracture.

In the acoustic emission study, significant refinements have been introduced, which are likely to improve the ability of the technique to quantify the AE signals. These include the study of the specimen acoustics, detailed attention to the selection of AE sensors, improvements in data recording and analysis procedures. There was considerable differences present in the acoustic emission behaviour of the five composite systems. In each of three systems, T300/5208, P75/ERLX 1902 and G3500/PES, and the AE signal amplitudes varied over nearly an order of magnitude, and the maximum amplitudes seen were below about 70 dB. The first two of these systems failed by the propagation of a single crack across the specimen width, while the third sytem failed by splintering into ligaments, having an average width of 0.05 inch. In the other two systems, namely AS6/F584 and G40-600/5245 , AE signals of amplitudes up to 100 dB were present. The very high amplitude events are likely to have been caused by fhe failure of large groups of fibers. Hence it appears that these two systems are

capable of surviving failure of relatively larger bundles of fibers, compared to the three systems discussed earlier.

A chart describing the failure process in unidirectional composite materials was constructed from the information obtained from the literature review and the results of the present investigation and this chart is shown in figure 28. This chart summarizes the hypothesis regarding the failure process in unidirectional composite materials and the influence of several important parameters in the evolution of damage.

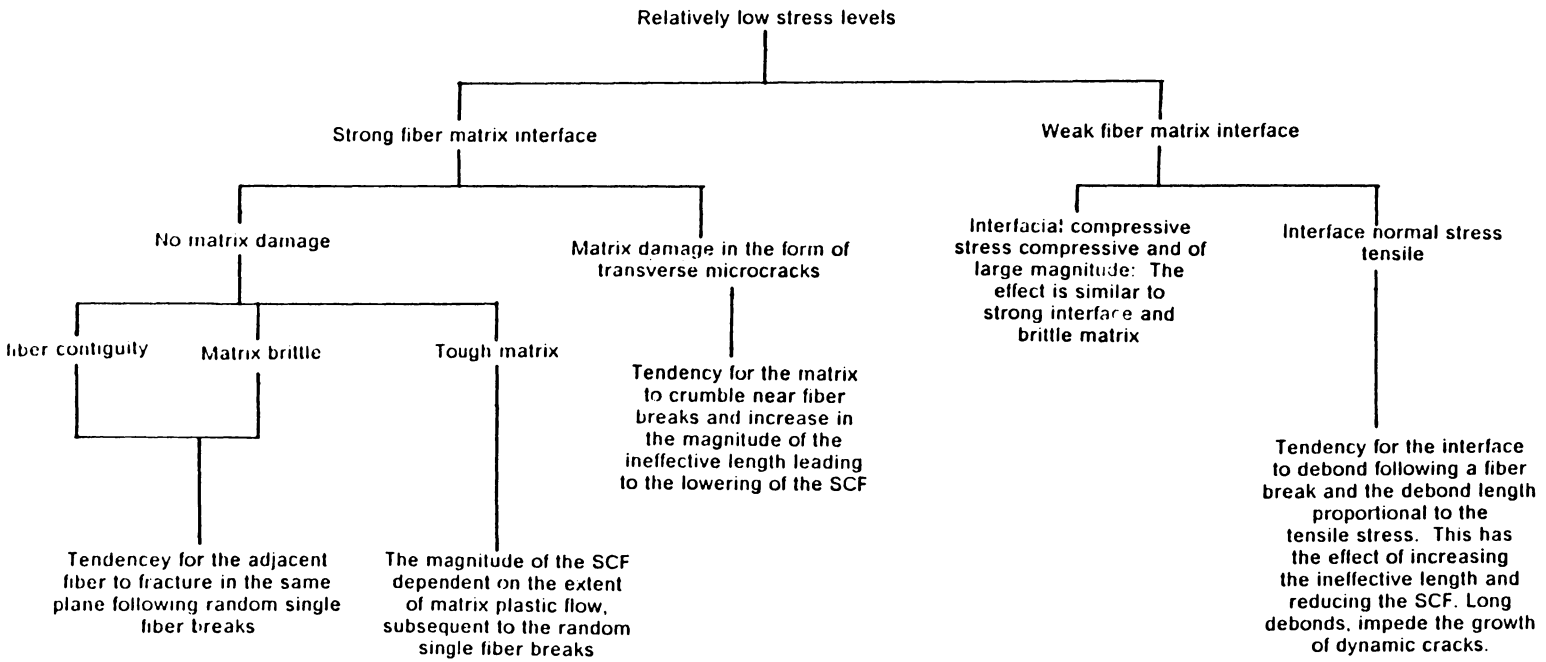

Fig. 28: A chart indicating possible trends in the influence of various parameters on unidirectional commposite material's strength (contd.)

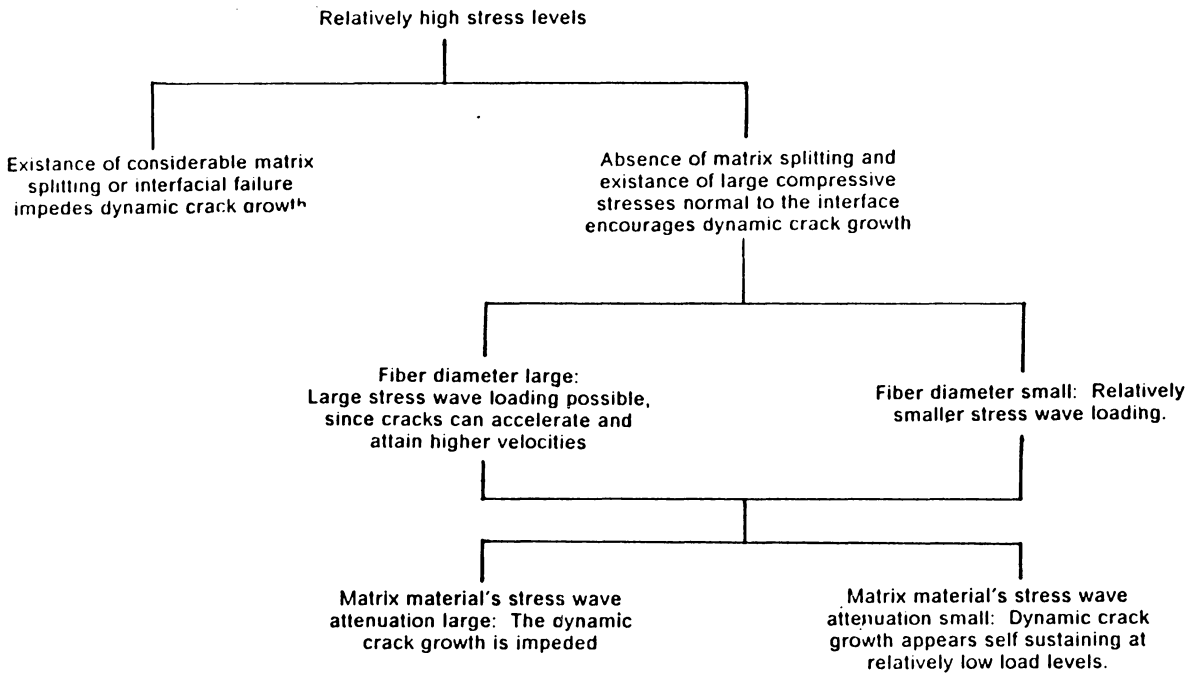

Fig. 28: A chart indicating possible trends in the influence of various parameters on unidirectional commposite material's strength.

6.0: References

1. J.D. Achenbach and J.G. Harris, "Acoustic Emission from a Brief Crack Propagation Event", J. Applied Mechanics, Vol. 46, pp 107-112, 1979.

2. D.F. Adams, "Influence of the Polymer Matrix on the Mechanical Response of a Unidirectional Composite", ICCM-IV, "Progress in the Science and Engineering of Composites", eds. T. Hyashi, et. al., pp. 507-517, 1982.

3. D.F. Adams, " A Micromechanics Analysis of the Influence of the Interface on the Performance of Polymer atrix Composite Materials", J. Reinforced Plastics and Composis , Vol. 6,pp. 66-88, 1987.

4. B.D. Agarwal and R.K. Bansal, "Effect of an Interfacial Layer on the Properties of Fibrous Composites: A Theoretical Analysis", Fibre Science and Technology, pp. 149-158, 1979.

5. B.D. Agarwal, J.M. Lifshitz and L.J. Broutman, "Elastic-Plastic Finite Element Analysis of Short Fibre Composites", Fibre Science and Technology, Vol. 7, pp. 45-62, 1974.

6. A.S. Argon, "Statistical Aspects of Fracture", in Composite Material Vol.5, Eds. L.J. Broutman Academic Press, New York 1974.

7. A.S. Argon, "Stresses in and Around Slender Elastic Rods and Platelets of Different Modulus in an Infinite Elastic Medium Under Uniform Strain at Infinity", Fiber Science and Technology, vol. 9, pp. 265-75, 1976.

8. A.E. Armenakas, et. al.,"Experimental Study of the Failure Mechanism and Strength Characteristics of Fiber Bundles and Composites" , Experimental Mechanics, pp. 1-10, January, 1972.

9. A.E. Armenakas and C.A. Sciammarella, "Experimental Investigation of the Failure Mechanism of Fiber-reinforced Composites Subjected to Uniaxial Tension", Experimental Mechanics, pp. 49-58, February, 1973.

10. A.E. Armenakas and C.A. Sciammarella, "Response of Glass-fiber-reinforced Epoxy Specimens to High Rates of Tensile Loading", Experimental Mechanics , pp. 433-438, October, 1973.

11. C. Atkinson, et. al., "The Rod Pull Out Problem, Theory and Experiment", J. Mech. Phys. Solids, Vol. 130, pp. 97-120,1982.

12. W. B. Avery and C.T. Herakovich, "Effect of Fiber Anisotropy on Thermal Stress in Fibrous Composites", J. Applied Mechanics, Vol.53, pp. 751-756, 1986.

13. J. Aveston, "Strength and Toughness in Fiber-reinforced Ceramics", in "The Properties of Fiber Composites", Conference Proceedings, National Physical Laboratory,England, Nov. 1971, IPC Science & Tech Press Ltd.

14. M.G. Bader and A.M. Priest, "Statistical aspects of Fiber and Bundle Strength in Hybrid Composites" in Proceedings of ICCM IV, Eds. T. Hayashi et. al., 1982.

15. W.D. Bascom, R.M. Jensen and L.W. Cordner, "The Adhesion of Carbon Fibers to Thermoplastic Polymers", pp. 5.424-5.438, Proceedings of the 6th international conference on composite materials, Eds. F.L. Mathews et. al., Elsevier Applied Science Publishers, 1987.

16. S.B. Batdorf, "Note on Shear Interaction Between Two Fibers", Engineering Fracture Mechanics, Vol.18, pp. 1207-1210, 1983.

17. S.B. Batdorf, "Tensile Strength of Unidirectionally Reinforced Composites -- I", J. Reinforced Plastics and Com[posites, Vol. 1, pp. 153-63, April, 1982.

18. S.B. Batdorf and Reza Gaffarian, "Tensile Strength of Unidirectionally Reinforced Composites --II", J. Reinforced Plastics and Composites, Vol. 1, pp. 165-176, April 1982.

19. S.B. Badtdorf and R. Gaffarian, "Stress Distributions in Damaged Composites", ASTM STP 836, pp. 56-70, 1984.

20. S.B. Batdorf and Reza Gaffarian, "Size Effect and Strength Variability of Unidirectional Composites", Int. J. Fracture, Vol. 26, pp. 113-23, 1984.

21. S.B. Batdorf and Reza Gaffarian, " Statistical Treatment of Stress Concentration Factors in Damaged Composites", J. Materials Science Letters, Vol. 1, pp. 295-97, 1982.

22. S.B. Batdorf and R.W.C. Ko, "Use of Shear Lag for Composite Microstructural Analysis - Linear Array", AIAA Journal, Vol. 23, pp. 1749-52; - Rectangular array, pp. 906-910, 1985.

23. S.B. Batdorf, "Experimental Determination of Stress in Damaged Composites Using an Electric Analogue", J. Applied Mechanics, Vol. 50, pp. 190-193 , March 1983.

24. P.W. Barry, "Experimental Data for the Longitudinal Tensile Strength of Unidirectional Fibrous Composites- Part 1: Fiber and Matrix", Fiber Science and Technolog , vol. 11, pp. 245-55, 1978.

25. P.W. Barry, "Experimental Data for the Longitudinal Tensile Strength of Unidirectional Fibrous Composites -- Part 2: Composites", Fibre Science and Technology, Vol. 11, pp. 319-327, 1978.

26. P.W. Barry, "The Longitudinal Tensile Strength of Unidierctional Fibrous Composites", J. Materials Science, Vol. 13, pp. 2177-2187.

27. W.D. Bascom, R.M. Jensen and L.W. Cordner, "The Adhesion of Carbon Fibers to Thermoplastic Polymers", pp. 5.424-5.438, Proceedings of the 6th international conference on composite materials, Eds. F.L. Mathews et. al., Elsevier Applied Science Publishers, 1987.

28. P.W.R. Beaumont and Bryan Harris, "The Energy of Crack Propagation in Carbon Fibre-reinforced Resin Systems", J. Materials Science, Vol. 7, pp. 1265-79, 1972.

29. P.W.R. Beaumont and P.D. Antice,"A Failure Analysis of the Micromechanism s of Fracture of Carbon Fibre and Glass Fibre Composites in Monotonic loading", J. materials Science, Vol. 15, pp. 2619-35,1980.

30. B. Bergman, "On the Probability of Failure in the Chain of Bundle Model", J. Composite Materials, Vol. 15, pp. 92-98, 1981.

31. B. Bender et. al. "Effect of Fiber Coatings and Composite Processing on Properties of Zirconia Based Matrix SIC Fiber Composites", American Ceramic Society Bulletin, Vol. 65. pp. 363-69, 1986.

32. W.L. Bradley and R.N. Cohen, "Matrix Deformation and Fracture in Fiber Reinforced Epoxies", ASTM STP 864, pp. 389-410, 1985.

33. F.G. Buchholz, N. Schulte - Frankenfeld and B. Meiners, "Fracture Analysis of Mixed Mode Failure Processes in a 3D Fiber/matrix composite Cylinder, pp. 3.417-3.428, Proceedings of the 6th international conference on composite materials, Eds. F.L. Mathews et. al., Elsevier Applied Science Publishers, 1987.

34. R.E. Bullock, Strength Ratios of Composite Materials in Flexure and Tension", J. Composite Materials, Vol. 8, pp. 200-206, 1974.

35. A.R. Bunsell, et. al., "Damage and Failure in Carbon Fiber Reinforced Epoxy Resin", ASTM STP 813, pp. 38-54, 1983.

36. I.Y. Chang, "Static Mechanical Properties of Thermoplastic Matrix Composites", Intl. Symposium on Composite Materials, Beijing, China, pp. 20-25, 1986.

37. G.P. Cherapanov, "Mechanics of Brittle Fracture", pp 647-660, McGraw-Hill, 1979.

38. Z. Chi and T.W. Chou, "An Experimental Study of the Effect of Prestressed Loose Carbon Strands on Composite Strength", J. Composite Materials, Vol. 17, pp. 196-209, May, 1983.

39. T.T. Chiao, et. al., "Tensile Properties of an Ultrahigh strength Graphite fiber in an Epoxy Matrix", ASTM STP 580, pp.612-620, 1975.

40. T.C. Chu, et.al., "Application of Digital Image Correlation Techniques to Experimental Mechanics", Experimental Mechanics, Vol. 24, pp 232-244, 1985.

41. D.A. Clarke and M.G. Bader, "Influence of Polymer Matrix and Polymer Coatings on the Strength of Silicon Carbide Reinforcing Fibers", pp. 5.382-5.392, Proceedings of the 6th international conference on composite materials, Eds. F.L. Mathews et. al., Elsevier Applied Science Publishers, 1987.

42. L.L. Clements and P.R. Lee, "Influence of Quality Control Variables on Failure of Graphite/Epoxy Under Extreme Moisture Conditions", ASTM STP 768, pp. 161-171, 1982.

43. L.L. Clements, "Fractography of Unidirectional Graphite/Epoxy as a Function of Moisture, Temperature and Specimen Quality", J. Materials Science, Vol. 21, pp.1853-62, 1986.

44. R.J. Clifton, "Dynamic Plasticity", J. Aplied Mechanics, Vol. 50, pp. 941-952, 1983.

45. F.N. Cogswell, "Microstructure and Properties of Thermoplastic Aromatic Polymer Composites", SAMPE Quarterly, pp. 33-37, July, 1983.

46. G. A. Cooper, "Micromechanics Aspects of Fracture and Toughness", in "Composite materials", vol. 5, pp. 415-448, Academic Press, 1974.

47. G.A. Cooper and M.R. Piggot, "Cracking and Fracture in Composites", Fracture 1977, Vol.1, pp. 557-605, ICF4, Proc. Intl. Conference on Fracture, Waterloo, Canada, 1977.

48. J.W. Dally, " Dynamic Photoelastic Studies of Fracture", Experimental Mechanics, pp 349-361, 1979.

49. J.W. Dally and T. Kobayashi, "Crack Arrest in Duplex Specimens", Int. J. Solids and Structures, Vol. 14, pp. 121-129, 1978.

50. I.M. Daniel,"Photoelastic Investigation of Composites", in Treatise on Composite Materials Eds. L.J. Broutman and R.H. Krock, Vol. 2.

51. H.E. Daniels, "The Statistical Theory of the Strength of Bundles of Theories I", Proc. Roy. (London), Series A, 183, pp. 405-435 (1945).

52. C.K.H. Dharan, "Fracture Mechanics of Composite Materials", J. Engg. Materials and Technology, Vol. 100, pp. 233-247, 1978.

53. L.R. Dharani, W.F. Jones and J.G. Goree "Mathematical Modeling of Damage in Unidirectional Composites", Engineering Fracture Mechanics, Vol. 17, pp. 555-573, 1983.

54. L. Di Landro and M. Pegoraro, "Carbon Fiber - Thermoplasic Matrix hesion", J. Materials Science, Vol. 22, pp. 1980-1986, 1987.

55. G.D.M. Disalvo and S.M. Lee, "Fracture Tough Composites-The Effect of Toughened Matrices on the Mechanical Performance of Carbon Fiber Reinforced Laminates", SAMPE Quarterly, pp. 14-17, January, 1983.

56. L.T. Drzal, M.J. Rich, J.D. Camping and W.J. Par, Proceedings of the 35th Aannual Technical Conference of the Reinforced Plastics, section 20-c, pp. 1-7, The Society of the Plastics Institute Inc., 1980.

57. L.T. Drzal and M.J. Rich, "Effect of Graphite Fiber/Epoxy Matrix Adhesion on Composite Fracture Behaviour", ASTM STP 864 pp. 16-26, 1985.

58. L.T. Drzal, "Composite Property Dependence on the Fiber, Matrix and the Interphase", "Tough Composites", NASA Conference Publication 2334, pp. 227-243, 1984.

59. J.C. Duke, Jr, and E.G. Henneke, II, "Acoustic Emission Monitoring of Advanced Fiber Reinforced Composite Materials: Review", pp. 147-162, Fifth Acoustic Emission Symposium, Tokyo, Japan, 1980.

60. S.J. Fariborz, C.L. Yang and D.G. Harlow, "The Tensile Behaviour of Interply Hybrid Composites I: Model and Simulation", J. Composite Materials, Vol. 19, pp. 334-354.

61. H. Fukuda and K. Kawata, "On the Stress Concentration Factor in Fibrous Composites", Fibre Science and Technology, Vol. 9, pp. 189-203, 1976.

62. H. Fukuda, et. al., "Probabilistic Approach on the Strength of Fibrous Composites", Proc. of U.S. - Japan Conference : Composite Materials, pp. 181-193, Tokyo, 1981.

63. H. Fukuda and T. W. Chou, "Stress Concentrations in a Hybrid Composite Sheet", J. Applied Mechanics, Vol. 50, pp. 845-48, December, 1983.

64. H. Fukunaga, et. al., "Probabilistic Initial Failure Strength of Hybrid and Non-Hybrid Laminates", J. Materials Science, Vol. 19, pp. 3546-53, 1984.

65. H. Fukunaga et. al., "Strength of Intermingled Hybrid Composites", J. Reinforced Plastics and Composites, Vol. 3, pp. 145-159, 1984.

66. M. Fuwa, et. al., "Tensile Failure Mechanisms in Carbon Fibre Reinforced Plastics", J. Materials Science, Vol. 10, pp. 2062-70, 1975.

67. S.K. Garg, V. Svalbonas and G.A. Gurtman, "Analysis of Structural Composite Materials", Marcel Dekker Inc. 1973.

68. M.R. Gecit and F. Erdogan, "The Effect of Adhesive Layers on the Fracture of Laminated Structures", J. Engg. Materials and Technology, Vol. 100, pp. 2-9, 1978.

69. C.A. Ginty, "Progressive Damage, Fracture Predictions and Postmortem Correlations for Fiber Composites", NASA TM-87101, 1985.

70. J.G. Goree, "The Accuracy of Approximate Solutions in the Analysis of Fracture of Composites", pp. 584. Composite Structures 3, Eds. Marshall, Elsevier applied Science Publishers, 1985.

71. W.I. Griffith, M.F. Kanninen and E.F. Rybicki, "A Fracture Mechanics approaches to the analysis of Graphite/Epoxy Laminated precracked Tension Panels", ASTM STP 696, pp. 185-201, 1979.

72. T. Gottesman and M. Mikulinsky, "Influence of Matrix Degradation on Composite Properties in Fiber Direction", Engg. Fracture Mechanics, Vol. 20, pp. 667-674, 1984.

73. R. Grove and B. Smith, "Compendium of Post-Failure Aanalysis Techniques for Composite Materials", AFWAL-TR-86-4137, January, 1987.

74. D.F. Gucer and J. Gurland, "Comparison of the Statistics of Two Fracture Modes", J. Mech. Phys. Solids. Vol. 10, pp. 365-373, 1962.

75. M. A. Hamstad, "A Review: Acoustic Emission, a Tool for Composite Materials Studies", Experimental Mechanics, pp. 7-13, March 1986.

76. M.A. Hamstad and T.T. Chiao, "Acoustic Emission from Stress Rupture and Fatigue of an Organic Fiber Composite", ASTM STP 580, pp. 191-201. 1975.

77. J.R. Hancock, Fatigue of Metal-Matrix Composites, pp. 371-414. in "Composite Materials", Vol. 5, Eds. L.J. Broutman, Academic Press, New York 1974.

78. D.G. Harlow, "Properties of the Strength Distribution for Composite Materials", ASTM STP 674, pp. 484-501, 1979.

79. D.G. Harlow and S.L. Phoenix, "The Chain-of-Bundles Probability Model For the Strength of Fibrous Materials I: Analysis and Conjectures", J. Composite Materials, Vol. 12, pp. 195-214, 1978.

80. D.G. Harlow and S.L. Phoenix, "Probability Distribution for the strength of Composite Materials II: A Convergent Sequence of Tight Bounds", J. Fracture, Vol. 17, pp. 601-630, 1981.

81. D.G. Harlow and S.L. Phoenix, "The Chain-of-Bundles Probability Model for the Strength of Fibrous Materials II: A Numerical Study of Convergence",J. Composite Materials, Vol. 12, pp. 314-34, 1978.

82. J. Heaner and N. Ashbaugh, "Three Dimensional Stress Distribution in a Unidirectional Composite", J. Composite Materials, Vol. 1, pp. 54-63, 1967.

83. J.M. Hedgepeth, "Stress Concentrations in Filamentary Structures", NASA TN D-882, 1961.

84. J.M. Hedgepeth and P.Van Dyke, "Local Stress Concentrations in Imperfect Filamentary Composite Materials", J. Composite Materials, Vol. 1, pp. 294-309, 1967.

85. E. G. Henneke, II and Jones, "Description of Damage in Composites by Acoustic Emission", Materials Evaluation, vol. 37, no. 8, pp. 70-75, 1979.

86. H.W. Herring, J.L. Lytton and J.H. Steele, "Experimental Observations of Tensile Fracture in Undirectional Boron Filament Reinforced Aluminium Sheet", Metallurgical Transactions, vol. 4, pp. 807-817, March 1973.

87. T. Hiramatsu, T. Higuchi and J. Matsui, "Torayca T1000 Ultra High Strength Fiber and its Composite Properties", Looking Ahead for Materials and Processes, Eds. J. De Bossu, et al., pp. 1-8, Elsvier Science Publishers, 1987.

88. J.W. Hitchon and D.C. Philips, "The Dependence of the Strength of Carbon Fibres on Length", Fibre Science and Technology, Vol. 12, pp. 217-234, 1979.

89. J.D.H. Hughes, "Strength and Modulus of current Carbon Fibers", Carbon, Vol. 24, pp.551-556, 1986.

90. T. Ishikawa, "Strength and Thermal Residual Stresses of Unidirectional Composites", J. Composite Materials, Vol. 16, pp. 40-52, 1982.

91. R.D. Jamison, et. al., "Characterization and Analysis of Damage Mechanisms in Tension-Tension Fatigue of Graphite/Epoxy Laminates", ASTM STP 836, pp. 21-55, 1984.

92. R.D. Jamison, "On the Interrelationship Between Fiber Fracture and Ply Cracking in Graphite/Epoxy Laminates", ASTM STP 907, pp.252-273, 1986.

93. X. Ji, "On the Hybrid Effect and Fracture Mode of Interlaminated Hybrid Composites", Proc. ICCM-IV, "Progress in Science and Engineering of Composites", eds. T. Hayashi, et. al., pp. 1137-1144, 1982.

94. X. Ji, X.R. Liu and T.W. Chou, "Dynamic Stress Concentration Factors in Unidirectional Composites", J. Composite Materials, Vol. 19, pp. 269-275, 1985.

95. J.B. Jones, J.B. Barr and R.E. Smith, "Analysis of Flaws in High Strength Carbon Fibers from Mesophase Pitch", J. Materials Science, Vol. 15, pp. 2455-2465, 1980.

96. M.F. Kanninen and C.H. Popelar, "Advanced Fracture Mechanics", Oxford Univ. Press. New york, 1985.

97. R.M. Jones, "Mechanics of Composite Materials", pp. 128-134, McGraw-Hill, 1975.

98. Y. Kasai and M. Saito, "Weibull Analysis of Strength of Various Reinforcing Filaments", Fibre Science and Technology, Vol. 12, pp. 21-29, 1979.

99. I. Kimpara and T. Ozaki, "Dynamic Simulation on Stochastic Tensile Fracture of Unidirectional Fiber Reinforced Composite Materials", Intl. Symposium on Composite Materials, Beijing, China, pp. 682-86, 1986.

100. J.N. Kirk, M. Munro and P.W.R. Beaumont, "The Fracture Energy of Hybrid Carbon and Glass Fibre Composites", J. Materials Science, Vol. 13, pp. 2197-2204, 1978.

101. W.L. Ko, "Finite Element Microscopic Stress Analysis of Cracked Composite Systems", J. Composite Materials, Vol. 12, pp. 97-115 1978.

102. R.D. Kriz, "Influence of Ply Cracks on Fracture Strength of Graphite/ Epoxy Laminates at 76k", ASTM STP 836, pp. 250-265, 1984.

103. R.A. Larder and C.W. Beadle, "The Stochastic Finite Element Simulation of Parallel fiber Composites", J. Composite Materials, Vol. 10, pp. 21-31, 1976.

104. I. Leddet and A.R. Bunsell, "Fatigue Damage in Boron-Aluminium", ASTM STP 674, pp. 581-596, 1979.

105. S. Lehmann, C. Megerdigian and R. Papalia, "Carbon Fiber/Resin Matrix Interphase: Effect of Carbon Fiber Surface Treatment on Composite Performance", SAMPE Quarterly, pp. 7-13, April, 1985.

106. L. Lorenzo and H.T. Hahn, "Fatigue Failure Mechanisms in Unidirectional Composites", ASTM STP 907, pp.210-232, 1986.

107. D.R. Lovell, "A Comparison of Available Carbon Fibers", Proceedings of 3rd International Conference on Carbon fibers, Technology, Uses and Prospects, The Plastics and Rubber Institute, Noyes Publications, 1986.

108. Kelly and Zweben, "Poisson Contraction in Aligned Fibre Composites Showi Showing Pull-out",J. Materials Science, Vol. 11, pp. 582-586, 1975.

109. A. Kobayashi and H. Suemasu, "On Fracture Behaviour During Crack Propagation in Carbon-Fiber Composites", Proc. ICCM-IV, "Progress in Science and Engineering of Composites", eds. T. Hayashi, pp. 633-640, 1982.

110. J.T. Lim, M.R. Piggott and W.J. Bailey, "Toughness of Fibre Composites with Controlled Matrix Shrinkage", SAMPE Quarterly, pp. 25-30, July, 1984.

111. J.M. Mahishi and D.F. Adams, "Micromechanical Predictions of Crack Initiation and Crack Growth Resistance in Boron/Aluminum Composites", J. composite Materials, Vol. 16, pp. 457-469, 1982.

112. J.M. Mahishi and D.F. Adams, "Fracture Behaviour of a Single-Fibre Graphite/Epoxy Model Composite Containing a Broken fibre or Cracked Matrix", J. Materials Science, Vol. 18, pp. 447-456, 1983.

113. J.M. Mahishi, "An Integrated micromechanical and Macromechanical Approach to Fracture Behaviour of Fiber Reinforced composites", Engineering Fracture Mechanics, Vol. 25, pp. 197-228, 1986.

114. G. Maier, et. al., "Damage Development in Carbon Fibre-Reinforced Polyimides in Fatigue Loading as a Function of Stress Ratio", Composites, Vol. 17, pp. 111-120, April, 1986.

115. L.E. Malvern, "Experimental and Theoretical Approaches to Characterization of Material Behaviour at high rates of Deformation", in Conference Serial No. 70. The Institute of Physics, Bristol, Eds. J. Harding, "mechanical Properties at high rates of Strain 1984".

116. P.W. Manders and M.G. Bader, "The Strength of Hybrid Glass/Carbon fiber Composites", parts I & II, J. Materials Science, Vol. 16, pp. 2233-2256, 1981.

117. P.W. Manders, M.G. Bader and T.W. Chou, "Monte Carlo Simulation of the Strength of Composite Fibre Bundles", Fibre Science and Technology, pp. 183-204, 1982.

118. P.W. Manders and T. W. Chou, "Enhancement of Strength in Composites Reinforced with Previously Stressed Fibers", J. Composite Materials, Vol. 17, pp. 26-44, January, 1983.

119. D.B. Marshall, B.N. Cox and A.G. Evans, "The Mechanics of Matrix Cracking in Brittle Matrix Fiber Composites", Acta Metallurgica, Vol. 33, pp. 2013-2021, 1985.

120. W.P. Mason, "Electromechanical Transducers and Wave Filters", Van Nostrand, New York, 1942.

121. L.N. McCartney and R.L. Smith, "Statistical Theory of the Strength of Fiber Bundles", J. Applied Mechanics, Vol. 50, pp. 602-608, 1983.

122. P.E. McMahon and D.G. Taggart," Effect of Carbon Fiber Strain and Resin Characteristics on Optimum Composite Performance", Proc. ICCM-IV, "Progress in Science and Engineering of Composites", eds. T. Hayashi, et. al., pp. 529-536, 1982.

123. A.G. Metcalfe and G.K. Schmitz, "Effect of Length on the Strength of Glass Fibers", Proceedings of ASTM, Vol. 64, pp. 1075-1093, 1964.

124. Y. Mikata and M. Taya, "Stress Field in a Coated Continuous Fiber Composite Subjected to Thermo-Mechanical Loadings", J. Composite Material s, Vol. 19, pp.554-578, November, 1985.

125. A.G. Miller and A.L. Wingert, "Fracture Surface Characterization of Commercial Graphite/Epoxy Systems", ASTM STP 6%, pp. 223-273, 1979.

126. G.J. Mills, G.G. Brown and D.R. Waterman, "Reducing Variability in Compos ite Tensile-Strength Properties", ASTM STP 580, pp. 352-363, 1975.

127. M. Morita, "A Study of Relationship between Composite Strength and Monofilament Strength", Proc. ICCM-IV, "Progress in Science and Engineeri ng of Composites", eds. T. Hayashi, et. al., pp. 107-111, 1982.

128. R. Moreton, "The Tensile Strengths of PAN Based Carbon Fibers", Handbook of Composites, Vol. I: Strong Fibers, Eds. W. Watt andB.W. Perov, p . 446-473, 1985.

129. J. Mullin, J.M. Berry and A. Gath, "Some Fundamental Fracture Mechanisms Applicable to Advanced Filament Reinforced Composites", J. Composite Materials, Vol. 2, pp. 82-103, January, 1968.

130. J.V. Mullin, "Influence of Fiber Property Variation on Composite Failure Mechanisms", ASTM STP 521, pp. 349-366, 1973.

131. J.A. Nairn, "Thermoelastic Analysis of Residual Stresses in Unidirectional, High Performance Composites", Polymer Composites, Vol. 6, pp. 123-130, April, 1985.

132. J.A. Nairn and P. Zoller, "Matrix Solidification and the Resulting Residual Thermal Stresses in Composites", J. Materials Science, Vol. 20, pp. 355-367, 1985.

133. K.P. Oh, "A Monte Carlo Study of the Strength of unidirectional Fiber-Reinforced Composites", J. Composite Materials, Vol. 13, pp.311-328 ,1979.

134. C. Ouyang and M.Z. Lu, "On a Micromechanical Fracture Model for Cracked Reinforced Composites", Intl. J. Nonlinear Mechanics, Vol. 18, pp. 171- 177, 1983.

135. E.P. Papadakis, "Broad Band Flaw Detection Transducers", Acoustica, Vol. 48, pp.293-298, 1980.

136. W.H. Peters and W.F. Ranson, "Digital Imaging Techniques in Experimental Stress Analysis", Optical Engineering, Vol. 21, pp. 427-431, 1982.

137. S.L. Phoenix, "Statistical Analysis of Flaw Strength Spectra of High Modulus Fibers", ASTM STP 580, pp. 77-89, 1975.

138. S.L. Phoenix and R.L. Smith, "Comparison of Probabilistic Techniques for the Strength of Fibrous Materials Under Local Load-Sharing Among Fibers", Intl. J. Solids and Structures, Vol. 19, pp. 479-496, 1983.

139. R.E. Pitt and S.L. Phoenix,"Probabilistic Distributions for the Strength of Composite Materials IV: Localized Load Sharing with tapering", Intl. J. Fracture, Vol. 22, pp. 243-276, 1983.

140. M.R. Piggot, "How the Interface Controls the Properties of Fibre Composit es", Proc. ICCM-IV, "Progress in Science and Engineering of Composites", eds. T. Hayashi, et. al., pp. 193-202. 1982.

141. M.R. Piggot, "Load Bearing Fiber Composites", Pergaman Press, 1980.

142. M. R. Piggot and D. Andison, "The Carbon Fiber-Epoxy Interface", J. Reinforced Plasti and Composites, Vol. 6, pp. 290-302, 1987.

143. R.T. Potter and D. Purslow, "The Environmental Degradation of Notched CFRP in Compression", Composites, pp206-225, 1983.

144. K.M. Prewo, "The Notched Tensile Behaviour of Metal Matrix Composites", ASTM STP 546, pp. 507-522, 1974.

145. T.M. Proctor, "An Improved Piezoelectric Acoustic Emission Transducer", J. Acoustic Society of America, Vol. 71, pp.-1163-1168, 1982.

146. T.M. Proctor, F.R. Breckenridge and Y.H. Pao, "Transient Waves in an Elastic Plate: Theory and Experiment Compared", Journal of Acoustical Society of America, Vol. 74, pp. 1905-1906, 1983.

147. D. Purslow, "Some Fundamental Aspects of Composites Fractography", Composites, pp. 241-247, October 1981.

148. D. Purslow, "Fratographic Analysis of Failure in CFRP", AGARD CP-355, pp. 1-1 to 1-11, 1983.

149. D. Purslow, "Matrix Fractography of Fiber Reinforced Epoxy Composites", Composites, 1986.

150. E.D. Reedy, "Fracture of Notched, Unidirectional Boron/Aluminum: Experiments and Analysis", in "Mechanics of Composite Materials - 1983", Eds. G.J. Dvorak, ASME - AMD, Vol. 58, 1983.

151. E.D. Reedy, "Fiber Stress Concentrations in Kevlar/Epoxy Monolayers", J. Composite Materials, Vol. 19, pp. 533-542, november, 1985.

152. E.D. Reedy, "Fiber Stresses in a Cracked Monolayer Comparison of Shear - Lag and 3-D Finite Element Predictions", J. Composite Materials, Vol. 18, pp. 595-607, 1984.

153. K.L. Reifsnider, et. al., "Long Term Fatigue Behaviour of Composite Materials", ASTM STP 813, pp. 136-159.

154. K.L. Reifsnider and R. Jamison, "Fracture of Fatigue-Loaded Composite Laminates", Intl. J. Fatigue, pp.187-197, 1982.

155. P.G. Riewald, A.K. Dhingra and T.S. Chern, "Recent Advances in Aramid Fiber and Composite Technology", pp. 5.362-5.370, Proceedings of the 6th international conference on composite materials, Eds. F.L. Mathews et. al., Elsevier Applied Science Publishers, 1987.

156. B.W. Rosen, "Tensile Failure of Fibrous Composites", AIAA Journal, Vol. 2, p. 1985, 1964.

157. N. Sato, et. al., "In Situ SEM Observation of Fracture Processes in Short Glass Fiber Reinforced Thermoplastic Composites", ASTM STP 868, pp. 493-503, 1985.

158. N. Sato, T. Kurauchi and O. Kamigaito, "Fracture Mechanism of Unidirectional Carbon Fiber Reinforced Epoxy Resin", J. Materials Science , Vol. 21 pp. 1005-1010, 1986.

159. Y. Sawada, A. Shindo and Y. Nakanishi, "Interphacial Adhesion in a Carbon Fiber - Polyimide Ccomposite", pp. 5.44-5.457, Proceedings of the 6th international conference on composite materials, Eds. F.L. Mathews et. al., Elsevier Applied Science Publishers, 1987.

160. A.V.S.R.J. Sarma, P.N. Murthy and P.S. Kushwaha, "Stress Diffusion in a Pull Out Model", Fibre Science and Technology, Vol. 12, pp. 129-138, 1979.

161. A.R. Sanadi and M.R. Piggot, "Interfacial Effects in Carbon-Epoxies , Part 3, Toughness with Short Fibers", J. Materials Science, Vol. 21, pp. 1642-2646, 1986.

162. P.M. Scop and A.S. Argon, "Statistical Theory of Strength of Laminated Composites II", J. Composite Materials, Vol.3, pp. 30-47, 1969.

163. G.C. Shih and L. J. Elbert, "Theoretical Modelling of the Effect of the Interfacial Shear Strength on the Longitudinal Tensile Strength of Unidirectional composites", J. Composite Materials, Vol. 21, pp. 207-224, 1987.

164. R.L. Smith, et. al., "Lower-tail Approximations for the Probability of Failure of Three-Dimensional Fibrous Composites with Hexagonal Geometry", Proc. Royal Soc. London, series A, Vol. 388, pp. 353-391, 1983.

165. R.L. Smith, "Probabilistic Models for Composites: Are there Flaws in the Theory?" , in " Probabilistic Methods in the Mechanics of Solids and Structures", pp. 291-298, Eds. S. Eggwertz and N.C. Lind, Springer Verlag, 1984.

166. A.J.M. Spencer and G.E. Smith, "Interfacial Tractions in Fibre-Reinforced Composites", Proc. Conf. on "The Properties of Fibre Composites", National Physical Laboratory, IPC Science and Technology Press Ltd., Nov. 1971.

167. W.W. Stinchcomb et. al., " Effect of Ply Constraint on Fatigue Damage Development in Composite Material Laminates", ASTM STP 723, pp. 64-74, 1981.

168. R.V. Subramanian and A.S. Crasto, "Electrodeposition of a Polymer Interface in Carbon Fiber Composites", Polymer Composites, Vol. 7, pp. 201-218, 1986.

169. C.T. Sun and S.E. Yamada, "Strength Distribution of Unidirectional Fiber Composite", J. Composite Materials, Vol. 12, pp. 169-176, 1978.

170. M. J. Sundaresan, L. C. Manoharan, H. N. Sudheendra and Viveka Naik, "Evaluation of Damage Growth in Composite Materials by Acoustic Emission Energy Measurement", proceedings of the Sixth International Acoustic Emission Symposium, Ed. M. Onoe, Japanese Society of Nondestructive Testing, 1982.

171. M.J. Sundaresan, " The Interaction Between Stress Waves and Fracture in Brittle Materials - an Experiment to Verify Cleaving Waves", Intl. J. Fracture, pp. R19-R21, 1984.

172. M. J. Sundaresan and E. G. Henneke, "Scanning Electron Microscopic Observations of the Evolution of Damage in Composite Materials", presentated in the Ninth Symposium on Composite Materials: Testing and Design, American Society for Testing and Materials, Ren, Nevada, April, 1988.

173. J.V. Suvorova, "The Influence of Time and Temperature on the Reinforced Plastic Strength", in Handbook of Composites, Vol. 3, eds. G.C. Sih and A.M. Skurda, Vol. 3, Elsevier Science Publishers B.V., 1985.

174. R. Talreja, "Estimation of Weibull Parameters for Composite Materials Strength and Fatigue Life Data",ASTM STP 723, pp. 291-311, 1981.

175. L.F. Tenn, "Statistical Analysis of Fiber Composite Strength Data"' ASTM STP 734 pp. 229-244, 1981.

176. P.S. Theocaris and J. Milios,"Crack Arrest at a Bimaterial Interface", Int. J. Solids and Structures, Vol. 17, pp. 217-230, 1981.

177. P.S. Theocaris and J. Milios, "Crack Arrest Modes of a Transverse Crack Going Through a Longitudinal Crack or a Hole", J. Engg. Materials and Technology, Vol. 103, pp. 177-182, 1981

178. P.S. Theocaris and J. Milios, "Dynamic Crack Propagation in Composites", Int. J. Fracture, Vol. 16, pp. 31- 51, 1980.

179. P.S. Theocaris et. al., "Crack Propagation and Bifurcation in Fiber Composite Models", Parts I & II, J. Reinforced Plastics and Composites, Vol. 5, pp. 23-50, 120-140, 1986.

180. P.S. Theocaris and G.C. Papanicolaou, "The Effect of the Boundary Interface on the Thermomechanical Behaviour of Composites Reinforced with Short Fibres", Fibre Science and Technology, pp. 421-433, 1979

181. R.Y. Ting, "Rubber Modified matrices", in "The Role of Polymer Matrix in the Processing and Structural Properties of Composite Materials", eds. J.C. Serafis, et. al., Plenum Press, 1983.

182. S.W. Tsai and H.T. Hahn, "Introduction to Composite Materials", pp. 405 - 413, Technomic Publishing Co., 1980.

183. T.Twardy and H.W. Bergman, "Strain Capabilities and Strain Rate Effects in Epoxy Resins and Composites", Intl. Symposium on Composite Materials, Beijing, China, pp.124-129, 1986.

184. H. Vangerko and A.J. Barker, "The Stiffness of Unidirectionally Reinforced CFRP as a Function of Strain Rate, Strain Magnitude and Temperature", Composites, pp. 19-22, 1985.

185. A. Vary and R.F. Lark, "Correlation of Fiber Composite Tensile Strength With Ultrasonic Stress Wave Factor", NASA TM-78846, 1978.

186. A. Vary, "Correlation Between Ultrasonic and Fracture Toughness Factors in Metallic Materials", NASA TM 73804.

187. T. Vinh and T. Khalil, "Adiabatic and Viscoplastic Properties of some Polymers at High Strain and Strain Rate", in "Mechanical Properties at High Rates of Strain - 1984", Eds. J. Harding, 1984.

188. J.K. Wells and P.W.R. Beaumont, "Debonding and Pull-Out Process in Fibrous Composites", J. Materials Science, Vol. 20, pp. 1275-1284, 1985.

189. A.S. Watson, and R.L. Smith, "An Examination of Statistical Theories for Fibrous Materials in the light of Experimental data", J. Material Science Vol. 20, pp. 3260-3270, 1985.

190. J. M. Whitney and L.T. Drzal, "Axisymmetric Stress Distributions around an Isolated Fiber fragment", Toughened Composites, AM STP 937, Ed. Norman J. Johnston, pp. 179-196, 1987.

191. J.M. Whitney and M. Knight, "The Relationship Between Tensile Strength and Flexure Strength in Fiber-reinforced Composites", Experimental Mechanics, pp. 211-216, June 1980.

192. J.G. Williams, "Fracture Mechanics of Polymers", John Wiley and Sons, p 162, 1984.

193. J. Xing, G.C. Hsiao and T.W. Chou, "A Dynamic Explanation of the Hybrid Effect", J. Composite Materials, Vol. 15, pp.443-461, 1981.

194. A. R. Zak and M. L. Williams, " J. Applied Mechanics, Vol. 30, pp. 143-145,1963.

195. R.S. Zimmerman, D.F. Adams, and D.E. Walrath, "Investigation of the Relation Between Neat Resin and Advanced Composite Mechanical Properties", NASA CR 172303, 1984.

196. C.Zweben, "Tensile Failure of Fiber Composites", AIAA Journal,PP.2325-31, 1968.

197. C.Zweben and B.W. Rosen, "A Statistical Theory of Material Strength with Application to Composite Materials", J. Mechanics and Physics of Solids, Vol. 18, pp. 189-206, 1970.

198. C. Zweben, " A Bounding Approach to the Strength of Composite Materials", Engg. Fracture Mechanics, Vol. 4, pp1-8,1972.

The vita has been removed from the scanned document